INTERACTIVE MUON CATALYZED

AND

INERTIAL CONFINEMENT FUSION

By

GREGORY RONALD CRIPPS, B.ENG, M.ENG

A Thesis

Submitted to the School of Graduate Studies

in Partial Fulfilment of the Requirements

for the Degree

Doctor of Philosophy

McMaster University

July 1993

INTERACTIVE MUON CATALYZED AND INERTIAL CONFINEMENT FUSION

DOCTOR OF PHILOSOPHY (1993)
(Nuclear Engineering)

McMASTER UNIVERSITY
Hamilton, Ontario

TITLE : Interactive Muon Catalyzed and Inertial Confinement Fusion

AUTHOR : Gregory Ronald Cripps. B.Eng. (McMaster University)

M.Eng. (McMaster University)

SUPERVISOR : Professor A.A. Harms

NUMBER OF PAGES : xxiv, 237

ABSTRACT

Energetic viability calculations of nuclear fusion energy systems based on two distinct approaches to a symbiotic combination of Muon Catalyzed Fusion (μCF) and Inertial Confinement Fusion (ICF) have been performed. The first approach involves a deuterium-tritium ICF pellet ignited by muon catalyzed fusion heating; the second approach is based on the energy generated by μCF reactions in deuterium-tritium compressed to high density.

Viability evaluations rely upon modelling of identified critical energy gain parameters for energy systems based upon each of the μCF-ICF approaches. Analysis leading to viability evaluation consists of outlining the general technological requirements of an interactive μCF-ICF system and developing muon catalyzed reaction models in conditions found in high density compressions.

An energy system based on μCF in compressed deuterium-tritium was found to be non-viable due primarily to the sharp decrease in the muon induced fusion rate for temperatures greater than 40 eV. The viability of a fusion energy system based on the μCF triggered spark ignition is favourable provided that technology can be developed which allows for the deposition of sufficient quantities of muons into a very small volume within a very short duration.

ACKNOWLEDGEMENTS

I would like to express my appreciation to Prof. A.A Harms for his kindness and direction. He always gave me support and never failed to inspire me when I needed it most.

My study period at the Kernforschungzentrum Karlsruhe laid the foundation of my thesis work and I express my thanks to Dr. Balbir Goel who supervised my stay at the Kernforschungszentrum and also to Dr. R. Frohlich, Dr. G. Kessler who made my visit possible.

I would also like to recognize the members of my thesis committee, Dr. B. Garland and Dr. D.W.L. Sprung for their time and useful suggestions.

During my past four years here at McMaster, I have had the privilege of learning from some very special colleagues: Zoran Bilanovic, Phil Roberts, Dr. Victor Sosnin, Dr. Klaus Schoepf, Peter Arberg, Wojtek Fundamenski, Mohammed Mansor and Rachid Ouyed. All of these people helped me immeasurably to complete this work.

Financial support form the Natural Science and Engineering Research Council (NSERC), the Canadian Fusion Fuels Technology Project (CFFTP) and the Deutscher Akademischer Austauschdienst (DAAD) is gratefully acknowledged.

My mother, my two musician brothers, the rest of my family and friends were always supportive and understanding during my studies. Special thanks goes to Klaus and Helga Stegemann for their kindness and wisdom. I would

also like to make a special mention of my late father who continues to inspire me.

Finally, I wish to acknowledge and dedicate this thesis to the most important influence in my life and the person who was always there with support, guidance and love: my wife Julia.

for Julia

TABLE OF CONTENTS

TABLE OF CONTENTS

TABLE OF CONTENTS

TABLE OF CONTENTS

LIST OF FIGURES

LIST OF FIGURES

LIST OF FIGURES

LIST OF FIGURES

LIST OF TABLES

NOMENCLATURE

α	-	alpha particle, helium 4, ^4He
α	-	fine structure constant
α_d	-	fraction of molecules undissociated
α_i	-	fraction of atoms unionized
A_{brems}	-	bremsstrahllung power loss constant
brems	-	brestrahllung
B	-	fusion cross-section constant
B	-	magnetic field
B_t	-	tritium breeding ratio
B(T)	-	temperature dependent fuel burn-up fraction variable
c	-	speed of light
c_s	-	sound speed
cat	-	catalyzed
c_p	-	constant pressure specific heat
c_v	-	constant volume specific heat
X_μ	-	muon efficieny, muon catalyzing efficiency, number of fusions induced per muon
C_d	-	fuel fraction of deuterium
C_t	-	fuel fraction of tritium
CANDU	-	Canadian Natural Uranium/Heavy Water fission reactor
d	-	deuteron, deuterium, ^2H
$\varepsilon_{(\,)}$	-	energy level
ε	-	permittivity
$\eta_{(\,)}$	-	efficiency
e	-	electron
e	-	2.71...
e	-	electronic charge
$E_{(\,)}$	-	energy
E	-	electric field
f_{burn}	-	fuel burn-up fraction
f_m	-	molecular fraction
f_a	-	atomic fraction
f_{deg}	-	degeneracy fraction
f_i	-	ion fraction
f_μ	-	muonic fraction
fermi	-	fermi degenerate gas
F	-	hyperfine structure
FLIBE	-	Li_2BeF_4

NOMENCLATURE

γ	- gamma ray
γ	- material equation of state constant
G	- energy gain
GPa	- giga pascal
h	- helium 3, ^3He
h	- Plank's constant
HIBALL	- ICF fuel pellet design
ign	- ignition
$I_{(\ )}$	- ionization energy
I_{max}	- maximum intensity
ICF	- Inertial Confinement Fusion
k	- Boltzmann's constant
keV	- kilo electron volt
K	- molecular rotational state
KrF	- Krypton Fluoride
$\lambda_{(\ )}$	- reaction rate
λ_0	- alpha particle range constant
λ_c	- muon cycling rate
$\ln\Lambda$	- coulomb logarithm
LAMPF	- Los Alamos Meson Physics Facility
LHD	- liquid hydrogen density
LINAC	- linear accelerator
μ	- muon
μd	- muo-atom, muo-deuterium
μt	- muo-atom, muo-tritium
μdt	- muo-molecular ion
μCF	- Muon Catalyzed Fusion
MCF	- Magnetic Confinement Fusion
$m_{(\ )}$	- mass
M_{ab}	- reduced mass of particle a and b
M_{dt}	- energy multiplication of a deuterium-tritium reactor blanket
MeV	- mega electron volt
M_{tamp}	- total mass of tamper material
M_{fuel}	- total mass of fuel
MJ	- mega joule
$\nu_{(\ )}$	- vibrational state
n	- neutron
ns	- nanoseconds
N(v)	- velocity distribution of particles
$N_{(\ )}$	- number density

NOMENCLATURE

ω	- vibrational freqeuncy
Ω	- ratio of the ignition wave speed and the sound speed in a deuterium-tritium plasma
p	- proton, hydrogen, ^1H
π	- pion
ϕ	- density with respect to liquid hydrogen
p	- momentum
p_{1s}	- fraction of muo-tritium in the ground state
ps	- picoseconds
$P_{(\ )}$	- power
$P_{(\ )}$	- pressure
$P_{(\ )}$	- probability
q_{1s}	- fraction of muo-deuterium in the ground state
$Q_{(\ )}$	- energy
$\rho_{(\ )}$	- mass density
ρr	- areal density
$\rho_s r_s$	- spark region areal density
r_α	- alpha particle range
r	- radius
$R_{(\ )}$	- reaction rate
R	- radius
R	- muon regeneration probability
RPA	- random phase approximation
$\sigma_{(\ )}$	- cross-section
$\langle\sigma v\rangle_{ab}$	- fusion sigma-vee of particles a and b
S(E)	- strong force component of the fusion cross-section
S(E)	- stopping power
S_n	- fuel injection rate
S_α	- alpha particle removal rate
SI	- spark ignition
t	- triton, tritium, ^3H
$\tau_{(\ )}$	- characteristic time
$t_{(\ )}$	- time
$T_{(\ )}$	- temperature

NOMENCLATURE

T_{keV}	- temperature in keV (temperature in energy units includes Boltzmann's constant k)
TW	- tera watt
u_s	- shock speed
u_p	- particle speed
U	- coulomb barrier energy
v	- velocity
v_{ab}	- relative velocity of particle a with repect to particle b
V	- volume
V_{cm}	- center of mass velocity
VI	- volume ignition
$w_{( )}$	- muon sticking probability
W	- watts
Z	- electronic charge
Z_{eff}	- effective electronic charge
Z_{vib}	- vibrational partition function

CHAPTER 1

INTRODUCTION

Many methods of generating energy exist, but the harnessing of nuclear fusion energy is considered to be an ultimate energy technology due primarily to the almost inexhaustible supply of fusion fuel. The exploitation of fusion energy as an energy source relies on the successful development of technology for releasing nuclear energy from selected elements and also for collecting and converting this energy into a useful form. The world-wide effort to develop fusion energy technology currently focuses on the following three approaches:

1. Magnetic Confinement Fusion (MCF),
2. Inertial Confinement Fusion (ICF), and
3. Muon Catalyzed Fusion (μCF).

The first two technologies are based on heating a fusion fuel (e.g. deuterium-tritium) to temperatures of several hundred million degrees and confining it by using magnetic fields or by using the fuel's own inertia, such that sufficient fuel burns to yield an adequate energy return. The largest current effort in MCF is based on the Tokamak concept. However, this technology is very complex and expensive, and will be difficult to operate due to stability problems of a magnetically confined fusion plasma[1].

An ICF energy system consists of technology that can initiate and contain a micro-explosion of a small quantity of fusion fuel and then extract and convert the blast energy. Such an inherently pulsed ICF energy system will provide an average constant supply of output energy at a high repetition rate. The key issue in ICF is devising a "driver" that can initiate the thermonuclear burn of a small fusion fuel pellet. Although ICF technology is not as well developed as MCF, recent experiments have demonstrated that the basic principles are sound and that high energy gains can indeed be achieved[2-4].

Muon Catalyzed Fusion (μCF) of two hydrogen isotopes occurs through screening of the Coulomb force by the heavy negative particle known as the muon. Considered by some to be an esoteric fusion technology, μCF has some advantages over the other two mainstream technologies. One notable property is that it operates at room temperature. The main obstacle to μCF is that the muon catalyzed reaction rates and muon losses limit the energy gain at low temperatures to non-viable values.

As of yet, none of the above technologies has been developed into an energetically practical system and currently it is uncertain which will succeed ultimately to become commercially useful. In this light, additional possible approaches to fusion energy should be investigated. The existence of common features among the three main fusion technologies suggests that a complementary combination of available technologies may yield favourable results[5]. Indeed, there are some examples of ventures to combine the technologies of MCF and ICF, notably the MIICF (Magnetically Insulated Inertial Confinement Fusion) study by Hasegawa[6,7]. As well, many μCF reactor designs rely greatly upon MCF design concepts[8,9].

Some recent experiments and theoretical formulations have suggested that μCF could be enhanced in deuterium-tritium fuel elevated to densities greater than liquid hydrogen density (LHD)[10-13]. Elevated densities are an integral part of ICF technology and a course of study to investigate the possible symbiotic relationship between ICF and μCF[14-17] thus seems most appropriate.

1.1 Objectives

Specific objectives of this dissertation are the following:

1. to conceptualize possible μCF-ICF synergetic energy systems,
2. to discuss technological requirements of a μCF-ICF energy system,
3. to investigate high density muon catalyzed fusion processes, and
4. to evaluate overall viability of μCF-ICF synergism.

Evidently it is only after the technology requirements and the critical issues of high density and temperature muon catalysis have been examined, that a clear view of the domain of viability of an symbiotic ICF-μCF energy system will emerge.

1.2 Organization

This introductory chapter is followed by a background chapter to clarify some topics of nuclear fusion, fusion energy systems, ICF and μCF. Chapter 3 will introduce conceptual energy systems based upon μCF-ICF synergism, and Chapter 4 will concentrate on the important components of the conceptual systems. Chapter 5 is dedicated to modelling the various μCF reaction

processes to be found under high temperature and high density ICF conditions. Using knowledge gained in Chapters 4 and 5, the viability of the μCF-ICF energy system approaches introduced in Chapter 3 are discussed in Chapter 6. To finish this work, conclusions and suggestions for further studies are presented in Chapter 7.

CHAPTER 2

BACKGROUND

The following overview of selected basic nuclear fusion concepts provides a basis for future elements of this work.

2.1 Nuclear Fusion

Nuclear fusion is a process in which light nuclei, i.e hydrogen isotopes, are brought together in order to liberate some of their nuclear binding energy in forming new nuclei. The basic nuclear fusion reaction,

$$a + b \rightarrow x + y + Q \ , \tag{2.1}$$

involves an interaction of reactants a and b to form reaction products x and y, releasing a quantity of energy Q. The energy released can be calculated from the well-known Einstein relation,

$$Q = [\Delta m]\, c^2 = [(m_a + m_b) - (m_x + m_y)]\, c^2 \ . \tag{2.2}$$

Here Δm is the change in total rest mass between the reactants and products, and c is the speed of light. The magnitude of the energy released during a fusion reaction can be comprehended by considering the magnitude of the reaction mass decrement and the speed of light and therefore indicates why the quest for fusion energy is of so much interest.

2.1.1 Nuclear Fusion Reactions

Figure 2.1 illustrates the potential between two nuclei resulting from the combination of the attractive nuclear force and the repulsive Coulomb force. As is depicted in Fig.2.1, the strong nuclear force is assumed to have only a short range and will be felt by the nuclei only when the separation distance r between two nuclei is less than a critical value, r_s. This critical value may be approximated as

$$r_s = r_o A^{1/3} \quad , \tag{2.3}$$

where r_o = 3.0 fm and A is the atomic mass number[18]. For example, if two deuterium nuclei reach a separation distance less than approximately 3.8 fm they will have a high probability of fusing.

For distances greater than r_s, the Coulomb potential between two nuclei with a separation distance r is

$$U = \frac{Z_a Z_b e^2}{4 \pi \epsilon_o r} \quad , \tag{2.4}$$

where Z_a and Z_b are the atomic numbers of the nuclei. For two deuterium nuclei at the boundary of the strong force attractive force, the Coulomb potential is U_{peak} = 350 keV. Thus, if a deuteron is accelerated to a kinetic energy of about 400 keV and directed to a solid deuterium target, fusion can be induced to create about 3.7 MeV. This simplistic picture does not include the energy losses due to scattering and radiative collisions of the energetic nuclei, nor the possibility of nuclear fusion occurring at lower particle kinetic energies by quantum mechanical tunnelling through the Coulomb barrier.

The effect of Coulomb barrier penetration by quantum mechanical tunnelling in the interaction between particle a and particle b yields the

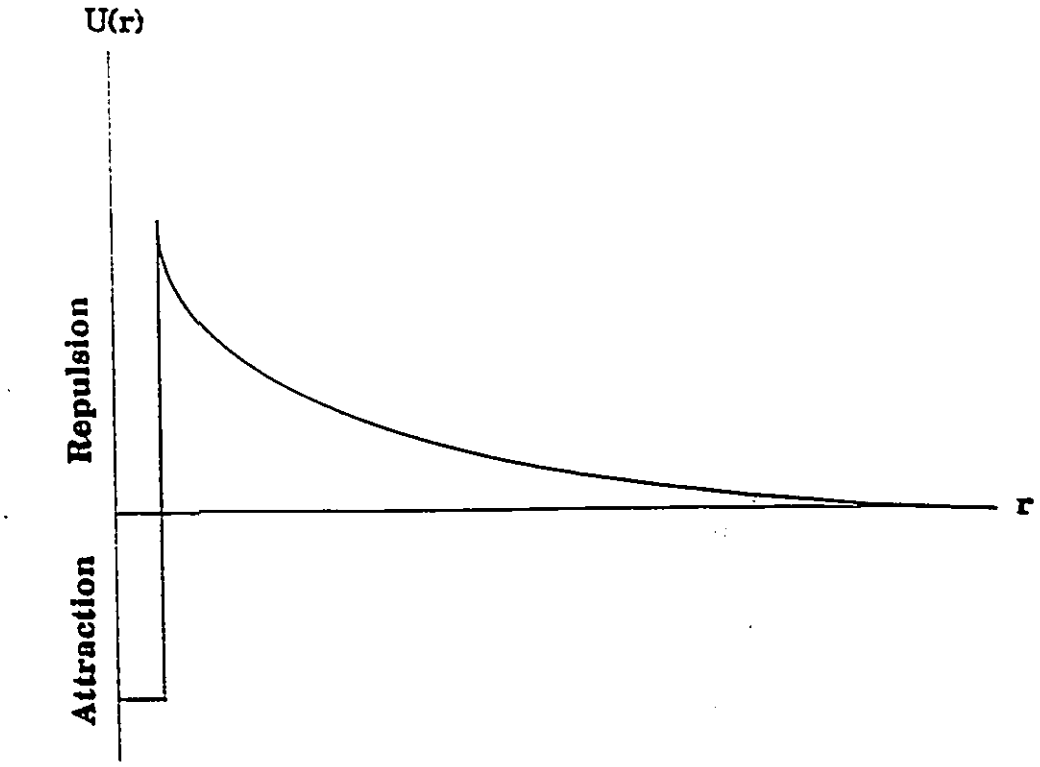

Figure 2.1 : Schematic of the attractive nuclear and repulsive Coulomb potentials between two nuclei.

Gamow cross-section for nuclear fusion[9]

$$\sigma(E) = \frac{S(E)}{E} \exp(-\frac{B}{\sqrt{E}}), \tag{2.5}$$

where E is the energy of the interaction, S(E) represents the intrinsically nuclear or strong force component and

$$B = 2\pi(\frac{e^2}{hc}) Z_a Z_b (\frac{M_{ab} c^2}{2})^{1/2}. \tag{2.6}$$

Here

$$M_{ab} = \frac{m_a m_b}{m_a + m_b} \tag{2.7}$$

is the reduced mass of the interacting particles, e is the electron charge constant, h is Plank's constant and c is the speed of light.

2.1.2 Thermonuclear Fusion

The translational velocity distribution N(v), assuming three degrees of freedom in the mutually orthogonal x, y and z directions, of a collection of particles at equilibrium can be characterized by the following Maxwell-Boltzmann distribution,

$$\begin{aligned} N(v)\, dv_x dv_y dv_z &= N(\frac{m}{2\pi kT})^{3/2} \exp(-\frac{m v^2}{2kT})\, dv_x dv_y dv_z \\ &= N(\frac{m}{2\pi kT})^{3/2} \exp(-\frac{m v^2}{2kT})\, d^3 v \end{aligned} \tag{2.8}$$

where the total velocity, v, may be calculated from the expression

$$v^2 = |v_x|^2 + |v_y|^2 + |v_z|^2 , \tag{2.9}$$

and where T is the temperature, k is Boltzmann's constant and N is the total number of particles.

The Maxwell-Boltzmann distribution is characterized by an exponential decrease in the number of particles at elevated velocities at a given temperature. At sufficiently high temperatures, a significant fraction of the particles in the high velocity or high energy tail will reach energies for which nuclear fusion is highly probable. This thermonuclear approach is more efficient than energizing all particles to energies required to overcome the fusion barrier.

The reaction rate of the fusion reaction characterized in Eq. 2.1 is calculated from

$$R_{fusion} = \int_{v_b}\int_{v_a} \sigma(|v_a - v_b|)\,|v_a - v_b|\,N_a(v_a)\,N_b(v_b)\,d^3v_a\,d^3v_b \tag{2.10}$$

where v_a and v_b are the total velocities of reactants a and b respectively and $N_a(v_a)$ and $N_b(v_b)$ are the velocity distributions of the reacting particles. In calculating the thermonuclear fusion reaction rate, the particle distribution part of the integral in Eq. 2.10, uses the Maxwell-Boltzmann distribution and becomes

$$N_a(v_a)\,N_b(v_b)\,d^3v_a\,d^3v_b = N_a N_b \frac{(m_a m_b)^{3/2}}{(2\pi kT)^3} \exp\left(-\frac{m_a v_a^2 + m_b v_b^2}{2kT}\right) d^3v_a\,d^3v_b . \tag{2.11}$$

The reaction rate expression in Eq. 2.10 can be converted to a centre of mass frame by using the following transformations:

$$v_a = V_{cm} + \frac{m_b}{m_a + m_b} v_{ab} \tag{2.12}$$

and

$$v_b = V_{cm} - \frac{m_a}{m_a + m_b} v_{ab} \ , \tag{2.13}$$

where V_{cm} is the velocity of the centre of mass and

$$v_{ab} = v_a - v_b \tag{2.14}$$

is the relative velocity of particles a and b.

Substituting Eq. 2.12 and 2.13 into Eq. 2.11 yields

$$N_a(v_a)\, N_b(v_b)\, d^3v_a\, d^3v_b$$

$$= N_a N_b \frac{(m_a m_b)^{3/2}}{(2\,\pi\, kT)^3} \exp\left(-\frac{(m_a + m_b)\, V_{cm}^{\,2}}{2\,kT} - \frac{M_{ab}\, v_{ab}^{\,2}}{2kT}\right) d^3v_a\, d^3v_b \ . \tag{2.15}$$

The integration over the velocity distributions v_a and v_b in Eq. 2.10 is transformed to an integration over dV_{cm} and dv_{ab} using the following relation:

$$d^3v_a\, d^3v_b = d^3V_{cm}\, d^3v_{ab} \ , \tag{2.16}$$

evaluated by the associated Jacobian determinant. The fusion reaction rate integral of Eq. 2.10 can now be integrated over the centre of mass velocity and the relative velocity separately, yielding

$$R_{fusion} = N_a N_b \int_{V_{cm}} \left(\frac{m_a + m_b}{2\,kT}\right)^{3/2} \exp\left(-\frac{(m_a + m_b)\,V_{cm}^2}{2\,kT}\right) d^3 V_{cm} \times \int_{v_{ab}} \sigma(v_{ab})\, v_{ab} \left(\frac{M_{ab}}{2\,kT}\right)^{3/2} \exp\left(-\frac{M_{ab}\, v_{ab}^2}{2kT}\right) d^3 v_{ab} \,. \tag{2.17}$$

Since a normalized Maxwell-Boltzmann distribution was used, the integral over the centre of mass velocity reduces to

$$\int_{V_{cm}} \left(\frac{m_a + m_b}{2\,kT}\right)^{3/2} \exp\left(-\frac{(m_a + m_b)\,V_{cm}^2}{2\,kT}\right) d^3 V_{cm} = 1 \tag{2.18}$$

and because the velocity distributions are assumed isotropic, the volume of velocity space for which the relative velocity between particles v_{ab} is constant is defined by the shell volume $4\pi\, v_{ab}^2\, dv_{ab}$ and thus,

$$d^3 v_{ab} = 4\,\pi\, v_{ab}^2\, dv_{ab} \,. \tag{2.19}$$

Using the expression for the total energy of a collision between particle a and particle b,

$$E = \frac{1}{2}\, M_{ab} v_{ab}^2 \,, \tag{2.20}$$

the fusion reaction rate can now be represented by

$$R_{fusion} = \langle \sigma v \rangle_{ab}\, N_a N_b \,, \tag{2.21}$$

where $\langle \sigma v \rangle_{ab}$, the "sigma-vee" of the fusion reaction of nuclei a and b, evaluated from Eqs. 2.17 - 2.20, is

$$\langle \sigma v \rangle_{ab} \sim \left(\frac{8}{\pi\, M_{ab}}\right)^{1/2} \frac{S_o}{(kT)^{3/2}} \int \exp\left(-\frac{E}{kT} - \frac{B}{\sqrt{E}}\right) dE \,. \tag{2.22}$$

The factor S(E) is only slightly dependent on energy and it can be assumed that $S(E) \approx S_0$.

2.1.3 Thermonuclear Fusion Fuels

Candidate fuels for first generation fusion energy systems are deuterium alone (^{2}H, D or d), deuterium with helium 3 (^{3}He or h) or deuterium with tritium (^{3}H, T or t). These fuels are characterized by the reactions listed in Table 2.1. The sigma-vee values of the fusion reactions involving these fuels can be calculated using a semi-empirical version of the expression in Eq. 2.22. Peres has developed such a model based upon a Pade expansion that yields very accurate values for a temperature range $T = 0 \rightarrow 100$ keV (Ref. 20). The parameters in Table 2.1 were used with this model,

$$\langle \sigma v \rangle = S_0 c \theta \sqrt{\frac{32\zeta}{3(mc^2)T^3}}\, e^{-3\zeta}, \tag{2.23}$$

where

$$\theta = T\left(1 - T\frac{P_2 + TP_4 + T^2P_6}{1 + TP_3 + T^2P_5}\right) \tag{2.24}$$

and

$$\zeta = \left(\frac{B^2}{4\theta}\right)^{1/3}, \tag{2.25}$$

to calculate sigma-vee values for the main fusion fuels.

Figure 2.2 clearly shows a 50%-50% deuterium-tritium mixture requires the lowest temperatures to obtain significant thermonuclear fusion reaction rates. Deuterium and D-^{3}He (50%-50% mixture) fusion fuels will require much higher temperatures for comparable fusion reaction rates. Therefore, deuterium-tritium fuel is the choice for the first generation fusion reactors. All

Reaction	$^3H(d,n)^4He$	$^2H(d,n)^3He$	$^2H(d,p)^3H$	$^3He(d,p)^4He$
mc^2 (keV)	1 124 656	937 814	937 814	1 124 572
S_0c	2.907161E-10	1.652735E-12	1.833600E-12	1.781357E-10
P_2	2.818421E-2	3.328985E-3	2.543079E-3	8.681070E-3
P_3	6.116184E-2	2.948735E-3	2.216964E-3	1.010217E-3
P_4	2.834474E-3			-3.516677E-6
P_5	8.955113E-3			3.671273E-4
P_6	-5.734052E-5			

Table 2.1 : Fusion cross-section parameters used in the models of Peres[29] for the fusion reactions of interest.

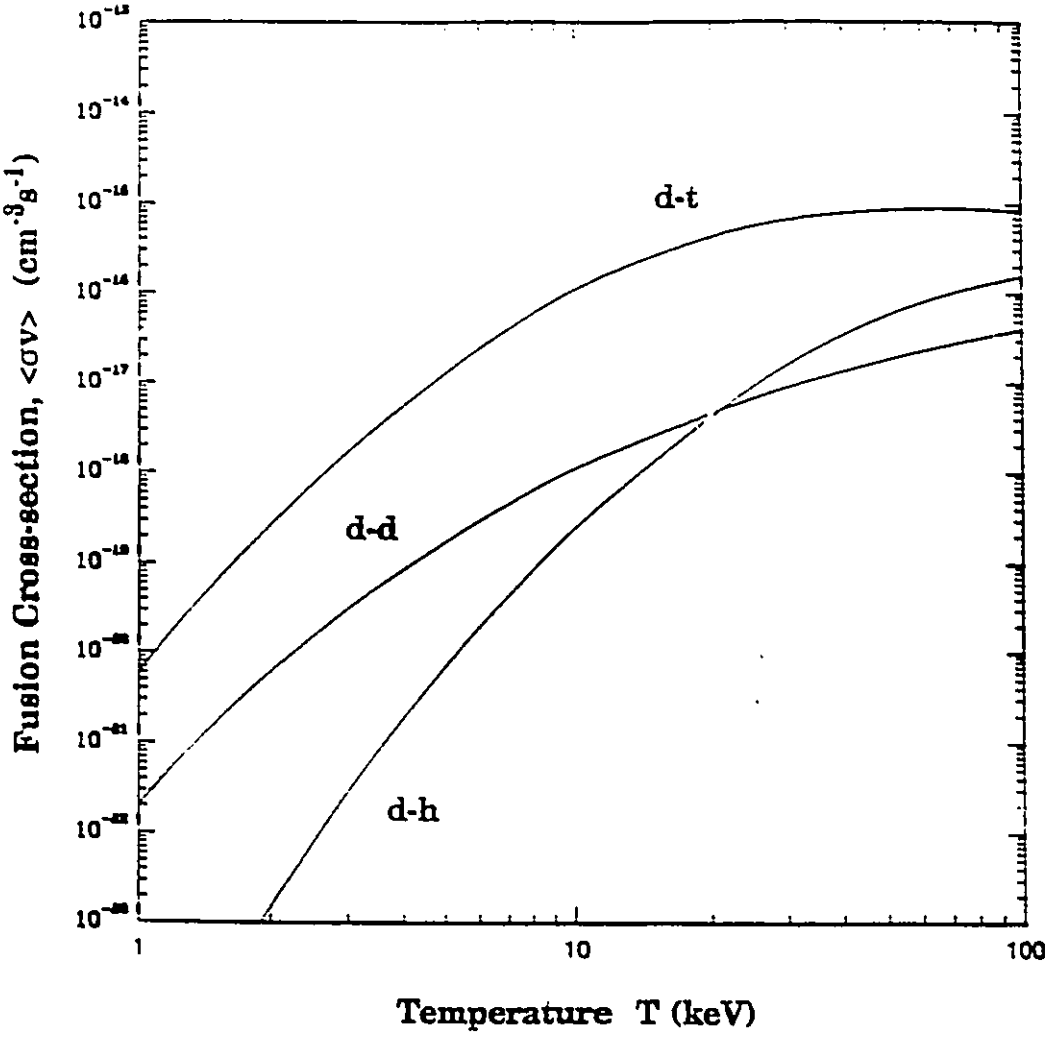

Figure 2.2 : The <σv> values for deuterium-tritium, deuterium and deuterium-^{3}He using the Peres models[20]. (Note: d - ^{2}H, t - ^{3}H, h - ^{3}He)

further references to deuterium-tritium fuel denote a 50%-50% mixture.

Once fusion temperatures are attained, the key issues in a thermonuclear approach to nuclear fusion are containment of heated fusion fuel for sufficient time periods for energy multiplication, and also extraction of the generated energy. Further discussions of these issues follow in Section 2.2 on Fusion Energy System Concepts and also in Section 2.3 on Inertial Confinement Fusion. Meanwhile, a second approach to overcoming the Coulomb barrier in order to initiate nuclear fusion will be pursued.

2.1.4 Catalyzed Nuclear Fusion

The Coulomb barrier may be overcome by placing an intervening particle between the two nuclei which will screen one positive charge. The screening particle reduces the repulsion between the two nuclei such that the separation distance reduces to where quantum mechanical tunnelling of the Coulomb barrier and subsequent fusion becomes highly probable. An example of a screening particle is a negative muon which has the same charge as an electron but has 207 times the mass[21,22] thus the Bohr radius of the muon ground state is approximately

$$a_\mu \sim \frac{a_e}{207} \tag{2.26}$$

where a_e is the electronic Bohr orbit radius.

As a muon has a single negative charge, it is only effective in screening nuclei with unit atomic number. Whereas it is theoretically possible to have two or more muons involved in a fusion reaction of nuclei with Z greater than 1, the rarity and expense of muons makes such interaction unrealistic.

Other negatively charged particles such as heavy mesons and baryons have been considered as possible candidates for catalyzing fusion, however the muon has been shown to be the only negatively charged particle with the required heavy mass, long-life, and inertness with respect to the reactants[23-24].

A muon can induce a fusion reaction in two ways. Firstly, a muo-atom, for example a muo-triton, μt, in which the electron is replaced with a muon, induces the following "direct" fusion reaction,

$$\mu t + d \rightarrow {}^4He + n + \mu + 17.6\,MeV\,. \tag{2.27}$$

Secondly, a muo-triton and deuteron initially form the muo-molecular ion μdt which has an analogous structure to the H_2^+ molecular ion. Fusion occurs within the molecular state according to the reaction,

$$\mu dt \rightarrow {}^4He + n + \mu + 17.6\,MeV\,. \tag{2.28}$$

It will be shown that the rates of the two muon induced fusion reactions are related, based upon the following discussion muo-molecular fusion.

2.1.4.1 Muo-Molecular Fusion

In muo-molecular fusion, the overall fusion rate is limited by the formation rate of the muo-molecular ion, but the essential rate limiting step is fusion within the muo-molecular ion. Figure 2.3 illustrates the potential energy between the nuclei in a muo-molecule where the molecular state allows a close approach of deuterium and tritium in the ground state of the muo-molecule. The separation distance between deuterium and tritium within the ground state μdt muo-molecule will be

$$r_{\mu dt} \approx 2\,a_\mu \approx \frac{2\,a_e}{207} \approx 500\,fm\,. \tag{2.29}$$

At this distance, the fusion rate within a muo-molecule is

$$\lambda_{fusion}^{molecular} = A|\Psi(0)|^2 \qquad (2.30)$$

where A is a constant representing the strong nuclear force component of the reaction and $\Psi(0)$ is the muo-molecular wave function at the interaction distance expressed as

$$|\Psi(0)|^2 \approx \frac{1}{4\pi a_\mu^{\,3}} \exp(-p_b) . \qquad (2.31)$$

The ground state fusion reaction rate for the μdt^* muo-molecule is predicted as $\lambda_{fusion}(\mu dt) \approx 10^{12}$ s^{-1} (Ref. 25) using $A \approx 2 \times 10^{-14}$ cm^3/s and $p_b \approx 9.5$.

The fusion reaction rate formula in Eq. 2.30 presumes that the muo-molecule is in the ground state. However, muo-molecules involving two hydrogen isotopes have the highest probability to form initially in the J=1 rotational state and v=1 vibrational state. Fusion from this state is complicated by the centripetal force experienced by the muo-molecule. Therefore, decay to the J=0 state is required for fast fusion rates. For the μdt muo-molecular ion, decay to the rotational ground state by collision induced or radiative excitation is rapid, indeed greater than 10^{12} s^{-1} at Liquid Hydrogen Density (LHD). For symmetric muo-molecular ions such as μdd and μtt, a $\Delta J = \pm 1$ transition is forbidden by the Pauli Exclusion Principle and nuclear fusion must occur in the J=1 state which has a relatively slow fusion rate. The observed values of the fusion rates for the possible muo-molecular ions are[25,26]:

$$\lambda_f(\mu dd) \approx 4.3 \times 10^8 \text{ s}^{-1},$$
$$\lambda_f(\mu dt) \approx 1.2 \times 10^{12} \text{ s}^{-1},$$
$$\lambda_f(\mu tt) \approx 1.5 \times 10^7 \text{ s}^{-1}.$$

The muon is not consumed in the fusion reaction and may initiate further fusions, yielding a catalyzed chain of reactions. An unfortunate limitation of the effectiveness of the muon catalyzing ability is the life-time of the muon in the reaction chain. The muon is radioactive with a half-life of $\tau_\mu \approx 2.2\ \mu s$, and decays into an electron, a neutrino and an anti-neutrino,

$$\mu \rightarrow e + \nu_\mu + \bar{\nu}_e \,. \tag{2.32}$$

With a single muon energy cost of about 4 GeV (see Section 4.2 Muon Production Concepts), the muon must "catalyze" many fusions in order to pay for its existence. Accordingly, the fastest possible fusion rate is desired. This has been demonstrated to occur for deuterium-tritium fuel. However, it is also critical to determine if the μdt muo-molecular ion formation reaction rate, and all prior processes leading to it, are sufficiently fast to yield economically acceptable catalyzed fusion chain lengths.

The highest muo-molecular ion formation rates occur when the difference between the binding energy of the muo-atom and the subsequently formed muo-molecular ion is lowest. As a guideline the muo-molecular formation rate will follow,

$$\lambda_{formation} \propto e^{k/\Delta\varepsilon} \,, \tag{2.33}$$

where $\Delta\varepsilon$ represents the energy difference between the muo-atom and the muo-molecular ion[27] and k is a constant.

Table 2.2 lists the binding energy differences for the muo-molecular ions possible in deuterium-tritium fuel at the various spin states J, and vibrational states v. From Table 2.2, the hierarchy of energy differences in deuterium-tritium fuel is: μdt_{11} formation from the ground state μt_1, μdd_{11} formation from the ground state μd_1 and μtt_{11} formation from the ground state μt_1 with

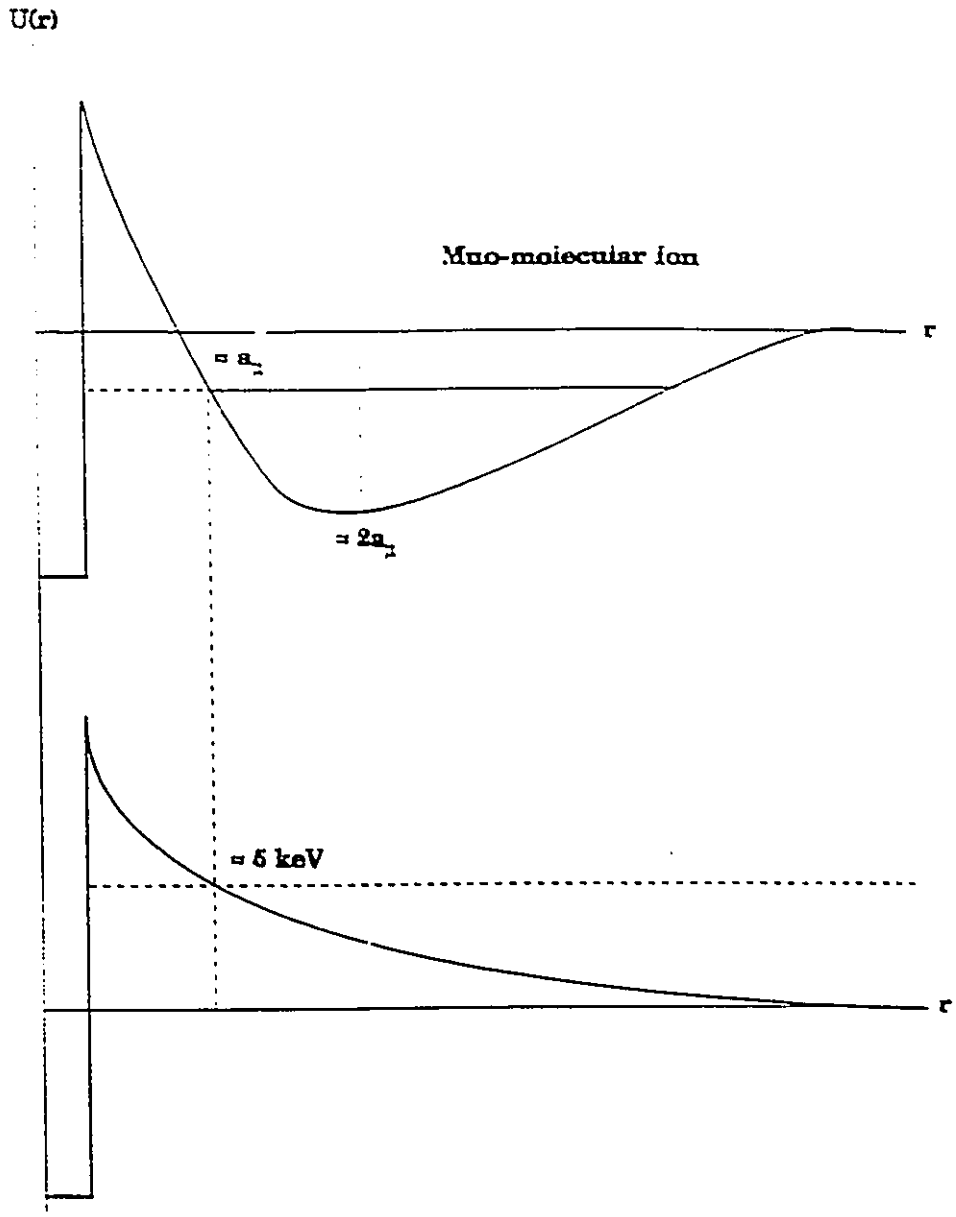

Figure 2.3 : Depiction of the attractive and repulsive forces between two hydrogen nuclei in a muo-molecule contrasted to the normal Coulomb repulsion and strong force attraction (see Fig. 2.1). The minimum at $r \approx 2a_\mu$ is the approximate size of a two hydrogen muo-molecule and the distance of closest approach of about a_μ corresponds to an effective temperature of about 5 keV.

binding energy differences of -0.66 eV, -1.98 eV and -45.2 eV respectively[26]. All other muon and hydrogen isotope pairs have much larger binding energy differences. From Eq. 2.33, the μdt_{11} formation rate will far exceed all others, thus only muon catalyzed fusion processes leading to μdt_{11} formation need be considered.

2.1.4.2 Direct Muon Fusion

Returning to the first route to muon induced fusion, as shown in Eq. 2.27, the rate of direct fusion involving a muon can be approximated by

$$\lambda_{fusion}^{Inflight} \sim \left(\frac{a_\mu}{a_e}\right)^3 \phi \, \lambda_{fusion}^{molecular}, \tag{2.34}$$

where ϕ is the local fuel density with respect to liquid hydrogen density (LHD) and the temperature is less than 5 keV (Ref. 25). Substituting the molecular fusion rate, the direct fusion rate is

$$\lambda_{fusion}^{Inflight} \sim 1.13 \times 10^5 \, \phi \quad (s^{-1}). \tag{2.35}$$

Considering the muon's decay rate of $\lambda_\mu \approx 4.5 \times 10^5 \, s^{-1}$, it is apparent that the utility of the direct fusion mechanism is limited unless very large fuel densities are considered.

If all processes leading to muon induced fusion have sufficiently fast rates, either through the muo-molecular or the direct process, it is possible that many fusion reactions can be "catalyzed" and a great deal of energy can be generated in the muon catalyzed chain before the muon decays. There are other factors involved in the muon catalyzing chain length and these issues are discussed in future sections of this work.

	J_v					
Molecular Ion	00	01	10	11	20	30
μdd	325.074	35.844	226.68	1.975	86.434	-
μdt	319.140	34.834	232.47	0.660	101.416	-
μtt	362.910	83.771	289.142	45.206	172.652	48.813

Table 2.2 : The binding energy differences in eV, between μd_1 and μdd_{J_v}, μt_1 and μdt_{J_v} and μt_1 and μtt_{J_v} (Ref. 26).

2.2 Fusion Energy System Concepts

This section elucidates some of the requirements of a generalized fusion energy system with the intent of developing energy gain expressions for the thermonuclear approach, focusing on the ICF concept, and also for the catalyzed fusion approach, concentrating on the μCF concept. Deuterium-tritium will be the only fusion fuel considered, as it is the optimal fuel for both the μCF and the ICF approaches.

2.2.1 General Fusion System Energy Balance

The fundamental goal of fusion energy system development is to create an environment where fusion reactions occur in a safe, controllable manner and where more energy is created than is used to generate the necessary environment. Figure 2.4 illustrates a schematic of a generalized fusion energy system. The core element of the energy system is the volume of fusion fuel in which fusion power P_{fusion} is generated and includes energy created in a surrounding breeding blanket. The vicinity around the fusion fuel volume is referred to as the reactor in Fig. 2.4 and encompasses all processes and materials necessary to sustain the fusion fuel in a configuration conducive to nuclear fusion. This necessary environment for fusion is initiated and sustained by the driver system which provides a power P_{driver} to the reaction domain. The efficiency for which the driver can create the fusion environment is expressed as η_d.

The power that exits the reactor, expressed as $P_{reactor}$, includes the fusion power created as well as the driver power deposited into the fusion environment. As depicted in Fig. 2.4, this exiting energy flow is directed to an energy conversion system and converted to a useable form (i.e. electricity).

Some fraction of this energy is diverted to the driver system. The efficiency of energy conversion of the reactor energy to electricity, η_c, will primarily involve thermal conversion of energy deposited into a reactor coolant. In order to maximize the overall system output, the waste energy from the driver is routed to the energy conversion system and thus partially recovered. This power recovery will be incorporated into the term $P_{reactor}$.

Accounting for the energy flows depicted in Figure 2.4, the net energy out can be expressed as

$$E_{out}^{net} = \eta_c \int_0^{\tau_r} P_{reactor}(t)\,dt - \frac{1}{\eta_d}\int_0^{\tau_r} P_{driver}(t)\,dt\,, \qquad (2.36)$$

where τ_r is the reaction duration and $P_{reactor}(t)$ is the power released by fusion reactions, breeder blanket reactions, the driver power deposited into the fusion fuel and also the waste energy from the driver, i.e.,

$$P_{reactor}(t) = P_{fusion}(t) + P_{driver}(t) + \frac{(1-\eta_d)}{\eta_d} P_{driver}(t)\,. \qquad (2.37)$$

The initial fusion power, P_{fusion}, contains a factor M_{dt}, where M_{dt} is a measure of the deuterium-tritium fusion energy multiplication in a surrounding blanket.

Defining the energy gain as the ratio of the total energy out of the reactor to the total energy injected into the reactor yields

$$G = \frac{\eta_c \int_0^{\tau_r} P_{reactor}(t)\,dt}{\frac{1}{\eta_d}\int_0^{\tau_r} P_{driver}(t)\,dt} = \eta_c\left(\eta_d \frac{\int_0^{\tau_r} P_{fusion}(t)\,dt}{\int_0^{\tau_r} P_{driver}(t)\,dt} + 1\right), \qquad (2.38)$$

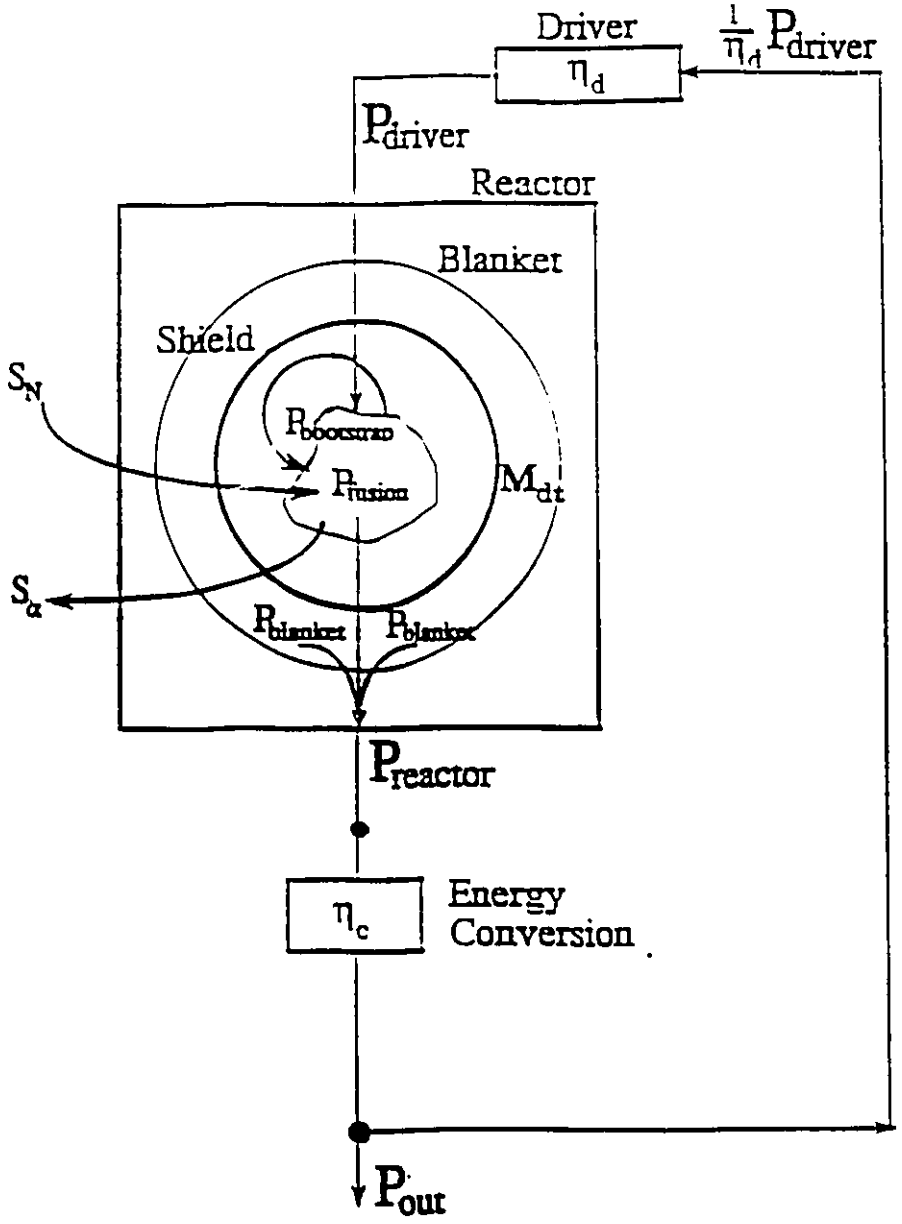

Figure 2.4 : Schematic of the energy and material flows in a generic fusion energy system. Here $P_{reactor}$, P_{driver}, $P_{blanket}$, P_{fusion} and P_{out} represent power flows.

and thus the net energy out of the reactor system can be reduced to the expression

$$E_{out}^{net} = (G - 1)\frac{\int_0^{\tau_c} P_{driver}(t)\,dt}{\eta_d}. \qquad (2.39)$$

It is obvious from the above analysis that a viable energy system must have an energy gain, G, much greater than unity. The estimate of the energy gain of a conceptual fusion energy system will be the focal point of the system viability evaluation. Concepts relevant to the energy gain calculation of a thermonuclear fusion system and a catalyzed fusion system will next be examined, stressing the key elements for viability assessment.

2.2.2 Thermonuclear Fusion Energy Balance

In order to calculate the thermonuclear fusion energy balance and energy gain, we consider a reaction domain in which a volume of deuterium-tritium fuel of density N is heated by a driver to a temperature such that thermonuclear fusion reactions are appreciable. The following energy flows are important:

1. The driving energy which creates and sustains the thermonuclear environment during the reaction duration τ_r.
2. The fusion energy produced.
3. The fusion energy deposited within the deuterium-tritium fuel, which is referred to as bootstrap heating.
4. Energy losses due to escaping radiation emissions.

Expressions for each of the above processes will be examined individually for

the case of deuterium-tritium fuel. Since our interest is specifically in the Inertial Confinement Fusion approach to thermonuclear fusion, the following conditions will apply:

1. No fuel replenishment or ash removal during the reaction duration (in Fig. 2.4, S_N=0 and S_α=0).
2. Radiation losses only by bremsstrahlung emission.
3. Compression of deuterium-tritium.

2.2.2.1 Driving Energy

In order to initiate thermonuclear fusion, very high ion temperatures are required. We refer to "ion" temperatures because at thermonuclear temperatures deuterium-tritium will be in a plasma state and the ion and the electron temperatures may be different. Laser energy, ion beam energy and fusion reaction product energy will deposit energy preferentially to electrons in lower temperature plasmas (T < 10 keV), however the fusion reaction rate depends upon the ion temperature. The energy deposition fraction will depend upon the local ion and electron temperatures, the local density and the mode of energy deposition. In a plasma, the ion temperature T_i and the electron temperature T_e have the following relationship:

$$\frac{dT_e}{dt} = \frac{T_e - T_i}{\tau_{ie}} . \tag{2.40}$$

The electron-ion collision characteristic time may be calculated as[28]

$$\tau_{ie} = \frac{3 m_e m_i}{8\sqrt{2\pi}\, N e^4 \ln\Lambda} \left(\frac{T_e}{m_e}\right)^{3/2} \sim 100 \frac{T_e^{3/2}}{\phi} \ (ps) \tag{2.41}$$

where m_e is the electron mass, m_i is the ion mass (i.e., the average mass of deuterium and tritium), e is the electron charge , lnΛ is the Coulomb logarithm, N is the density of ions and ϕ is the ion density with respect to LHD.

For relevant initial thermonuclear temperatures (T < 10 keV) and ICF densities (ϕ > 1000 LHD), ion-electron equilibrium occurs rapidly, with $\tau_{ie} <<$ 1 ns. Due to this rapid transfer time at lower temperatures and because energy is deposited more directly to ions at higher temperatures, it is reasonable to assume that the electron and ion temperatures are approximately equivalent in ICF environments and therefore, from here on, only one temperature for both electrons and ions, T, is used.

Fusion systems may be "driven" or "ignited". In a driven system, the fusion driver must deposit energy into the reaction domain during the fusion reaction period. An ignited fusion system is a system which only requires an initial energy injection from the driver. Thereafter, energy from the fusion reactions result in bootstrap heating, which keeps the reaction environment sufficiently hot to continue the fusion burn. The temperature for which this is true is known as the ignition temperature T_{ign}. An ICF energy system is inherently an ignited system and the driver is required to give the following initial energy to the fusion fuel,

$$E_{driver} = E_{compression} + E_{kinetic} \tag{2.42}$$

Here, $E_{compression}$ represents the energy required to compress the fuel and $E_{kinetic}$ is the required kinetic energy of the fusion fuel given by

$$E_{kinetic} = 3kTNV \tag{2.43}$$

where T exceeds the ignition temperature, N is the fuel number density and V is the volume of fusion fuel. The efficiency of energy transfer from the driver depends specifically on the heating and compressing mechanisms.

2.2.2.2 Fusion Power and Fuel Burn-up

The thermonuclear fusion power generated in a volume of deuterium-tritium with density N (assuming a 50%-50% deuterium-tritium fuel mixture then $N_d = N_t = N/2$) and temperature T is

$$P_{fusion} = R_{dt} Q_{dt} = \langle \sigma v \rangle_{dt} \frac{N^2}{4} Q_{dt} \tag{2.44}$$

where Q_{dt} is the energy generated per fusion. In general, during the fusion burn phase, the fusion power output will be a function of time, as the fuel will be depleted over time and the burn temperature will vary. To simplify the calculation of the fusion power, it is assumed that the average temperature during the fusion burn is constant and the fusion fuel inventory during the fusion burn can be determined from

$$\dot{N} = S_N - \langle \sigma v \rangle \frac{N^2}{2}, \tag{2.45}$$

where S_N is the replenishment rate of fusion fuel in the reaction domain during the reaction duration. The initial fuel charge is expressed as a multiple ϕ of LHD or N_0, i.e., $N_0\phi = \phi$ LHD. Assuming no fuel replenishment, the temporal depletion of fuel follows from solving Eq. 2.42 yielding

$$N(t) = \frac{N_0 \phi}{1 + N_0 \phi \frac{\langle \sigma v \rangle_{dt}}{2} t}. \tag{2.46}$$

Fuel consumption during the reaction burn period τ_r is calculated as a burn-up fraction,

$$f_{burn} = 1 - \frac{N(t)}{N_0 \phi} = \frac{N_0 \phi \frac{<\sigma v>_{dt}}{2} \tau_r}{1 + N_0 \phi \frac{<\sigma v>_{dt}}{2} \tau_r} . \qquad (2.47)$$

The fusion energy produced during the reaction burn is then

$$E_{fusion} = \int_0^{\tau_r} P_{fusion}\, dt$$
$$= \int_0^{\tau_r} <\sigma v>_{dt} \frac{N(t)^2}{4} Q_{dt}\, dt = f_{burn} N_0 \phi Q_{dt} . \qquad (2.48)$$

While the energy released from a single fusion reaction is Q_{dt} = 17.6 MeV, it is possible to multiple the 14.1 MeV neutron component in a breeding blanket surrounding the reactor. Indeed, the 14.1 MeV neutron is required to breed tritium from lithium. With the use of some neutron multiplication material, sufficient tritium breeding and some energy multiplication can be attained. This process is further discussed in Section 2.2.2 on Tritium Breeding where the multiplication factor, M_{dt}, for Q_{dt} is also described.

2.2.2.3 Bootstrap Heating

A deuterium-tritium fusion reaction produces a 3.5 MeV alpha particle and a 14.1 MeV neutron. Due to collisions with deuterium or tritium nuclei and/or electrons, some or all of the energy of the alpha particle and the neutron may be deposited within the reaction volume of the deuterium-tritium fuel. This process is referred to as bootstrap heating of the fuel and can be used to sustain the high temperatures needed for thermonuclear fusion. The critical issue in fusion energy bootstrapping is that the range of the energetic fusion

particles must be comparable to the reaction domain dimensions. In a deuterium-tritium plasma, the range of the 3.5 MeV alpha particle, r_α, has the following dependence on temperature and density[29],

$$r_\alpha = \frac{\lambda_0}{N} T_{keV}^{3/2}, \tag{2.49}$$

where $\lambda_0 \approx 2 \times 10^{-21}$ cm^{-3} keV$^{-1/2}$. Substituting $N = N_0\phi$ (cm^{-3}) into this expression yields

$$r_\alpha \sim 0.04 \frac{T_{keV}^{3/2}}{\phi} \ (cm), \tag{2.50}$$

where T_{keV} is the temperature in keV. For ICF, this range is sufficiently small, and alpha bootstrap heating plays a significant role.

The mass-mean-free path of a 14.1 MeV neutron in deuterium-tritium is $\rho r_n \approx 4.75$ g/cm^2 (Ref.30) where ρ is the mass density of deuterium-tritium (ρ_{dt}(LHD) ≈ 0.2 cm^{-3}). Thus, the neutron range is

$$r_n = \frac{2.25}{\phi} \ (cm). \tag{2.51}$$

Neutron bootstrap heating is appreciable only if the ρr of the fuel is near ρr_n.

2.2.2.4 Power Losses via Radiation

At thermonuclear temperatures, the fusion fuel will be fully ionized and energy can be lost from this plasma when charged particles, primarily electrons, decelerate through collisions. The decelerating electrons will emit radiation that may not be reabsorbed in the plasma medium and this will cool the plasma. This radiation, called bremsstrahlung radiation, is the principal radiation loss mechanism in a non-magnetized, thermonuclear plasma. Assuming a worst case, in which all bremsstrahlung radiation escapes, the

$$P_{brems} = A_{brems} Z_{eff}^2 N_e N_i \sqrt{T_e} \ \ (\frac{W}{cm^3}) . \qquad (2.52)$$

In this expression, the proportionality constant $A_{brems} = 4.8 \times 10^{-31}$. Z_{eff} is the effective charge, $N_e = Ni = N_0\phi$ is the density in cm^{-3}, and T_e is the electron temperature in keV. The effective charge Z_{eff} is calculated from

$$Z_{eff}^2 = \sum_{j \neq e} \frac{N_j Z_j^2}{N_e} . \qquad (2.53)$$

where N_j and Z_j are the density and charge of ion constituents. It is apparent from the above expressions that material other than hydrogen (i.e. Z > 1) will have much greater bremsstrahlung losses. Evidently, the absence of non-deuterium-tritium impurities in the reaction domain is critical.

2.2.2.5 Ignition Temperature

Ignition of a deuterium-tritium plasma can be obtained when the bootstrap power exceeds the bremsstrahlung radiation losses. Assuming that, at a minimum, all the alpha particles are absorbed, the energy deposition will have a range of $Q_{dep} = 3.5 - Q_{dt}$ and the bootstrap power will be

$$P_{bootstrap} = P_{fusion} \frac{Q_{dep}}{Q_{dt}} . \qquad (2.54)$$

Figure 2.5 displays the normalized bremsstrahlung power and the normalized fusion power in Eq. 2.54 with Q_{dep} = 3.5 MeV and 17.6 MeV, as a function of temperature. Since both the bootstrap power and the bremsstrahlung power depend upon the square of the fuel density (N^2), the powers are normalized by this factor. The intersection points depicted in Fig. 2.5 indicate the ignition temperatures T_{ign} for the deuterium-tritium plasma. At temperatures greater than the ignition temperature, the fusion power

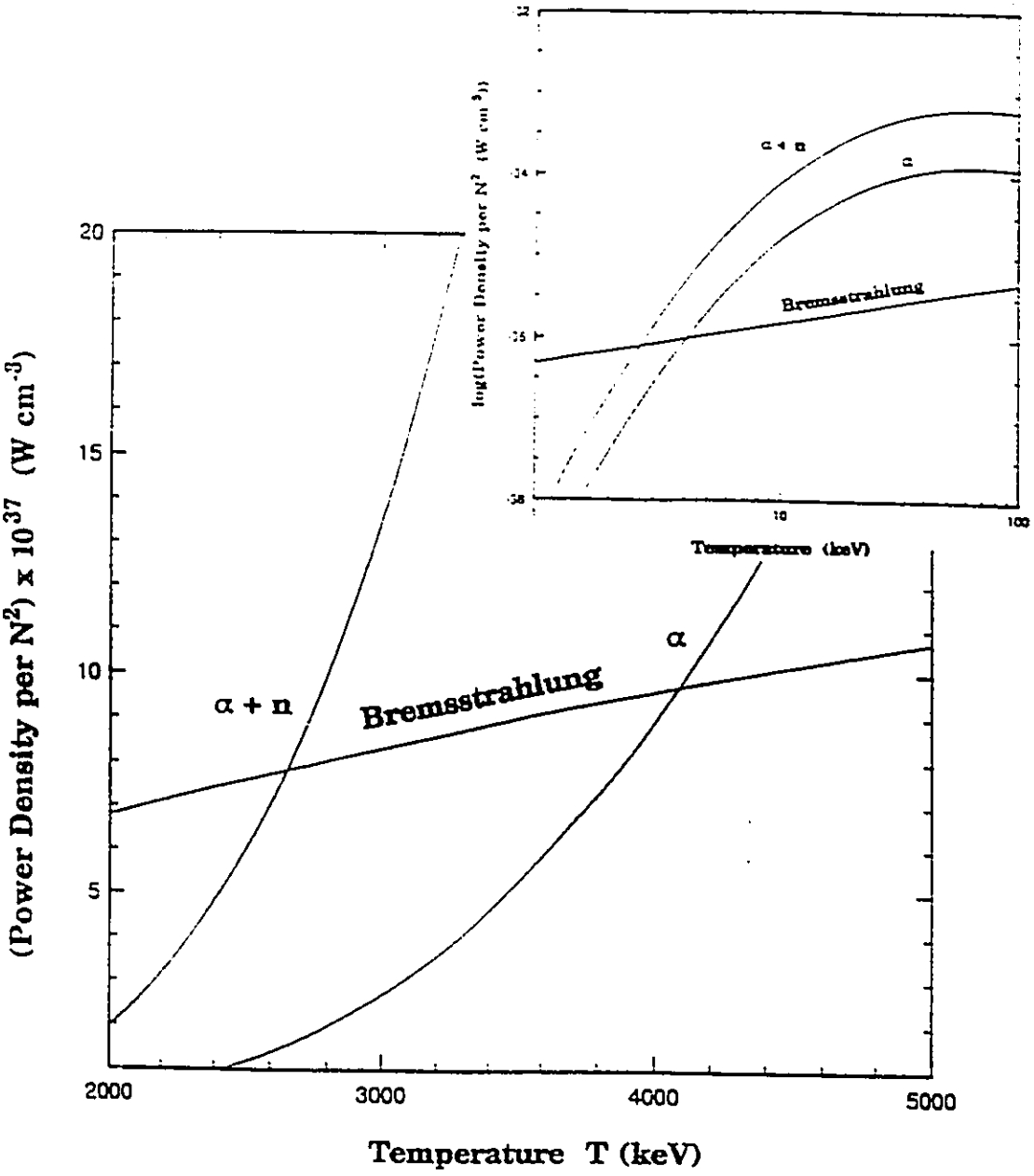

Figure 2.5 : Normalized bootstrap power for 3.5 MeV alpha particles alone and for 3.5 MeV alpha particles with 14.1 MeV neutrons plotted with the normalized bremsstrahlung power in a deuterium-tritium plasma. Curve intersection points represent the ignition temperatures. The powers are divided by N^2 where N is the deuterium-tritium density.

exceeds radiation power losses and the deuterium-tritium plasma is considered self-sustaining. Bootstrapping from alpha particles alone results in an ignition temperature of about 4 keV; if neutrons are also absorbed, the ignition temperature decreases to about 2.5 keV.

2.2.2.6 Lawson Criterion

From analysis of the energy flows in a fusion system, a criterion involving the fusion fuel density and the reaction time at a given temperature can be derived. This criterion, known as the Lawson criterion[31], is useful as a first approximation of the necessary requirements of a fusion energy system. A simplified variation of the derivation of the criterion, is described below.

Initially, energy is injected into a volume of deuterium-tritium fuel to elevate it to a temperature T and a density N. The temperature and density are assumed constant over the reaction time τ_r. The driver energy is simply the $E_{kinetic}$ of Eq. 2.43. We assume that most of this energy is required for fuel heating rather than fuel compression.

Substituting equations 2.43 and 2.48 into the energy gain formula of Eq. 2.38, the following condition emerges for net energy gain:

$$G = \eta_c(\eta_d \frac{Q_{dt} f_{burn}(\phi, T)}{3kT} + 1) > 1 . \qquad (2.55)$$

Lawson made the very optimistic assumption that $\eta_d \approx 1$, and assumed that the value of $\eta_c \approx 1/3$. By rearranging Eq. 2.55 using the fuel burn-up expression in Eq. 2.47, a criterion involving the product of the fuel density and the reaction time $N\tau_r$ for a minimally viable energy system emerges as

$$N\tau_r > f(T) = \frac{3kT(1-\eta_c)}{\eta_c \eta_d \langle \sigma v \rangle_{dt}(T) Q_{dt}} . \qquad (2.56)$$

The minimum of f(T) yields a lower bound for the product $N\tau_r$, referred to as "en-tau" of the fusion fuel. The deuterium-tritium $N\tau_r$ minimum occurs at T ≈ 10 keV and at this temperature it is necessary to have

$$N\tau_r > 10^{14} \left(\frac{s}{cm^3}\right) \qquad (2.57)$$

for an energetically viable system.

The implications of the above inequality can be appreciated when examining a specific approach to fusion energy, for example, a low density plasma confined by a magnetic field. Assuming a density of about 10^{14} cm^{-3}, magnetic confinement is reasonable in volumes needed for sufficient fusion power production, however the confinement time must extend for more than 1 second at a temperature of 10 keV. In this magnetic confinement approach, various plasma instabilities in the low density plasma that disrupt the fusion environment and reduce the confinement time are the prime obstacle to a viable fusion reactor.

At the other $N\tau_r$ extreme lies Inertial Confinement Fusion. Here a small deuterium-tritium pellet is compressed to a density in excess of $N > 10^{26}$ cm^{-3} and the inertia of the fuel itself will confine the fuel long enough that significant fusion occurs. ICF processes are further discussed in Section 2.3, entitled Inertial Confinement Fusion.

2.2.3 Catalyzed Fusion Energy Balance

The other approach to inducing nuclear fusion is via Coulomb screening.

The energy break-even and viable system criteria are different than for the thermonuclear approach. If the catalyzing particle is placed in deuterium-tritium and fusion is initiated, the energy balance is

$$E_{out}^{cat} = \eta_c \int_0^{\tau_c} P_{reactor}(t)\,dt - \frac{1}{\eta_{cat}} E_{cat}, \tag{2.58}$$

where E_{cat} is the average energy required for production of catalyzing particles and η_{cat} is the efficiency with which these particles are created and injected into the reactor. Assuming that the excess energy from the catalyst creation system (i.e. the driver) is recovered and sent to the energy conversion system, the total energy exiting the reactor in a reaction period τ_r is

$$E_{reactor} = E_{fusion} + E_{cat} + \frac{(1 - \eta_{cat})}{\eta_{cat}} E_{cat}. \tag{2.59}$$

For low fuel burn-up or constant fuel replenishment, the fusion power can be determined from

$$\int_0^{\tau_r} P_{fusion}^{cat}(t)\,dt = X_{cat} N_{cat} Q_{dt}, \tag{2.60}$$

where $\tau_r > \tau_{cat}$ (i.e., the lifetime of the catalyst), X_{cat} is the average number of fusions induced by one catalyst, and N_{cat} is the number of catalysts initially introduced. The total catalyst energy cost can be broken down to

$$E_{cat}^{total} = E_{cat} N_{cat} \tag{2.61}$$

where E_{cat} is the average energy cost of a single catalyst. From the above expressions, the catalyzed fusion energy gain becomes

The energy break-even and viable system criteria are different than for the thermonuclear approach. If the catalyzing particle is placed in deuterium-tritium and fusion is initiated, the energy balance is

$$E_{out}^{cat} = \eta_c \int_0^{\tau_c} P_{reactor}(t)\,dt - \frac{1}{\eta_{cat}} E_{cat}, \tag{2.58}$$

where E_{cat} is the average energy required for production of catalyzing particles and η_{cat} is the efficiency with which these particles are created and injected into the reactor. Assuming that the excess energy from the catalyst creation system (i.e. the driver) is recovered and sent to the energy conversion system, the total energy exiting the reactor in a reaction period τ_r is

$$E_{reactor} = E_{fusion} + E_{cat} + \frac{(1 - \eta_{cat})}{\eta_{cat}} E_{cat}. \tag{2.59}$$

For low fuel burn-up or constant fuel replenishment, the fusion power can be determined from

$$\int_0^{\tau_r} P_{fusion}^{cat}(t)\,dt = X_{cat} N_{cat} Q_{dt}, \tag{2.60}$$

where $\tau_r > \tau_{cat}$ (i.e., the lifetime of the catalyst), X_{cat} is the average number of fusions induced by one catalyst, and N_{cat} is the number of catalysts initially introduced. The total catalyst energy cost can be broken down to

$$E_{cat}^{total} = E_{cat} N_{cat} \tag{2.61}$$

where E_{cat} is the average energy cost of a single catalyst. From the above expressions, the catalyzed fusion energy gain becomes

such as Beryllium, which undergoes the (n,2n) reaction,

$$n + {}^{9}Be \rightarrow {}^{4}He + 2n - 1.57\,MeV \qquad (2.65)$$

enhances the tritium breeding ratio. Other (n,2n) materials such as Pb could also be utilized in the blanket. The blanket will also have structural material and will be designed not to interfere with the breeding capability. The high reactivity of lithium with air and water may be avoided by using the molten salt Li_2BeF_4, known as FLIBE, which has been found to have the overlapping qualities of being a good tritium breeding material as well as a safe coolant for a fusion reactor[35,36].

Fusion neutrons entering the breeding blanket will deposit their 14.1 MeV of energy into the blanket and induce reactions in the lithium and beryllium to generate tritium, but will also generate some excess energy. The tritium breeding ratio B_t, the ratio of tritium atoms created per neutron, and the multiplication of the deuterium-tritium fusion neutrons energy M_{dt} will depend upon the specifics of the blanket design. Values for $B_t \approx 1.2$ and $M_{dt} \approx 1.15$ are typical of FLIBE blankets yielding total energy released per fusion of $Q_{dt} \approx 20$ MeV (Ref.35,36).

2.3 Inertial Confinement Fusion

Inertial Confinement Fusion is based on the principle that appreciable fusion reactions will occur when a small spherical deuterium-tritium pellet is compressed to sufficient temperatures and densities by inertial forces. Compression and heating is facilitated by a driver which delivers energy to the pellet. An energy system based upon ICF is inherently pulsed and the driver would be required to fire at a fuel pellet at a rate sufficient to produce the requisite energy for the power plant. Figure 2.6 illustrates a basic ICF energy

system with the following primary components:

1. Deuterium-Tritium Pellet Fabricator and Injection System,
2. Compression Drivers,
3. Blast Chamber,
4. Tritium Breeding Blanket,
5. Coolant System and
6. Energy Conversion Unit.

In an ICF system, energy produced by an exploding fuel pellet after a successful fusion burn, impinges upon a blast protection wall, resulting in deposition of various forms of fusion energy (neutrons, gamma and x-rays, alpha particles, etc.) into the coolant surrounding the blast chamber. The repetition rate, the thermal capacity of the coolant and the energy conversion system would be designed for a steady electrical power output from the turbines.

Thus, the following course of events constitutes a single cycle of an ICF system:

1. A deuterium-tritium pellet descends into the blast chamber.
2. A driver is fired and impinges upon the pellet's surface, compressing and heating the fuel to initiate thermonuclear fusion reactions.
3. Fusion product alpha particles and neutrons deposit energy and sustain the high temperature fusion environment within the pellet.
4. As the pellet disassembles, the debris of the disintegrated fuel pellet hits the blast chamber wall with the consequent

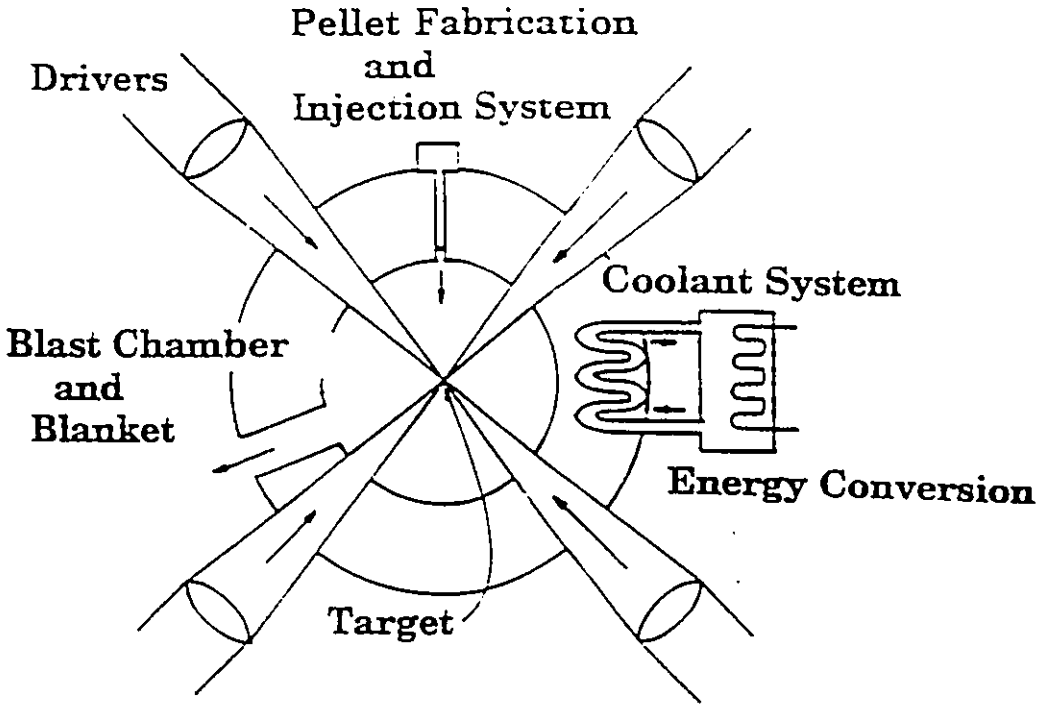

Figure 2.6 : Schematic of an energy system based on the Inertial Confinement Fusion (ICF) concept.

transfer of energy to the energy conversion system, via the coolant system.

5. Neutrons created during the fusion burn penetrate the surrounding lithium blanket, thereby breeding tritium. Neutron energy in the blanket is also transferred to the energy conversion system.
6. All systems are reset and another fuel pellet is injected.

Optimization of the energy gain of an ICF energy system requires study of the conditions for maximal deuterium-tritium pellet burn-up using a minimal amount of driver energy. The important physics issues in ICF technology development are:

1. fusion burn dynamics,
2. high temperature attainment, and
3. high density attainment.

Once an optimal fusion burn dynamic is derived, mechanisms that create the necessary density and temperature environment to initiate such a burn can be developed. Simple fusion burn dynamics are discussed in the following section for the purpose of developing some general conditions for maximum energy gain.

2.3.1 ICF Pellet Burn Schemes

Implosion compression and fusion burn initiation were first developed in the nuclear weapons programs in the US and USSR and it was from these projects that the ICF energy production concept initially sprang[37,38]. However,

much of this early work was classified until the 1970's, when some of the basic fusion burn physics was published and research into civilian applications of fusion began to accelerate.

The following sections will focus upon the derivation of the fuel burn-up fraction in an ICF pellet, which will then be used to calculate the energy gain of an ICF energy system.

2.3.1.1 Fusion Burn of a Free-Expanding Uniform Sphere

At temperatures greater than the ignition temperature, deuterium-tritium fuel is a plasma. A uniformly compressed, ignited, spherical fuel pellet plasma generates a rarefaction wave that moves from the surface towards the pellet's centre. As the rarefaction wave moves inward, the density and temperature of the material emitted from the surface of the pellet quickly decreases and thermonuclear fusion ceases. The rarefaction wave will move at the shock speed of a pressurized medium $u_{s,}$ and the time in which the pellet will entirely disassemble is determined from

$$\tau_r = \frac{r}{u_s}. \tag{2.66}$$

In this equation, r is the radius of the burning deuterium-tritium pellet. The shock speed is related to the pressure within the pellet by

$$u_s = \sqrt{\gamma \frac{P}{\rho}}, \tag{2.67}$$

where P is the local pressure, ρ is the fuel density and γ is determined by the equation of state of the material. It is assumed that the pressure within the material will be determined by a combination of the kinetic pressure of the ions and electrons and the degenerate electron pressure. The shock speed is then determined from

$$u_s = \sqrt{\frac{(\gamma_e + \gamma_i) T}{m_i} + \frac{\gamma_{fermi} P_{fermi}}{\rho}}, \qquad (2.68)$$

where $m_i \approx 4 \times 10^{-24}$ g is the average mass of a deuterium and tritium atom, T is the fuel temperature in energy units (i.e. eV), $\gamma_e=\gamma_i=\gamma_{fermi}=5/3$ and P_{fermi} is the pressure of degenerate electrons[39]. Assuming that the kinetic pressure always dominates the degenerate electron pressure, the shock speed can be expressed as

$$u_s = u_0 \sqrt{T} \qquad (2.69)$$

where $u_0 = 1.1 \times 10^6$ cm/(s $\sqrt{\text{eV}}$) and T is the temperature in eV.

It can be assumed that the temperature within the fuel plasma remains relatively constant during disassembly, provided that the fusion energy deposited by the resultant energetic alpha particles and neutrons offsets the bremsstrahlung radiation losses. Based on these assumptions, the total fusion energy generated by the disassembling sphere of radius r is calculated as

$$P_{fusion}^{total} = V(t) \frac{N(t)}{4} \langle \sigma v \rangle_{dt}(T) Q_{dt}, \qquad (2.70)$$

where the disassembling pellet volume V(t) is

$$V(t) = \frac{4\pi}{3} r(t)^3 = \frac{4\pi}{3} (r - u_s t)^3, \qquad (2.71)$$

N(t) represents the fuel density depletion given by Eq. 2.43.

The total fusion energy generated can then be calculated by integrating the total fusion power from t=0 to the disassembly time at t=r/u_s, yielding

$$E_{fusion} = \int_0^{\frac{r}{u_s}} \frac{4\pi}{3}(r - u_s t)^3 \frac{N(t)}{4} <\sigma v>_{dt}(T)\, Q_{dt}\, dt \qquad (2.72)$$

$$= \frac{4\pi}{3} r^3 \frac{N_0}{2} \frac{\rho r}{A(T)} I ,$$

where

$$I = \frac{1}{4} - \frac{1}{10}\frac{\rho r}{A(T)} + \frac{1}{20}\left(\frac{\rho r}{A(T)}\right)^2 - \frac{1}{35}\left(\frac{\rho r}{A(T)}\right)^3 + \ldots , \qquad (2.73)$$

$$A(T) = \frac{2 m_i u_s(T)}{<\sigma v>_{dt}(T)} , \qquad (2.74)$$

and

$$\rho = N m_i . \qquad (2.75)$$

From Eq. 2.72 the burn-up fraction f_{burn}(ICF), the fraction of deuterium-tritium nuclei that are consumed during a fusion burn, is represented by

$$f_{burn}(ICF) = \frac{\rho r}{A(T)} I . \qquad (2.76)$$

The burn-up fraction can be approximated as

$$f_{burn}(ICF) \sim \frac{\rho r}{\rho r + B(T)} \qquad (2.77)$$

where

$$B(T) = 4A(T) . \qquad (2.78)$$

The expression in Eq. 2.72 is a much better approximation to the fusion burn-up, however Eq. 2.77 is the one generally used in the ICF community and more clearly illustrates the required ρr values for large fuel burn-up. Figure 2.7 displays B(T) from Eq. 2.78 - 2.74, as well as an approximate value calculated from the following expression:

$$\begin{aligned} B(T) &= 10 && T \le 100\,keV \\ &= \frac{T}{5} - 10 && 100\,keV < T < 300\,keV \end{aligned} \tag{2.79}$$

where T is the temperature in keV.

2.3.1.2 Fusion Burn of a Uniform Sphere with a Tamper

The magnitude of B(T) will determine the deuterium-tritium burn-up fraction for a given areal density, ρr, at the operating temperature of the fusion burn. It is possible to reduce the value of B(T) by surrounding the spherical deuterium-tritium pellet with a heavy mass tamper. The tamper is compressed with the deuterium-tritium and retards the disassembly time because of its higher inertia. Considering Eq. 2.67, the magnitude of the reaction time increase can be approximated by

$$\tau_r' = \tau_r \left(1 + \frac{M_{tamp}}{M_{fuel}}\right)^{1/2} \tag{2.80}$$

where M_{tamp} is the mass of the tamper, M_{fuel} is the mass of the deuterium-tritium fuel and τ_r is the disassembly time defined in Eq. 2.66. Considering Eq. 2.78 and 2.74, the value of B(T) with a tamper, $B_{tamp}(T)$, is calculated using

$$B_{tamp}(T) = \frac{B(T)}{\left(1 + \frac{M_{tamp}}{M_{fuel}}\right)^{1/2}} . \tag{2.81}$$

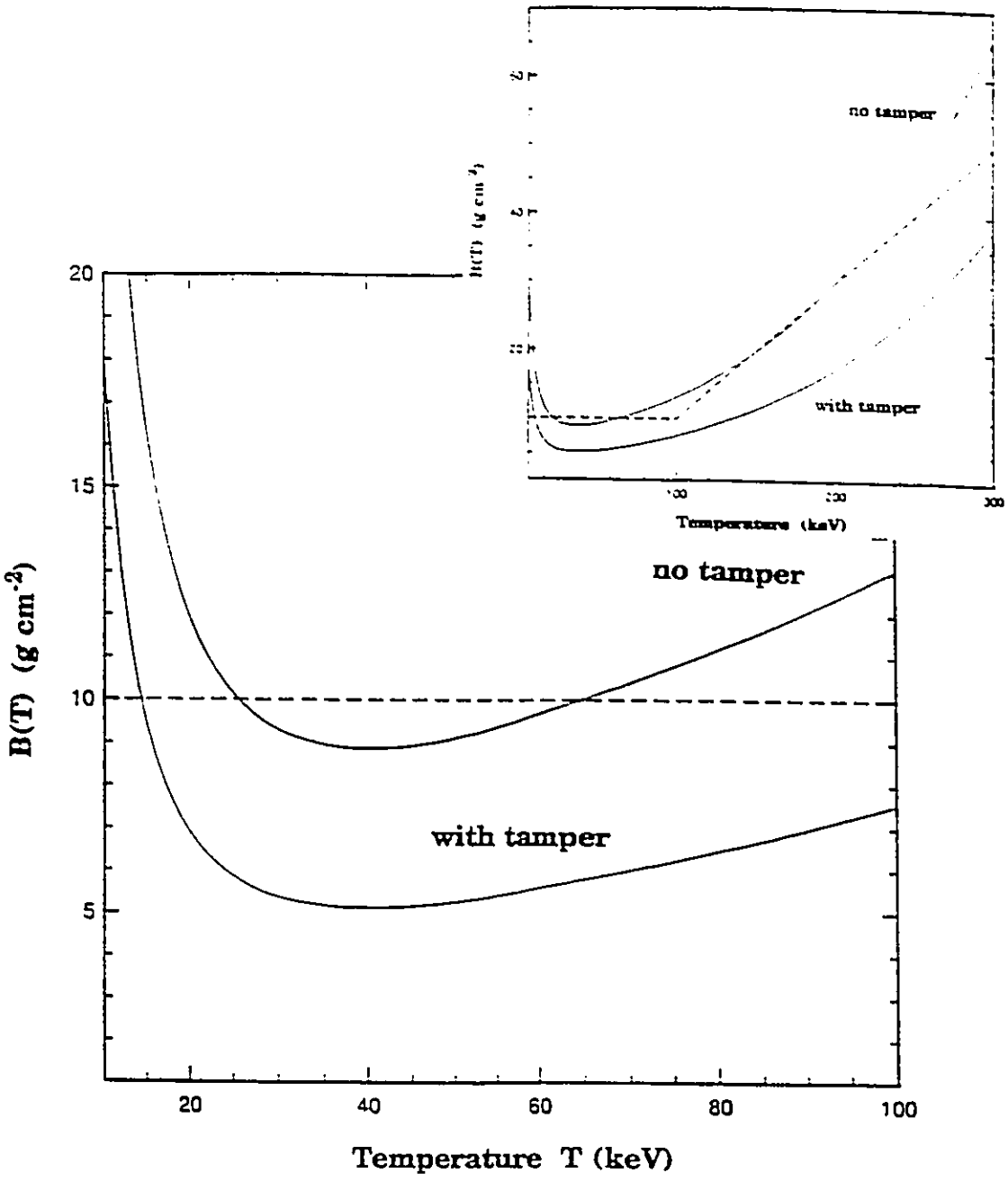

Figure 2.7 : The free sphere burn-up temperature factor B(T) of Eq. 2.78 (solid line), the tamped sphere burn-up temperature factor $B_{tamp}(T)$ of Eq. 2.81 with $M_{tamp}/M_{fuel} = 2$ (solid line), and a simple model of the free sphere burn-up temperature factor given by Eq 2.79 (dotted line) plotted against temperature for deuterium-tritium fuel.

The increase in the energy required to compress the tamper must be justified by a sufficient increase in the fusion burn-up gained by using the tamper. Potential Rayleigh-Taylor instabilities at the interface of the heavy tamper on the light mass fuel volume and degradation of the fusion burn by higher Z impurity cooling are a concern[40,41]. The HIBALL pellet design, a high yield design, can be considered an upper bound of the tamper mass where a value of $M_{tamp}/M_{fuel} \approx 2$ is used[42]. From Fig. 2.7, the HIBALL tamper size yields a minimum value of $B_{tamp}(T) = 6$ g/cm^2.

2.3.1.3 Operating Temperature

In the derivation of the energy generated in a disassembling deuterium-tritium sphere (Eq 2.72), it was assumed that the temperature was uniformly raised beyond the ignition temperature. The ρr dependent energy bootstrapping mechanism which raises the temperature of a just-ignited pellet to the operating temperature T_{op} is discussed in this section. After the relationship between the ρr and T_{op} is established, the ρr dependent fuel burn-up fraction is derived and two methods of attaining the minimum necessary ignition temperature in a deuterium-tritium pellet are outlined.

Consider first a deuterium-tritium sphere uniformly brought to a temperature just slightly greater than the ignition temperature of the pellet. The temperature will rise by bootstrap heating from fusion reaction products and the temperature change rate is given by

$$\begin{aligned} \frac{d}{dt}\left(3\,N(t)\,T(t)\right) &= P_{fusion}^{deposited}(t) \\ &= \langle \sigma v \rangle_{dt}(T(t))\,\frac{N(t)^2}{4}\,Q_{dep}(N(t),T(t)) \end{aligned} \quad , \tag{2.82}$$

where T(t) is the temperature in keV, N(t) is the deuterium-tritium fuel density and Q_{dep} is the fusion particle energy deposited into the deuterium-tritium fuel. In general, the value of Q_{dep} depends upon the range of fusion alpha particles and neutrons; however, due to the much smaller range of the alpha particles, it is assumed that only alpha particles deposit their energy. Thus,

$$Q_{dep} = Q_{\alpha} \frac{r}{r_{\alpha} + r} \tag{2.83}$$

where the alpha range, r_{α}, is determined by Eq. 2.49 and Q_{α} = 3.5 MeV.

The temperature will rise until the range of the alpha particles becomes greater than the pellet size and the energy deposited by the alpha particles will decrease until it is slightly greater than the bremsstrahlung radiation losses. This temperature is referred to as the operating temperature T_{op}. The volume heating would compete with the thermal energy loss which would occur at a rate proportional to the sound speed. The spherical volume effect described by Eq.2.71 results in a total energy residence time which is less than the radial transit time by a factor of approximately 0.25 (see Eq. 2.73). Based on Eq. 2.82, changing the integrand from a time basis to a space basis including the spherical volume effect by using

$$dr = 4\, u_s\, dt \tag{2.84}$$

yields the following expression after integration over the sphere radius,

$$\rho r = 48 \int_{T_{ign}}^{T_{op}} \frac{dT\, m_i\, u_s(T)}{\langle \sigma v \rangle_{dt}(T)\, Q_{dep}(T)} \,. \tag{2.85}$$

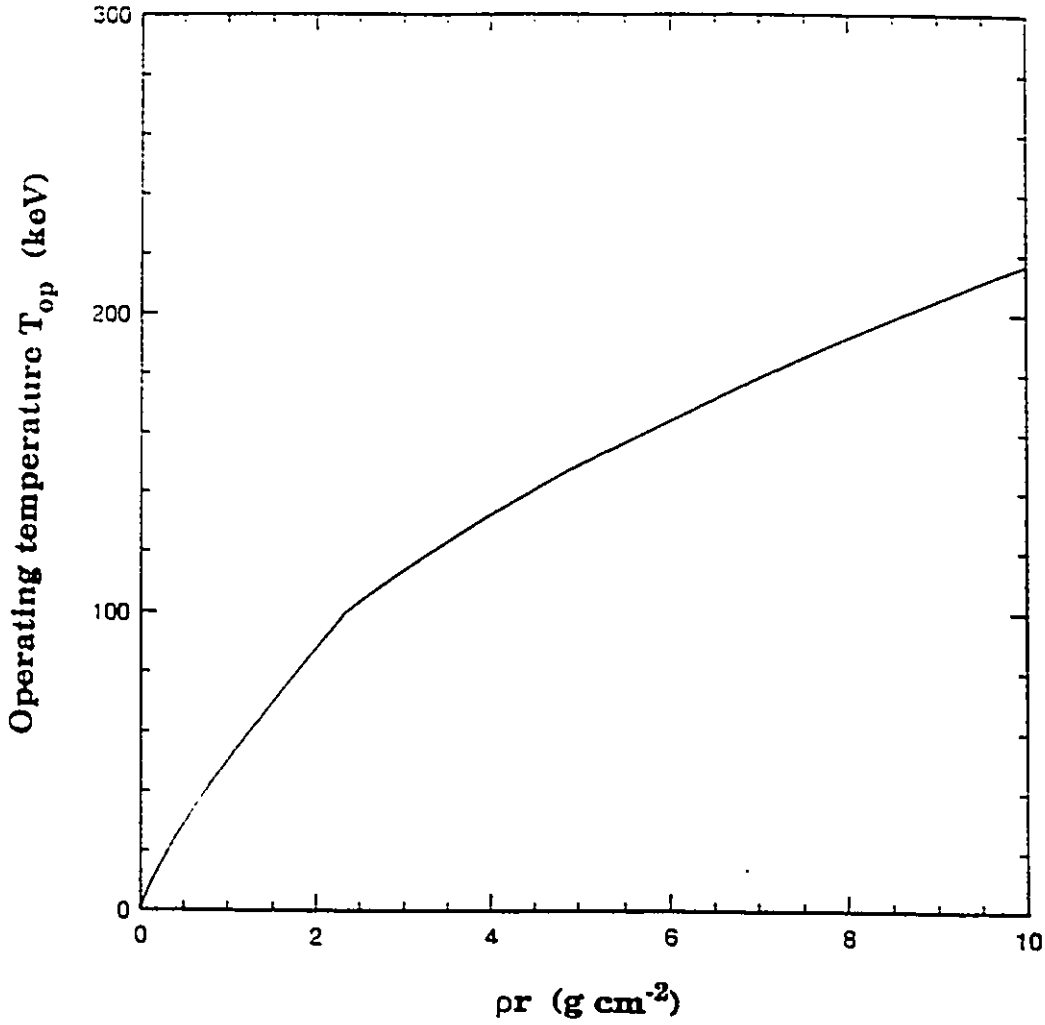

Figure 2.8 : The operating temperature, T_{op}, of an ignited deuterium-tritium sphere versus the areal density, ρr, using the expressions given in Eq. 2.87 and 2.88.

Recognizing B(T) from Eq. 2.78 and 2.74, Eq. 2.85 thus becomes

$$\rho r = \frac{6}{Q_\alpha} \int_{T_{ign}}^{T_{op}} \left(\frac{\lambda_0 m_i T^{3/2}}{\rho r} + 1 \right) B(T)\, dT \qquad (2.86)$$

where $\lambda_0 \approx 2.0 \times 10^{21}$ cm^{-2} keV$^{-3/2}$ and ρr is in g/cm^2. Using the approximation of B(T) in Eq. 2.79, the solution for T_{op} when $T_{op} \leq 100$ keV is

$$T_{op} \sim 50.6\, (\rho r)^{4/5} \quad (keV)\,, \qquad (2.87)$$

and the solution for T_{op} when $T_{op} > 100$ keV is

$$T_{op} \sim 55.6\, (\rho r)^{4/7} + 9.6 \quad (keV)\,. \qquad (2.88)$$

Figure 2.8 displays the operating temperature T_{op} as a function of ρr of the pellet.

The time required for a temperature rise from the ignition temperature to the operating temperature is calculated by

$$t_{VT} = \frac{12}{N_0} \int_{T_{ign}}^{T_{op}} \frac{dT}{\langle \sigma v \rangle_{dt}(T)\, Q_{dep}(T)} \sim \frac{10}{\phi} \ (ns)\,. \qquad (2.89)$$

For densities greater than $\phi \approx 10$ LHD, the assumption that the temperature rise is much more rapid than any appreciable hydrodynamic movement, is sound.

2.3.1.4 Fuel Burn-up

Rearranging Eq. 2.55 and using the ICF fuel burn-up in Eq. 2.77, the ICF Lawson Criterion can be written as,

$$\rho r > \frac{3\, kT(1 - \eta_c)}{\eta_d \eta_c Q_{dt}} B(T)\,. \qquad (2.90)$$

This break-even condition assumes that the heating energy required to sustain a fuel temperature T is provided externally, and no self heating occurs. Due to the assumptions used in the Lawson criterion, Eq. 2.90 is not well-suited to understanding the energy gain of an ICF energy system. Better energy gain models will be discussed in the following sections; however, it is now possible to determine the deuterium-tritium fuel pellet burn-up fraction. Using Eq. 2.77, 2.81, 2.87 and 2.88, the ρr dependent fuel burn-up fraction has been calculated for Fig. 2.9. It may be seen that, after a sharp rise to approximately

$$\rho r \sim 3 \quad (g/cm^2) , \tag{2.91}$$

which corresponds to $T_{op} \approx 120$ keV, the fuel burn-up fraction eventually levels off to $f_{burn} \approx 30$ %. Thus, the optimal areal density of the fuel is near 3 g/cm^2.

2.3.1.5 Fuel Pellet Size and Fuel Compression Requirements

For spherically symmetric compression of a solid fuel pellet, the fuel density is

$$\rho = \rho_0 \phi^3 \tag{2.92}$$

and the pellet radius,

$$r = r_0 \phi^{-1/3} \tag{2.93}$$

where ϕ is the fuel density with respect to LHD, $\rho_0 \approx 0.2$ g/cm^3 is the initial deuterium-tritium density at LHD and r_0 is the initial deuterium-tritium pellet radius before compression. Transforming Eq. 2.91 using Eq. 2.92 and 2.93, the 30 % deuterium-tritium burn-up condition is

$$r_0 \phi^{2/3} > 15 \quad (cm) . \tag{2.94}$$

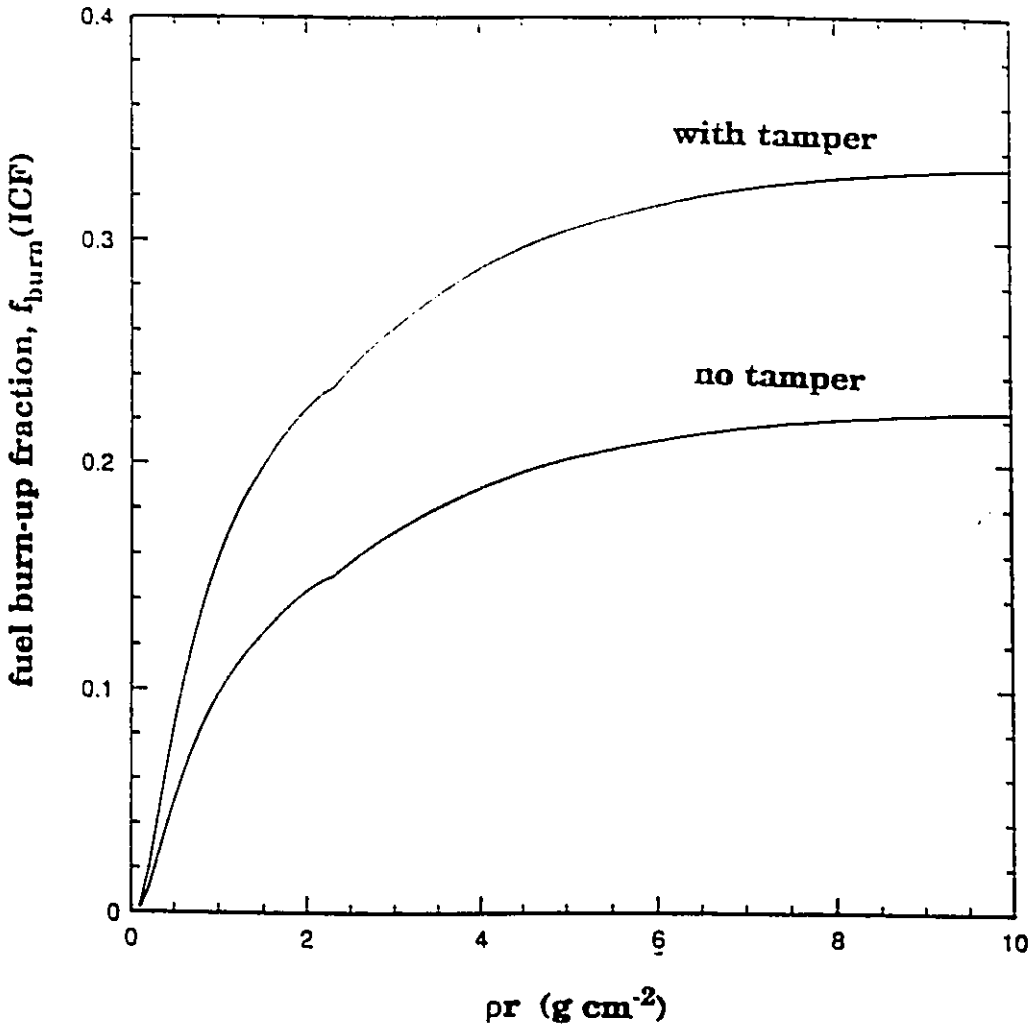

Figure 2.9 : The free sphere and the tamped sphere (M_{tamp}/M_{fuel} = 2) fuel burn-up fractions for deuterium-tritium fuel, f_{burn}(ICF), versus the fuel areal density, ρr.

The total energy generated in a deuterium-tritium pellet during a burn can be expressed as

$$E_{fusion} = \frac{4\pi}{3} r_0^3 \frac{\rho_0}{2 m_i} f_{burn}(ICF)\, Q_{dt} \sim 3.4 \times 10^5\,(MJ)\; r_0^3 f_{burn}(ICF)\,, \tag{2.95}$$

This energy must be limited to that which can be contained within a blast chamber.

The many presently existant blast chamber designs exhibit a variety of approaches to energy containment. A "wetted wall", where liquid metal or molten salt seeps through a porous wall, is appropriate for total fusion yields of less than 100 MJ per pellet burn[43]. The largest fusion yields envisaged would require a "waterfall" of liquid metal or lithium salt to protect the containment structure. Using the waterfall approach, the highest fusion yields judged feasible are about 4000 MJ per pellet burn[44,45]. An energy system using such high yield pellets with a waterfall blast shield could operate at about 1 Hertz and yield the 1000 MW of electrical power, an energy deemed necessary for an economical power plant. Using an upper limit energy yield of 4000 MJ per pellet, the initial pellet radius and the final pellet density are confined to

$$f_{burn}\, r_0^3 \le \frac{1}{82.5} \quad (cm^{-3})\,. \tag{2.96}$$

For fuel burn-up fraction of 30%, r_0 is limited to 4 mm.

2.3.1.6 Volume Ignition

Once the operating temperature exceeds the ignition temperature throughout a deuterium-tritium pellet, the pellet is considered volume-ignited

and the fusion burn dynamic of an uniform sphere applies. The volume ignition approach to ICF requires that a driver initially heats the deuterium-tritium pellet to the ignition temperature and also compresses the pellet to a $\rho r \approx 3$ g/cm^2.

The maximum ignition temperature is 4 keV for alpha particle heating. However, with $\rho r \approx 3$ g/cm^2, neutron bootstrap heating will tend to reduce the ignition temperature, as discussed in Sect. 2.2.2.3. As a first approximation, the neutron heating contribution is ignored and the energy gain of a volume ignited deuterium-tritium pellet is

$$\frac{G_{VI}}{\eta_c \eta_d} = \frac{\frac{4\pi}{3} r_0^3 \frac{N_0}{2} Q_{dt} f_{burn}(ICF)}{\frac{4\pi}{3} r_0^3 3 N_0 T_{ign}} = 220 . \qquad (2.97)$$

While an energy gain of 220 initially appears satisfactory, the maximum efficiency of a heavy ion driver needed to heat the entire pellet to the ignition temperature is about 30%. With a maximum conversion efficiency of 50 %, the gain reduces to $G_{VI} \approx 33$.

This energy gain is still acceptable, but a larger value would be preferable, in view of the ideal conditions assumed. In addition, the energy required by a driver to compress the fuel to high densities was not included in Eq. 2.97. The minimum compression energy, assuming ideal isentropic compression, is approximately the energy of degenerate electrons at the final density (see Section 4.2 : High Density Attainment). It is assumed that a tamper with $M_{tamp} \approx 2 \times M_{fuel}$ is appropriate for 30% fuel burn-up. Assuming that the tamper material electrons and the deuterium-tritium fuel electrons are both degenerate under compression, the energy to compress a given mass

of fuel will be approximately equal to the energy to compress an equivalent mass of tamper material. Therefore, the energy to compress a pellet with $M_{tamp}/M_{fuel} = 2$ may be determined:

$$E_{compression}(tamper + fuel) \sim (1 + \frac{M_{tamp}}{M_{fuel}}) E_{compression}(fuel) \sim 3 E_{compression}(fuel) . \quad (2.98)$$

Based on Appendix B, the degenerate electron compression energy is

$$E_{compression}(fuel) = E_d \phi^{2/3} N \frac{4\pi}{3} r_0^3 . \quad (2.99)$$

The ratio of the energy to compress to density ϕ and the energy to heat to the ignition temperature is

$$R_{VI} \sim 3 \frac{E_d \phi^{2/3} N \frac{4\pi}{3} r^3}{T_{ign} N \frac{4\pi}{3} r^3} = \frac{E_d \phi^{2/3}}{T_{ign}} . \quad (2.100)$$

Using $E_d \approx 5.1$ eV and $T_{ign} \approx 4$ keV yields $R_{VI} < (\phi/10^5)^{2/3}$. Therefore, it can be assumed that, for density enhancements of $\phi < 10^5$ LHD, the energy to volume heat the pellet exceeds the energy to compress, and the volume ignition gain is represented by Eq. 2.97.

2.3.1.7 Spark Ignition

Spark ignition is an efficient method of initiating a fusion burn in a sphere of deuterium-tritium and thus attaining volume ignition[29,37]. This method is analogous to the volume ignition approach in the sense that a solid volume of deuterium-tritium is compressed to a high burn-up ρr value, however, only a small central volume of the pellet is heated to the ignition temperature.

Consider a compressed deuterium-tritium fuel pellet consisting of a small hot region surrounded by a compressed relatively cold region. If the initial spark region temperature is just above the ignition temperature, the temperature there will quickly rise and the increasing fusion alpha particle range in the spark region will cause alpha particles to deposit energy into the surrounding cold material. For successful spark ignition, the proper conditions for propagation of this initial high temperature spark region throughout the whole fuel volume must exist. From this point on the deuterium-tritium pellet will burn in the same way as a volume ignited pellet, however it will have reached this juncture using much less driver energy. A simple calculation to determine the requirements of the initial spark region follows.

The following represents the energy balance in the spark region at the ignition temperature, where the kinetic energy comes from deposited alpha particles,

$$\frac{d}{dt}\left(\frac{4\pi}{3} r_s(t)^3 N_s(t)\, T(t)\right) = \frac{4\pi}{3} r_s(t)^3 P_{fusion}^{deposited}(t) = \frac{4\pi}{3} r_s(t)^3 \langle \sigma v \rangle_{dt}(T(t)) \frac{N_s(t)}{4} Q_{dep}(T(t)) . \tag{2.101}$$

Here r_s represents the radius of the spark region and N is the fuel density in the spark region. In order to simplify the above expression it is assumed that there is low fuel depletion until the volume is ignited, i.e., $N(t) \approx N_0$. It is also assumed that all alpha particles are deposited in the spark region, i.e., $Q_{dep} \approx Q_\alpha$.

The spark region will grow as the range of the alpha particles increases and an ignition wave moves outwards through the pellet with a speed

$$\dot{r}_s = \frac{d}{dt}\left(\frac{\lambda_0 T^{3/2}}{N_0}\right) = \frac{3}{2}\frac{\lambda_0}{N_0}\dot{T}\,T^{1/2} . \qquad (2.102)$$

Substituting Eq. 2.102 into Eq. 2.101, the ratio of the ignition wave speed and the sound speed from Eq. 2.69 is

$$\Omega = \frac{\dot{r}_s}{u_s} = \frac{3}{44}\frac{<\sigma v>_{dt}(T)\,Q_\alpha\,\lambda_0}{u_0} \sim \frac{<\sigma v>_{dt}(T)}{7.3\times10^{-17}} . \qquad (2.103)$$

The initial spark ignition will generate hydrodynamic disturbances, which will eventually meet the rarefaction wave generated by full pellet ignition. If the whole pellet is ignited and quickly reaches the operating temperature T_{op}, the rarefaction wave generated when the ignition wave reaches the outer pellet's surface will be so much more powerful than the oncoming initial spark shocks that the latter becomes negligible. Thus, for maximal fuel burn, the ignition wave speed must be much faster then any spark shock generated and therfore Ω should be greater than 1. At a temperature of $T \approx 15$ keV , $\Omega \approx 2$, which is considered sufficient for successful spark ignition[29]. Spark ignition then depends on the $\rho_s r_s$ value (the areal density of the spark region) that will result in rapid heating of the spark region to 15 keV. Utilizing the previous operating temperature analysis, which culminated in the derivation of Eq. 2.86 - 2.88, the necessary condition for a $\Omega \approx 2$ spark ignition becomes,

$$\rho_s r_s \sim 0.22 . \qquad (2.104)$$

The energy gain of spark-ignited deuterium-tritium pellet is

$$G_{SI} = \eta_c \eta_d \frac{\frac{4\pi}{3} r_0^3 \frac{\rho}{2 m_i} Q_{dt} f_{burn}(ICF)}{\frac{4\pi}{3} r_s^3 3 \frac{\rho_s}{m_i} T_{ign}} \qquad (2.105)$$

$$= (\frac{r}{r_s})^3 \frac{\rho}{\rho_s} G_{VI} \sim (\frac{\rho r}{\rho r_s})^3 G_{VI} .$$

Assuming that the density of the spark region is about the same as that of the remainder of the pellet, using ρr = 3 g/cm^2 for significant burn-up and Eq. 2. 104, a maximum spark ignition energy gain of 10^5 may be calculated.

The ratio of the energy required to compress compared to the energy required to spark ignite is

$$R_{SI} = \frac{3 \frac{4\pi}{3} r^3 \frac{\rho}{m_i} E_d \phi^{2/3}}{\frac{4\pi}{3} r_s^3 \frac{\rho_s}{m_i} T_{ign}} = (\frac{\rho r}{\rho r_s})^3 \frac{3 E_d}{T_{ign}} \phi^{2/3} \qquad (2.106)$$

This equation clearly shows that the energy to compress the fuel and the tamper (assume M_{tamp}/M_{fuel} = 2) dominates. The energy gain is modified to include the energy to compress the pellet and becomes

$$G_{SI}' = \frac{G_{SI}}{1 + R_{SI}} \sim \frac{2.1 \times 10^4}{\phi^{2/3}} . \qquad (2.107)$$

Using $\rho r = 3$ g/cm^2 to determine the $\sigma - r_0$ relationship. Eq. 2.107 reduces to,

$$G_{SI}' \sim 700\, r_0 . \qquad (2.108)$$

While spark ignition is a more efficient method of initiating a nuclear fusion burn in a spherical pellet, it is not simple to generate the necessary spark environment. Spark ignition may be achieved by coalescence of a series of compressive waves in a spherical deuterium-tritium pellet or by shock heating in a collapsing fuel shell. In both mechanisms, the coalescence timing of the pressure pulse will be critical to successful ignition and any spatial instabilities in the convergence of the compression waves will be detrimental. For spark ignition to occur, the ablation pressure drive must be spatially uniform. This requires high initial pellet surface smoothness, and even irradiation by the driver[47].

A compressing pellet will be susceptible to degradation of the symmetry of the spherical implosion by the Rayleigh-Taylor instabiiity[40,41]. The Rayleigh-Taylor instability occurs when a high density material compresses a low density material. Such a situation occurs when the heavy tamper compresses the deuterium-tritium fuel, and also when the cold compressed fuel surrounds the hot central spark region. The onset and the characteristic exponential growth of both of these instabilities tend to inhibit the formation of the central spark ignition region.

2.3.1.8 Summary

In order to achieve a high energy gain in a tamped deuterium-tritium pellet, it is important to have $\rho r \approx 3$ g/cm^2 and also initiate a spark ignition where the condition of the spark region is $\rho r_s \approx 0.22$ g/cm^2 and $T \approx 4$ keV.

2.3.2 ICF Drivers

With the development of intense energy density sources from laser research in the 1960s, it was possible to envisage using focused laser irradiation to drive an ICF implosion and thermonuclear ignition. The following list summarizes this and other current ICF driver concepts[46,47]:

1. Neodymium glass laser
2. KrF laser
3. CO_2 laser
4. Free Electron Laser (FEL)
5. X-rays
6. Electron beam
7. Light Ions (p,d,..)
8. Heavy Ions (Ar...U)
9. Hyper-velocity Projectiles
10. Chemical explosives
11. Micro-fission.

Of all the drivers listed above, the KrF laser, heavy ion beams and light ion beams have the greatest potential for eventual implementation into an ICF energy system because they are projected to have the combination of required properties.

The energy from any of the many possible drivers may be delivered to the fuel pellet directly, by illumination of the pellet surface of the driver, or indirectly, by placing the spherical fuel pellet within a hohlraum, a hollow high-Z shell. The driver illuminates only the inside of the hollow shell,

creating soft X-rays which then act as the driver. Two advantages are inherent to the indirect approach: 1) the X-ray driver is very efficient and compression instability seeding by variations of the driver power over the pellet surface is considered to be more manageable, and 2) the hohlraum pellet requires at most two defocussed driver beamlets, each of which deposits energy evenly over half of the inner spherical shell, whereas a direct driver must have many beamlets for even energy deposition.

The key issues in determining the suitability of an ICF driver are the following:

1. Maximum delivery of energy,
2. Efficiency of coupling of driver energy to the pellet,
3. Maximum power,
4. Pressure pulse shaping,
5. Repeatability.

The driver energy required in the spark ignition concept will be the energy required to create a compressed deuterium-tritium fuel pellet that satisfies $\rho r \approx 3$ g/cm^2,

$$E_{driver} \sim 7.7\,(MJ)\, r_0^3 \,. \tag{2.109}$$

If an energy yield per pellet of 100 MJ is desired, then a deuterium-tritium fuel radius of $r_0 \approx 0.25$ cm and a driver energy $E_{driver} \approx 0.16$ MJ are required.

A driver will have an efficiency, η_d, which increases the driver energy required to 0.16 MJ/η_d. Heavy ion beams have $\eta_d \approx 30$ % and light ion drivers exhibit efficiencies up to $\eta_d \approx 25\%$ (Refs.54-56). An efficiency of about 7%

	Osiris	Sombrero	Libra
Fusion Power (MW_{th})	1987	2668	960
Driver Energy (MJ)	5	3.4	4
Target Yield (MJ)	432	401	320
Repetition Rate (Hz)	4.6	6.7	3
Energy Gain	87	118	80
Blanket Mult.	1.26	1.08	1.21
Total Thermal Power (MW_{th})	2504	2903	1160
η_e (%)	45	47	38
Total Elec. Power (MW_e)	1015	1000	331
Driver	12 beam Xe^+	KrF laser	Li^+ ion beam
η_d (%)	28.2	7	23
Blanket	Flibe	Li_2O	$Li_{17}Pb_{83}$
Blast Chamber	Flibe/ Carbon mesh	Carbon mesh/ Xenon gas X-ray shield	$Li_{17}Pb_{83}$ soaked Carbon mesh
Coolant	Flibe	He	He

Table 2.3 : ICF energy system parameters[54-56].

(Ref.55) is estimated for the KrF laser, the prime candidate for a laser ICF energy system driver.

Compression of the fuel pellet should be as isentropic as possible in order to minimize driver energy. However, for an isentropic pressure pulse, a maximum attainable driver power density should be near 10,000 TW/cm^2 and should be suitably temporally shaped, as discussed in Section 4.2.

An ICF energy system is projected to burn pellets at a rate of between 1 and 10 Hz; hence, the driver must be able to be pulsed at this rate.

2.3.3 Current ICF Research

The major laser ICF research centres, OMEGA at University of Rochester's Laboratory of Laser Energetics[48], NOVA at Livermore[49] and GEKKO XII at Osaka University[50], use frequency multiplied Neodymium:glass lasers. The original 1054 nm fundamental laser wavelength generated by excited Neodynium dopants is converted to the 2nd or 3rd harmonic using a KDP crystal (Potassium-Dihydrogen-Phosphate) frequency multiplier. Frequency multiplied Nd:glass lasers are useful for driver:fuel pellet interface and burn physics research but are not thought of as energy system driver candidates due to their low efficiency and the low repetition rate. OMEGA is a frequency tripled (351 nm) 1.5 kJ Nd:glass laser and has achieved fuel densities in glass-covered solid deuterium-tritium targets of 20 - 40 g/cm^3. OMEGA is currently being upgraded to 30 kJ. GEKKO is a frequency doubled, 526 nm Nd:glass laser and has achieved densities of 600 g/cm^3 in compressed plastic targets. NOVA is also a frequency tripled Nd:glass laser with a maximum power of 17 kJ. There is currently a proposal to upgrade NOVA to

1-2 MJ. Research in KrF lasers is currently being performed in the NIKE program[51], a collaboration of Los Alamos National Laboratories (LANL) and the Naval Research Laboratories (NRL). As well, research into light ion beamdrivers at Sandia Laboratories and also at the Kernforschungzentrum Karlsruhe is progressing and a 1 TW/cm^2 Li^+ beam can be delivered[52]. Heavy ion driver research is still in its infancy, with concentrations of effort at Lawrence Berkeley Laboratories and the Institute für Schwerionenforschung in Garching, Germany[53].

2.3.4 ICF Energy System Designs

Table 2.3 lists the major parameters in three recent ICF energy system design studies. Osiris is based on a heavy ion driver[54], Sombrero is based on a KrF laser[55] and Libra is based on a light ion driver[56]. The key parameters in each of these designs are the thermal energy generated in burning pellets, represented by Fusion Power, the energy produced in the blanket, represented by Blanket Mult., the efficiency of thermal energy conversion, the driver energy required and the driver efficiency. The blanket material in each of the systemdesigns is some form of lithium necessary to breed tritium (see Section 2.2.4 Tritium Breeding). In the solid blanket designs, the coolant is helium, but it is possible to use Flibe both as a coolant, breeder and part of the blast shield. The blast containment in all designs is basically a carbon and ceramic mesh with some material shielding to effectively absorb the X-ray energy of the blast.

2.3.5 Issues in ICF

The key issue in the development of ICF for energy production is the generation of a spark ignition region in the core of a compressed deuterium-

tritium pellet. The basic concept of the fusion burn in an ICF pellet has been affirmed as a result of the classified Halite/Centurion program where an ICF pellet was driven by the blast of an underground nuclear test[57]. It is not yet known whether a driver and pellet can be designed to avoid instability problems and give a large energy gain.

2.4 Muon Catalyzed Fusion

Expanding on concepts introduced in Section 2.1.4, this section focuses on muon catalyzed fusion processes in molecular deuterium-tritium (i.e. low temperature) fuel at LHD and prepares for future analysis of similar μCF processes at high densities (densities greater than LHD) addressed in Chapter 5. The main topics examined are: 1) modelling of processes leading to resonant formation of the μdt_{11} muo-molecular ion, 2) fusion via the muo-molecular process and 3) the experimental values of muon catalyzed fusion rates and the muon sticking probability in molecular deuterium-tritium at LHD. In addition, the impact of the measured μCF reaction rates in molecular deuterium-tritium on the feasibility of an energy system based on low temperature muon catalyzed fusion are examined.

2.4.1 Introduction

In 1956, Luis Alvarez thought that he and his co-workers had solved mankind's energy problems forever[58]. They observed, in cosmic ray showers, evidence of the following muon induced fusion reaction at room temperature:

$$\mu d + p \rightarrow \mu pd \rightarrow h + \mu + 5.49\,MeV. \qquad (2.110)$$

Fusion reactions catalyzed by heavy negative particles, such as a muon, were first proposed in 1947 by Frank[21] and also independently a year later by Sakharov[22]. After careful analysis of Alverez's observation, it was concluded that the energy gain of a system based on the concept of muon induced proton-deuterium fusion was not energetically viable. Later theoretical analysis by Vesman and others proposed that muon catalyzed fusion of a μdt_{11} muo-molecule would exhibit a large reaction rate at room temperature due to a resonance in the formation[59]. This result heightened interest in μCF and experimental investigations of muon induced fusion in low temperature (T < 1000 K) molecular deuterium-tritium were pursued.

Subsequent experiments with muons in molecular deuterium-tritium at temperatures from 4 to 1000 K, and densities from a very low pressure molecular gas to liquid hydrogen densities (LHD) confirmed the existence of a loosely bound μdt_{11} muo-molecular state and the resonance formation mechanism[60-68]. Experimental studies focused on processes leading up to resonant muo-molecule formation and also on the muon loss to sticking to the alpha particle by-product.

The research groups involved in μCF experiments include: JINR (Joint Institute for Nuclear Research, Russia), KEK (National Laboratory for High Energy Physics, Japan), LAMPF (Los Alamos Meson Physics Facility, USA), PSI (Paul Scherrer Institute, Switzerland), TRIUMF (Tri-University Meson Facility, Canada) and RAL (Rutherford-Appleton Laboratory, UK). The work performed at each of the above facilities has generally been complementary, however some important results on the density dependence of muon sticking from the main groups at PSI and LAMPF have been in disagreement. The LAMPF group reports a significant density dependence reduction in muon

sticking[63,64] and the PSI group sees only a weak dependence[66-68].

2.4.2 Molecular Deuterium-Tritium

Before an analysis of the muon catalyzed fusion processes commences, a property of the molecular deuterium-tritium should be discussed. At low temperatures, gaseous or liquid molecular deuterium-tritium fuel will be made up of D_2, DT and T_2 molecules. The DT molecules are a result of the following exchange reaction which proceeds for T > 20 K (Ref.69),

$$D_2 + T_2 \rightarrow 2DT \tag{2.111}$$

The concentrations of D_2:DT:T_2 will equilibrate to a ratio of 1:2:1, however it is feasible to have purely DT or D_2:T_2 frozen fuel.

2.4.3 μCF in Molecular Deuterium-Tritium

Figure 2.10 illustrates the chain of linking reactions involving muons and molecular deuterium-tritium mixtures (D_2-DT-T_2). The dominant reactions in the reaction chain leading to muo-molecular formation and fusion within the muo-molecular ion are:

1. Muon injection, muon deceleration, capture of muons by deuterium or tritium molecules, molecular break-up and de-excitation to the muo-atomic ground state.
2. Isotopic transfer of muons between muo-atoms at excited and ground states.
3. Hyperfine μt_{1s} state transitions from the F=1 state to the F=0 state.
4. The μdt muo-molecular ion formation in the J=v=1 state and de-excitation to J=0 fusion channel states.

5. Nuclear fusion and release of the muon.
6. Muon sticking to and regenerative stripping from fusion by-product helium.

A muon will proceed through these steps and, once fusion occurs and the muon is released or regenerated, it will proceed through the reactions once again. The length of the fusion reaction chain generated by the cycling muon is determined by the rate of cycling, muon losses due to muon sticking to fusion by-products and ultimately by muon decay. Each of the above listed processes will be discussed individually in the following sections.

2.4.3.1 Muo-atom Formation via Molecular Interactions

A newly formed, initially relativistic muon will decelerate in LHD molecular deuterium-tritium in about 1 ns (Refs.70,71). Once the injected muons slow to energies in the range of $E_\mu \approx 30$ eV ($v_\mu \approx 2.0 \times 10^7$ cm/s), muon capture by a molecule proceeds. The following muon-molecule interactions may occur in deuterium-tritium:

$$\mu + D_2 \rightarrow \mu d + D + e, \tag{2.112}$$

$$\mu + DT \rightarrow \mu d + T + e, \tag{2.113}$$

$$\mu + DT \rightarrow \mu t + D + e, \tag{2.114}$$

$$\mu + T_2 \rightarrow \mu t + T + e. \tag{2.115}$$

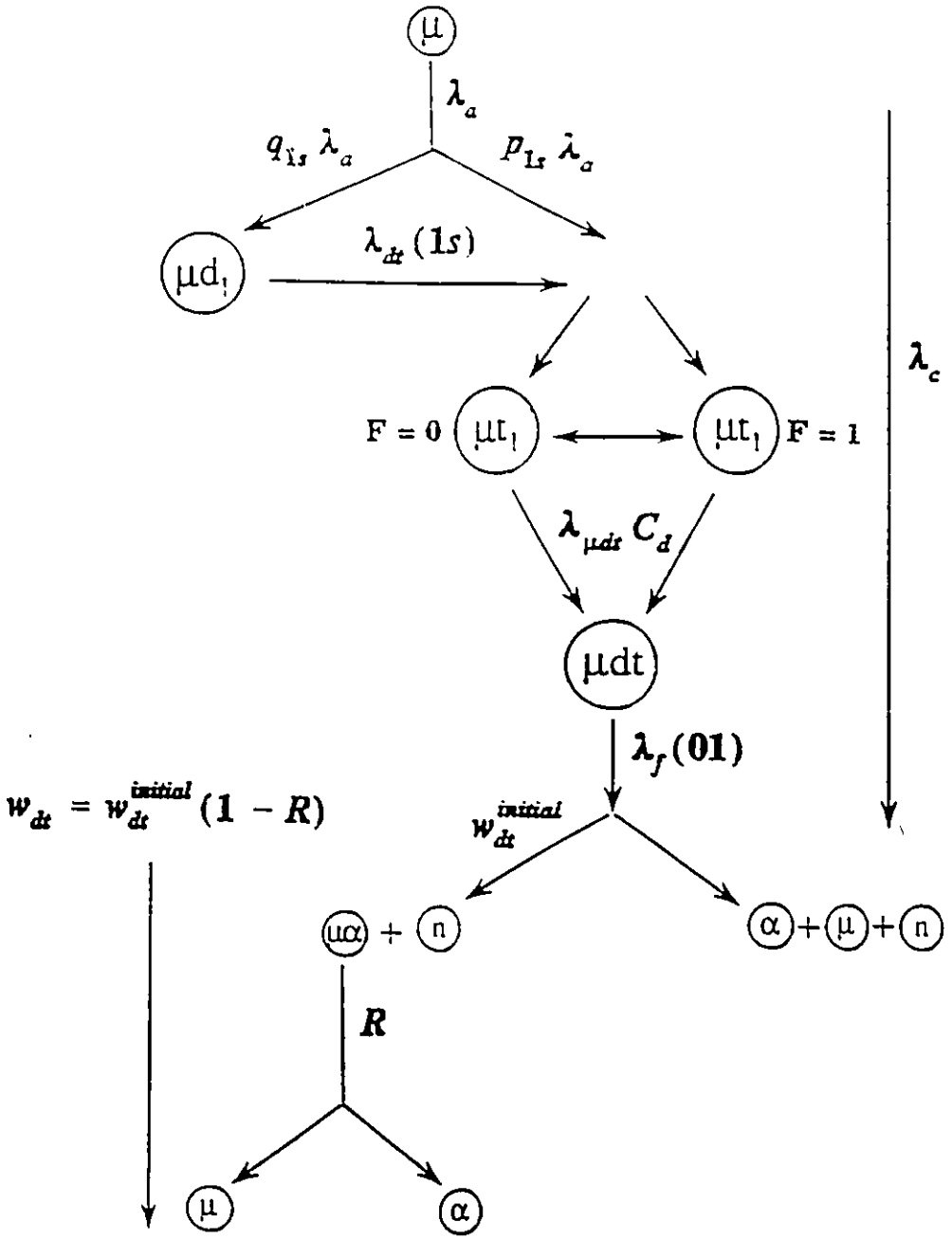

Figure 2.10 : Network of muon catalyzed fusion reactions in molecular deuterium-tritium.

Owing to its large momentum, a 30 eV muon in a collision with a molecule will dissociate the molecule and then "knock out" an electron, creating a highly excited bound muon. Using an approximate size for the D_2, T_2 or DT molecule of $d_o \approx 0.7$ Å, the cross-section for a muon capture collision, $\sigma_{molecule}$, is calculated as follows:

$$\sigma_{molecule} \sim \pi d_o^2 \ . \tag{2.116}$$

The molecular muon capture rate, λ_a(molecular), is calculated by using the following reaction rate expression:

$$\lambda = <\sigma_{molecule} v_\mu > N_{molecule} \ , \tag{2.117}$$

where $N_{molecule} = 4.8 \times 10^{22} \phi \ (cm^{-3})$ is the deuterium-tritium molecular density in LHD. Using Eqs. 2.116 and 2.117, the molecular capture rate is

$$\lambda_a (molecular) \sim 1.5 \times 10^{14} \ \phi \ f_m f_\mu \ (s^{-1}) \ . \tag{2.118}$$

2.4.3.2 Muon Transfer in Molecular Deuterium-Tritium

The binding energy of a muonic atom including first-order relativistic effects is expressed by

$$E_b = -M_{\mu X} c^2 \frac{(\alpha Z)^2}{2 n^2} \left(1 + \frac{(\alpha Z)^2}{n^2} \left(\frac{n}{j - 1} - \frac{3}{4}\right)\right) \tag{2.119}$$

where $M_{\mu X}$ is the reduced mass of muo-atom μX, Z is the nuclear charge of X, n is the principal quantum number, j is the angular momentum quantum number and α is the fine structure constant. For the μd and μt muo-atoms, the binding energies are $E_b(\mu d) = -2663.23$ eV and $E_b(\mu t) = -2711.27$ and there is a 48.04 eV binding energy difference between μt and μd muo-atom. In addition, the ground state μt muo-atom has a hyperfine splitting between a

total net spin state of F=1 and of F=0 equal to $\Delta E = 0.24$ eV (Ref.72).

The formation of the μdt_{11} muo-molecular ion from μd will have an extra 48.1 eV binding energy difference, greater than the 0.66 eV energy difference between μt and μdt_{11}. Considering Eq. 2.33, the formation rate from μd will be very much slower than the formation rate from μt.

Because the fusion precursor forms through the ground state μt muo-atom only, the formation of a μd restricts the further fusion catalyzing capacity of the muon. However, since μt has a lower binding energy than μd, the following muon transfer reactions proceed:

$$\mu d_n + t \rightarrow \mu t_n + d + \frac{48.1}{n^2}\ eV. \qquad (2.120)$$

During molecular muon capture, the initial muon energy level will be about $n = (m_\mu/m_e)^{1/2} \approx 15$. The initially excited muo-atoms will de-excite, both by radiative and collisional processes and it is assumed that the n=15 state will decay to the n=3 energy state after approximately[73,74]

$$t_{n-3} \approx \frac{1}{\phi}\ (ps)\ . \qquad (2.121)$$

The values of the de-excitation rates and transfer rates in Fig. 2.11 are taken from theoretical work performed by Menshikov and Ponomarev[73]. This study originally calculated the muon transfer rates of μd with atomic tritons and indicated that muon transfer competes with collisional de-excitation starting at n=5 energy levels. In a more recent study, Müller et. al.[74] have convincingly theorized that for $n > 2$ there will be a suppression of muon

transfer to molecules. Using this current result, it is assumed that the μd_3 and μt_3 are formed in the same ratio as the initial fuel mixture C_d:C_t, and the concentrations of the ground state populations μd_{1s} and μt_{1s} then depend on the relative strengths of subsequent de-excitation reactions.

The fraction of initial number of excited μd formed, compared to the number of ground state μd resultant is referred to as q_{1s} and the similar fraction for μt is referred to as p_{1s}. The combination of the density dependent collisional de-excitation processes and the density independent radiative processes will result in a non-linear density dependence of q_{1s}. At low densities the radiative transitions will dominate and few $n > 1$ muon transfers will occur. As the density increases, the increase in the collisional de-excitation rate and the dominance of the transfer rate over the radiative rates will cause q_{1s} to approach the limiting case of small dependence on density. For densities greater than LHD, q_{1s} and p_{1s} depend only on the tritium fraction of the fuel represented by C_t. Using Ponomarev and Menshikov's and Müller's models, the calculated value of p_{1s} versus initial tritium concentration C_t for low temperatures is illustrated in Fig. 2.12. Using values of $C_t = 0.5$, $\phi \approx$ LHD and $T < 1$ eV, a value of $q_{1s} \approx 0.2$ results.

If the muon does not transfer from μd in the excited state where the transfer rates are relatively high, it must transfer from the relatively slow μd_{1s} (ground state) with a rate given by[73]

$$\lambda_{dt}(1s) \sim 3 \times 10^8 \, \phi \quad s^{-1} \, . \tag{2.122}$$

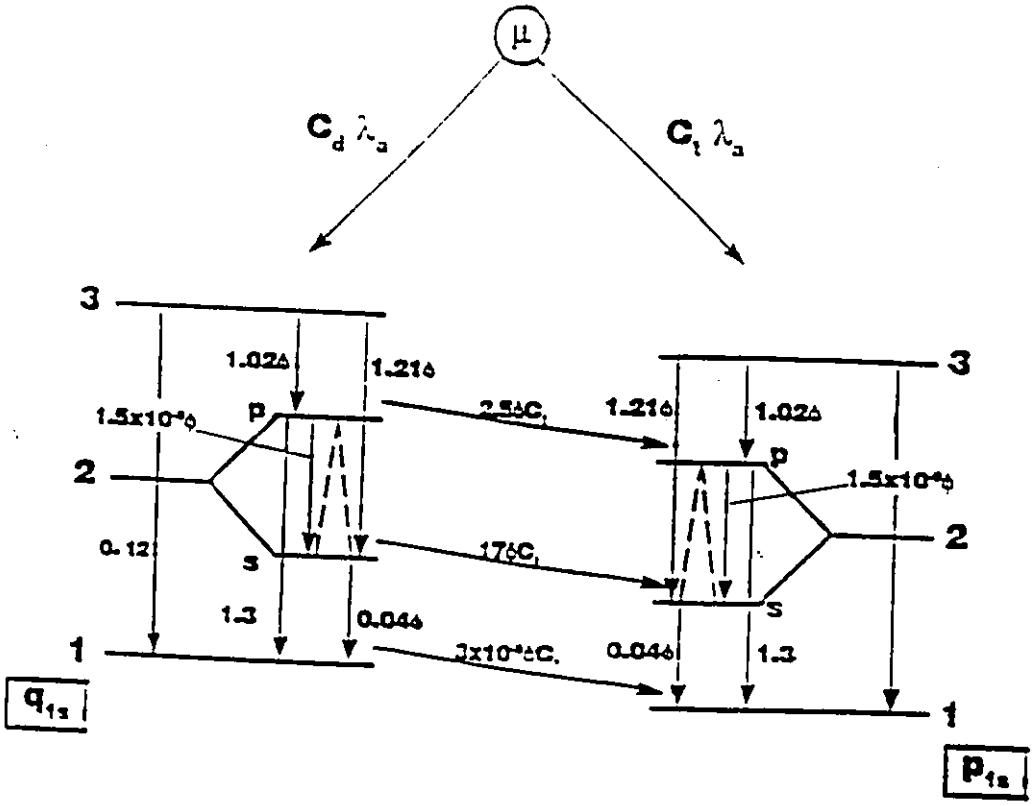

Figure 2.11 : Depiction of the possible de-excitation and transfer routes of a μd muo-atom whose ground state population is q_{1s} including the de-excitation routes of a μt muo-atom whose ground state population is p_{1s}.

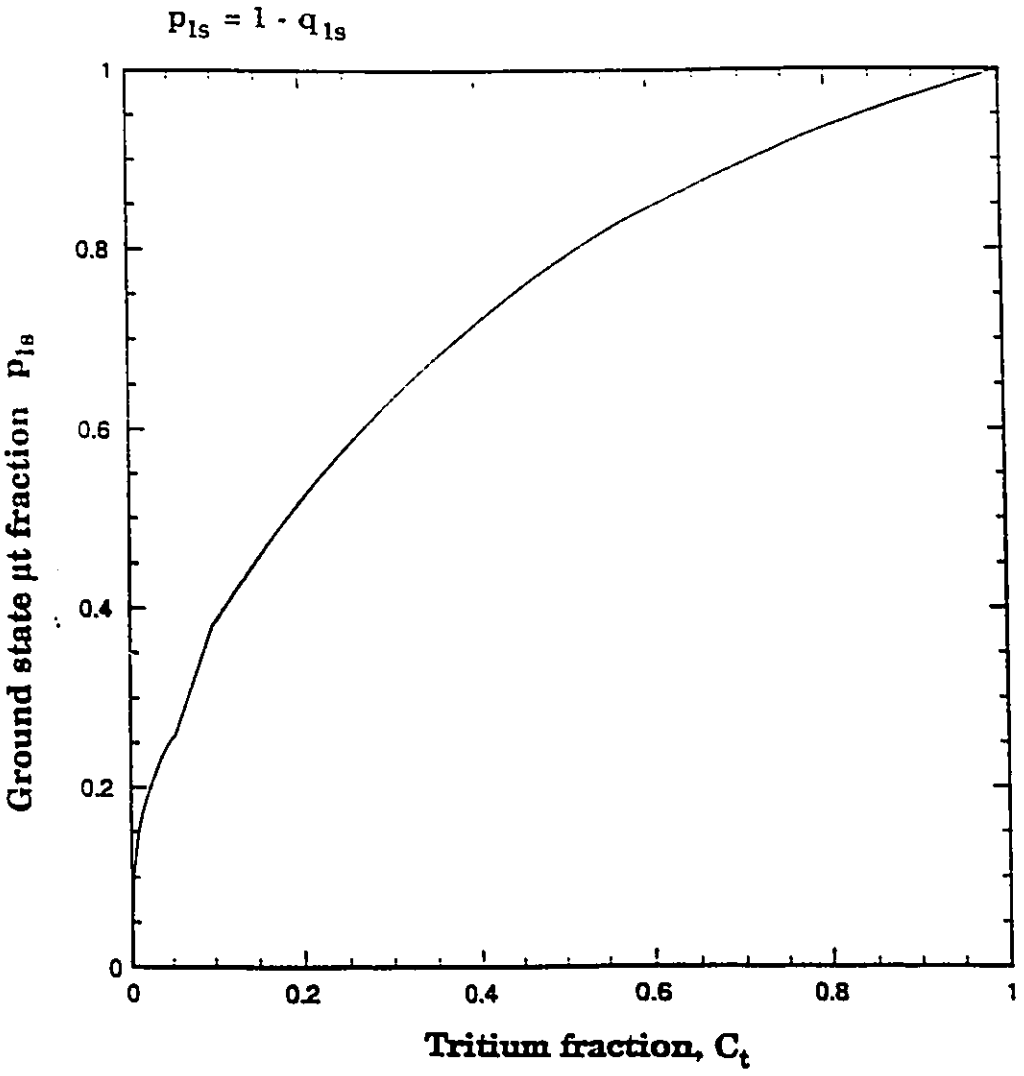

Figure 2.12 : Plot of the fraction of initially formed μt muo-atoms that make it to the ground state, referred to as p_{1s}, versus C_t the tritium fraction for temperatures T < 1 eV and $\phi \approx$ LHD.

2.4.3.3 Resonance Formation of the μdt_{11} Muo-molecular Ion

Once a μt_{1s} muo-atom is formed by muon capture or muon transfer, it can then move close to a D_2 or DT molecule and proceed to form muo-molecules. The desired result is the formation of a muo-molecular complex in which the fusible μdt_{11} muo-molecular ion is a constituent.

Referring to Table 2.2, the μdt_{11} muo-molecular ion formed via an interaction between a ground-state muo-atom μt_{1s} and a D_2 or DT molecule has a binding energy of approximately -0.66 eV. This energy is less than the hydrogen molecule dissociation energy of about 4 eV; therefore, the excess energy generated in a μt_{1s} and D_2 or DT collision can be assumed by the rotational and vibrational modes of the resultant H_2 molecule-like muo-molecular complex. Since the energy transferred to the muo-molecular complex is transferred to distinct energy states, the process of formation will be resonant. This process was first proposed by Vesman in 1967 and is referred to as the Vesman mechanism[59].

Figure 2.13 illustrates the potential energy surfaces for the reactants and products of the following resonant muo-molecule formation reactions:

$$(\mu t)_{1s} + (D_2)_{K_i,\nu_i} \rightarrow ((\mu dt)_{11}\, dee)_{K_f,\nu_f} \qquad (2.123)$$

where X = D or T, K_i and ν_i are the initial rotational and vibrational states of the reactant molecule DX and K_f and ν_i are the final rotational and vibrational states of the resultant muo-molecular complex.

The resonant conditions for the reactions depicted in Eq. 2.123 are:

$$\varepsilon_0 + |\varepsilon_{11}| = \Delta E_{K\nu} \qquad (2.124)$$

where ε_{11} is the μdt_{11} binding energy, ε_0 is the energy of the μt and DX reactants and $\Delta E_{K\nu}$ is the transition energy of the muo-molecule. In order to determine the resonance condition of Eq. 2.124, the following aspects of the resonant formation reaction must be included:

1. the initial K_i and ν_i states of the reactant molecule DX,
2. the hyper-fine state energy transition of the μt_{1s}, and
3. the fine and hyperfine splitting of the μdt_{11} muo-molecular ion energy as illustrated in Fig. 2.14.

The general expression for the formation rate is

$$\lambda_{\mu dt\text{-}X} = \pi \frac{N}{M_{\mu t,DX}} \sum_i P[K_i,\nu_i](T) \times \int_0^\infty dE \, |PM(K_i,\nu_i \rightarrow K_f,\nu_f)|^2 f(E,T)\, \delta(E - E_{res}(K_i,\nu_i \rightarrow K_f,\nu_f)) , \tag{2.125}$$

where $M_{\mu t,DX}$ is the reduced mass of the μt + DX collision, $PM(K_i,\nu_i \rightarrow K_f,\nu_f)$ is the interaction probability matrix using the initial $\mu t_{1s}(F)$ state, (K_i,ν_i) are the initial rotational and vibrational states of the reactant molecule DX, (K_f,ν_f) are the final rotational and vibrational states of the resultant μdt_{11}Xee muo-molecule, $P[K_i,\nu_i](T)$ is the probability of the DX molecule being in the K_i and ν_i states at temperature T, f(E,T) is the energy state distribution of the μt_{1s} and DX collisions assumed to be Maxwellian and the delta function $\delta(E\text{-}E_{res}(K_i,\nu_i \rightarrow K_f,\nu_f))$ is a consequence of the resonance condition in Eq. 2.124 (Ref.75). The summation of the two possible initial reactant molecules yields the following expression for the total μdt_{11} formation rate:

$$\lambda_{\mu dt} = \lambda_{\mu dt\text{-}d} + \lambda_{\mu dt\text{-}t} . \tag{2.126}$$

The following issues are important to the above reaction rate calculations:

1. The distributions of the reactants μt_{1s} and DX were assumed to be Maxwellian, but this may not be true for μt_{1s} formed by exothermic muon transfer reactions.
2. The interaction matrix element M is very sensitive to the transition energy $E_{res}(K_i,vi \rightarrow K_f,v_f)$.
3. Theory suggests that the resonant formation rate of the μdt_{11}dee and μdt_{11}tee muo-molecules are dominated by transitions from the initial vibrational state $v_i = 0$ to the final vibrational state $v_f = 2$.
4. Below threshold resonances, i.e. $E_{res} < 0$, are inaccessible if the resonances have negligible widths. However if the resonant states are collisionally broadened then the delta function in Eq. 2.125 is replaced by a Lorentzian function and it is possible that below threshold resonances could play a role in formation. The consequence of these processes is that as $T \rightarrow 0$ K , the formation rate will approach a constant value, rather than zero. This effect is experimentally observed for μt_{1s} - D_2 collisions but is not observed for μt_{1s}DT. In addition, because of the larger area of the Lorentzian function compared with the delta function, larger parts of the Maxwellian distribution of reactants can contribute to the formation mechanism[76]. Collisional broadening of the resonances increases with density due to higher probability of three body collisions. This results in a non-linear density dependence of the resonance formation

when the collisional broadening and three-body reactions are significant.

The very complex nature of the important factors discussed above provide for interesting experimental studies but modelling of the resonant formation reaction rate is difficult because of the high sensitivity to variables. A "first-order" model of resonance formation may be developed using the following simplifying assumptions:

1. the difference in the fine and hyperfine states of the μdt_{11} muo-molecular ion and the μt_{1s} muo-atom are negligible,
2. there is no difference between formation via D_2 and DT,
3. there are no three-body resonance reactions or resonance line broadening,
4. $v_i = 0$ and $v_f = 2$, and
5. the μt_{1s} and DX distributions are Maxwellian.

Using these simplifications, the approximate μdt_{11} formation rate is

$$\lambda_{\mu dt}(resonance) \sim 7.78 \times 10^6 \, T^{-3/2} \, e^{-0.07/T} \phi \quad (s^{-1}) , \qquad (2.127)$$

where T is in eV (Ref.77).

Once a muo-molecular complex forms through resonance, de-excitation of the μdt_{11} muo-molecular ion to the J=0 state is a requirement for quick fusion. The transition from the μdt_{11} state to μdt_{01} state is much more rapid than the μdt_{11} formation rate, $\lambda_{11\to01} \approx 10^{12}\ s^{-1}$; therefore, it is safe to assume that the μdt_{11} instantaneously fuses when it forms in molecular fuel. However, the muo-molecular ion may break-up upon collision with another body. De-excitation to the fusion channel will compete with break-up[78].

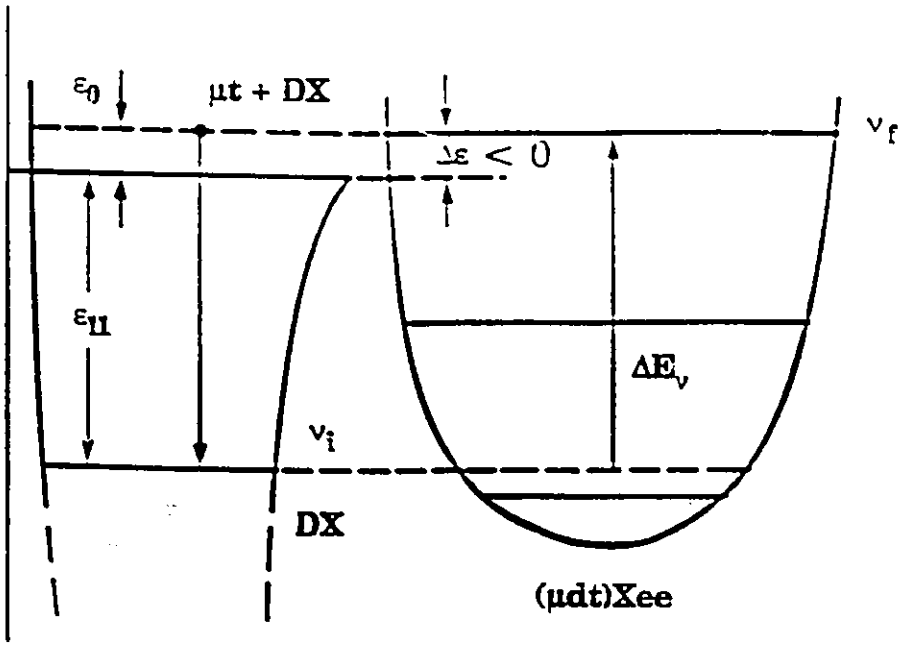

Figure 2.13 : Energy level schematic of a μt_{1s} + DX interaction forming a μdt_{11}Xee muo-molecule where X = D or T.

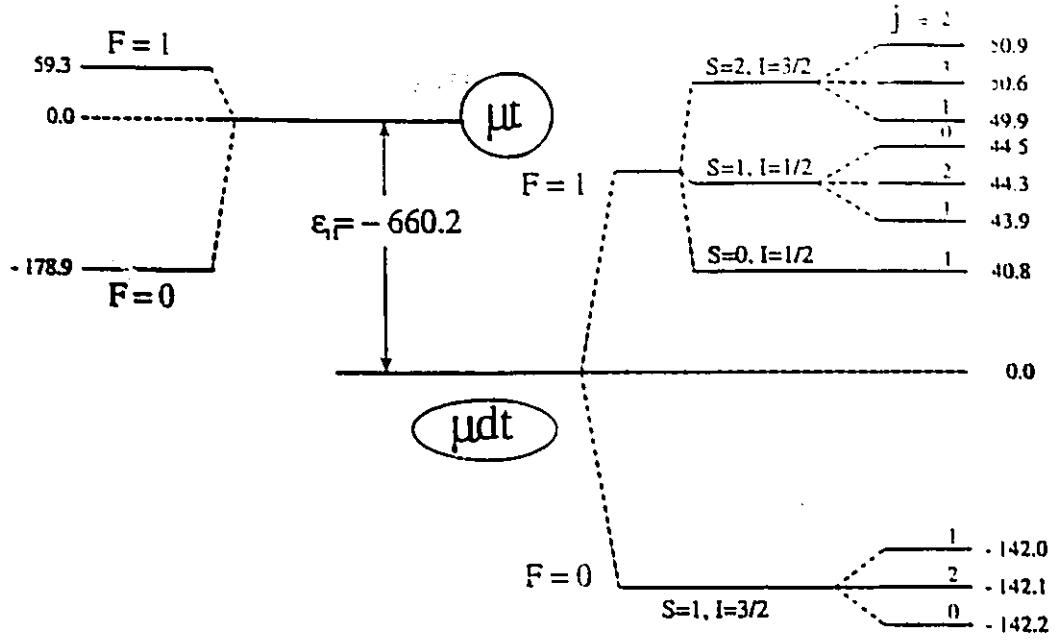

Figure 2.14 : Fine and hyper-fine splittings of the μt_{1s} muo-atom and the μdt_{11} muo-molecular ion[25].

Because the μdt_{11} muo-molecule has an energy of approximately 0.66 eV, and the de-excitation is so rapid, the breakup of the muo-molecular ion is not significant for temperatures less than the molecular dissociation energy of approximately 4 eV. This is discussed further in Chapter 5.

2.4.3.4 Introduction to Muon Sticking

After the μdt_{01} fusion event, the probability that the muon will be free to initiate another link in the muon catalyzed fusion chain is greater than 99%. However, there is a small probability that the muon will adhere to the by-product ^{4}He and remain there until it decays. This phenomenon is known as muon sticking.

Muon sticking in molecular deuterium-tritium can best be appreciated by regarding the experimental values of the sticking probability w_{dt}, as depicted in Fig. 2.15. The sticking probability tends to decrease as the deuterium-tritium density increases from that of a low density gas to approximately 1.3 LHD. The decrease in muon sticking is most appreciable for the LAMPF data. Although this density dependence has been the subject of some debate between the PSI group and the LAMPF group, it is now generally accepted that the LAMPF data is correct. The lowest muon sticking probability measured is $w_{dt} \approx 0.0036$ at a density of $\approx 5.5 \times 10^{22}$ cm^{-3}.

It is noteworthy that the solid line in Fig. 2.15, representing the best theoretical models of muon sticking in molecular deuterium-tritium, does not adequately explain the observed density dependence.

Further increases in the fuel density at temperatures where muon

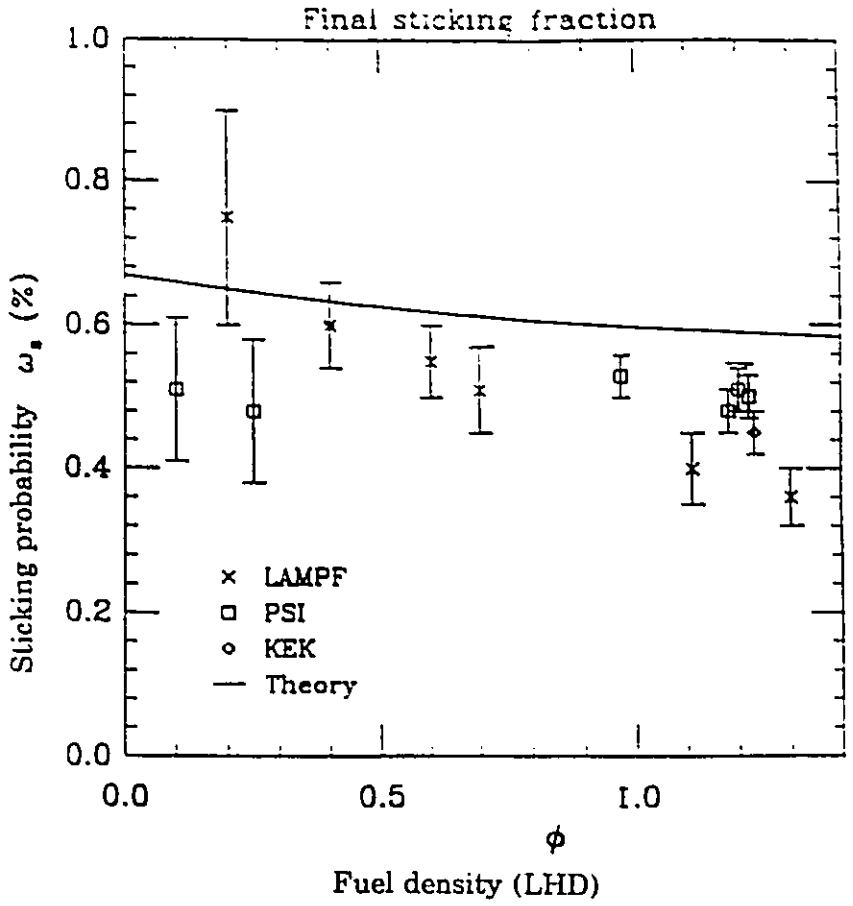

Figure 2.15 : Theoretical and measured values of the muon sticking probability in deuterium-tritium. Here ϕ is the fuel density with respect to a density of 4.25 x10^{22} cm^{-3} (Taken from Ref. 75).

catalyzed fusion reactions are appreciable are not possible due to the finite material strength of the reaction container. This thesis will endeavour to explore the attainment of dynamic density regimes where muon sticking is additionally reduced. Further analysis of muon sticking is discussed in Section 5.5 Muon Sticking and Regeneration; this analysis will apply to all temperatures and densities.

2.4.3.5 Muon Cycling Rate

The series of reactions leading to muon induced fusion shown in Fig. 2.11 will determine the overall muon cycling rate λ_c. Using the same assumptions previously used to develop the simplified resonance model (Eq.2.127) and the values of q_{1s} and λ_{dt} in LHD deuterium-tritium, the cycling rate can be approximated by the following expression[79]

$$\lambda_c^{-1} = \frac{q_{1s} C_d}{\lambda_{dt(1s)} C_t} + \frac{1}{\lambda_{\mu dt} C_d} \qquad (2.128)$$

where C_d is the fraction deuterium and C_t is the fraction of tritium in the fuel.

The cycling rate calculated using Eq. 2.128, for LHD and temperatures less than 1000 Kelvin is shown in Fig. 2.16, with experimental values by Jones et.al.[64]. It is apparent that there is a considerable disagreement between the calculated and experimental values for muon cycling. These differences are possibly due to the aforementioned collisional broadening and three body effects in the muo-molecule formation. The ultimate magnitude of the muon cycling is unknown, but will be restricted to $\lambda_c < 10^9\ s^{-1}$ at LHD by the q_{1s} and $\lambda_{dt}(1s)$ terms in Eq. 2.126.

2.4.3.6 Muon Catalyzing Efficiency

The average number of fusions induced by a muon in molecular deuterium-tritium fuel will be a function of the number of times a muon cycles through the processes leading to fusion before loss by decay or sticking. The following expression can be used to determine the number of fusions per muon also refered to as the muon catalyzing efficiency:

$$X_\mu = \frac{1}{\frac{\lambda_\mu}{\lambda_c} + w_{dt}}, \tag{2.129}$$

Using the maximum measured value of $\lambda_c \approx 1.6 \times 10^8$ s^{-1} in Fig. 2.16 at T ≈ 800 Kelvin, $\phi \approx$ LHD and the minimum measured muon sticking probability, the maximum muon efficiency in molecular deuterium-tritium at a density of $\phi \approx$ 1.3 LHD, correcting for the density difference, is

$$X_\mu \sim 173 . \tag{2.130}$$

Assuming that each fusion reaction generates about 20 MeV, i.e., that the neutron energy multiplication in a FLIBE breeder blanket is approximately 1.15, the energy produced per muon is about 3460 MeV. The key to the viability of μCF in molecular deuterium-tritium will be minimizing the energy cost of the muon.

2.4.3.7 Muon Energy Cost

It is known that there is a steady flux of muons striking the earth as a result of cosmic ray showers. The cost of these muons is a function of the energy required to collect them into a reaction volume. The flux of negative muons to the earth's surface is about 500 - 3000 m^{-2} s^{-1}. Analysis by Harms and Shani[80] concluded that a μCF reactor utilizing this free muon source

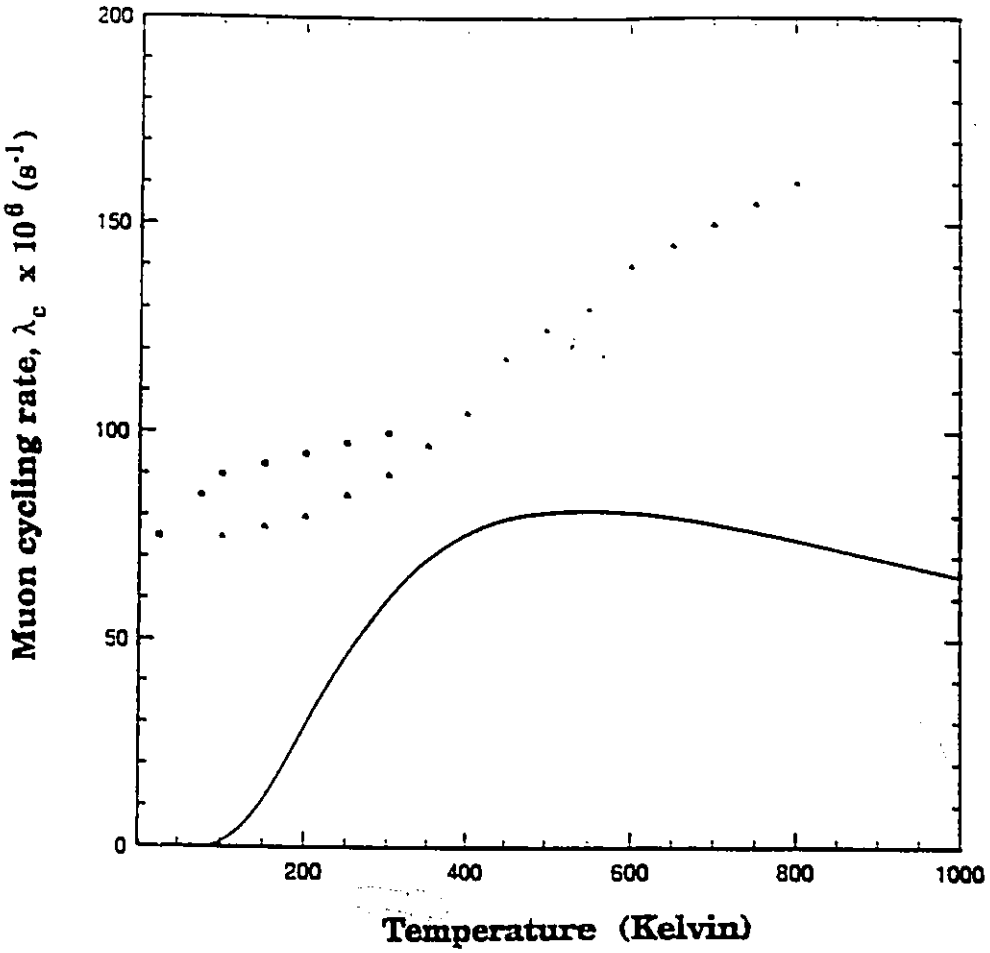

Figure 2.16 : Theoretical values of the muon cycling rate calculated with Eq. 2.126 (solid line) compared to the experimental values of muon cycling by Jones et. al.[84] in LHD deuterium-tritium.

would be prohibitively large. Use of a magnetic lens to concentrate the muon flux and reduce the size of the reactor was recently analyzed by Fundamenski and Harms[81], but concluded that such a lens would not yield a reactor scale muon flux.

As the rest mass energy of a muon is about 106 MeV, a scientific gain of approximately 32 was achieved in the LAMPF experiments. Unfortunately, the efficiency of creating muons by the best method known, accelerated charged particle interactions, is very low. Technology for the production of the muon fluxes required by a μCF reactor is discussed in Section 4.2. The technical difficulties in creating a large muon flux are non-trivial, but a sufficient flux for significant fusion power production is thought to be achievable with further accelerator and target development. The most promising muon production schemes converge on an energy value of approximately 4 GeV per muon (see Table 4.2).

2.4.3.8 Molecular Deuterium-Tritium μCF Reactor Concepts

Substituting values of $E_{cat} = E_\mu \approx 4$ GeV, $Q_{dt} \approx 20$ MeV and maximum $X_\mu \approx 173$ into the catalyzed fusion energy gain formula given in Eq. 2.58, the raw energy gain of an energy system based on μCF in molecular deuterium-tritium is

$$G \sim \frac{X_\mu Q_{dt}}{E_\mu} \sim 0.87 . \qquad (2.131)$$

While energy break-even is nearly achieved, higher energy gains in molecular deuterium-tritium are not possible because of the huge expense of the muon, and muon sticking losses.

While energy break-even is nearly achieved, higher energy gains in molecular deuterium-tritium are not possible because of the huge expense of the muon, and muon sticking losses.

In order to increase the energy gain, the value of Q_{dt} may be increased by placing fertile material such as ^{232}Th and ^{238}U within the blanket and breeding fissionable fuel. The effective value of Q_{dt} is then multiplied by the average number of fissile nuclei generated per fusion neutron and by the energy released per fission. Such a scheme was first suggested by Petrov[8] and many analyses of fissile fuel breeding using μCF have been performed[82,83].

The dilemma of fusion-fission hybrid schemes is that the prime advantages of fusion over fission, that is, the avoidance of long-lived radionuclides and proliferation, are lost. Thus, it is desirable to develop a purefusion system, and the fissile breeding option will not be considered further here.

2.4.4 Requirements for a μCF Energy System

From the above energy gain calculation it is apparent that μCF in molecular deuterium-tritium is presently not an option for energy production. Muon catalyzed fusion can only be an alternative for fusion energy production if a reaction regime can be found where the muon sticking probability is low and the muon cycling rate is rapid. The LAMPF muon sticking and muon cycling data suggests that higher deuterium-tritium densities may provide these requirements.

CHAPTER 3

MUON CATALYZED - INERTIAL CONFINEMENT FUSION SYNERGISM

3.1 Fusion Synergism

Synergism is defined as the joint action of two dissimilar processes to achieve an action neither could independently. Considering the interaction between two distinct technologies and searching for a domain in which a symbiotic effect results can be a very effective method of attaining a technological goal[5,84]. Review of the basic principles of ICF and μCF points to the existence of complementary qualities in these two fusion systems.

Although there have been some previous attempts to investigate μCF-ICF synergism, none were comprehensive enough to be conclusive[13,42,77,85-88]. Preliminary re-evaluation work[14-17] suggests that a closer look at the concepts determining the overall viability of a μCF-ICF combination would be beneficial.

3.2 μCF-ICF Synergism Approaches

The apparent density dependence of muon sticking described in Chapter 2 is intriguing, and indicates that muon catalyzed fusion at elevated densities may provide a route to an energetically viable μCF energy system. Because of the finite strength of fuel containment materials, elevated fuel densities in a reactor domain can only be procured in a pulsed mode, i.e., the fuel is

imploded by explosively driven compression within a suitable reactor cavity. High fuel compression is easily obtained in ICF pellets.

In considering options for μCF-ICF symbiosis, there are two obvious courses:

1. ICF enhanced by μCF,
2. μCF enhanced by ICF.

In the first approach, muons are used to initiate spark ignited fusion of an ICF pellet. This concept will be referred to as μCF triggered spark ignition.

In the second approach, the density of deuterium-tritium fuel is elevated, as in an ICF fuel pellet, which facilitates muon catalyzed fusion reactions upon muon injection. This approach is referred to as high density μCF.

Common features and technology requirements of both approaches are:

1. Deuterium-tritium fusion fuel
2. Solid spherical fuel pellets
3. Muon production and injection system
4. Compression driver system
5. Reactor, energy conversion system and other ancillary systems required in a pulsed power plant.

The analysis of interactive μCF-ICF converges on modelling parameters which determine the overall energetic viability of the energy systems based on each of the approaches. This entails an examination of the technological

aspects of a μCF-ICF system as well as an analysis of the effects of elevated density and temperature on muon catalyzed fusion reaction processes.

Analytic models will be used to extrapolate μCF reaction rates at elevated densities, for processes relevant to both approaches. Since there is no experimental data with which to compare these models, "order-of-magnitude" calculations are used.

3.2.1 Introduction to μCF Triggered Spark Ignition

The notion of muon catalyzed fusion reactions heating the centre of a solid core deuterium-tritium pellet to induce spark ignition was first suggested by Tan[85]. A schematic diagram of this approach is provided in Figure 3.1. Firstly, a deuterium-tritium pellet is lowered into a ICF blast chamber; then, a compression pulse is applied to the pellet, while a pulse of muons is injected into the pellet. The muon pulse is tailored such that the muons are preferentially deposited in the middle of the pellet where the spark ignition will occur. Stopping of muons in the middle of the pellet could be enhanced by surrounding the core of the deuterium-tritium pellet with a higher Z material to moderate the incoming muon pulse.

When muons are deposited into the centre of the deuterium-tritium pellet they initiate muon catalyzed reactions which generate 14.1 MeV neutrons and 3.5 MeV alpha particles. If the muon induced fusion alpha particles can heat fuel with a areal density of $\rho_s r_s \approx 0.22$ to the deuterium-tritium ignition temperature $T_{ign} \approx 4$ keV, then μCF triggered spark ignition is possible. Once spark ignition occurs, this concept functions identically to the ICF scheme outlined in Section 2.3.

The primary advantage of μCF triggered spark ignition over conventional spark creation by converging shock waves is the decreased significance of compression instabilities. The presence of hydrodynamic instabilities severely reduces the probability of a spark ignition occurring; hence, spark region creation by convergent compression shocks requires stringent symmetry. The hydrodynamic stability problem is the central theme of current ICF research and there is no assurance of a viable solution. Since muons act independently to generate alpha particles, using muons as the spark initiator greatly reduces the effect of the instabilities.

The main concerns in Tan's μCF triggered ignition concept are the volume in which muons must be deposited, and the feasibility of obtaining a sufficient number of muon induced fusion reactions to heat the fuel to the ignition temperature. Shortly after Tan published his ideas on μCF triggered spark ignition, Hincks et al.[86] criticized Tan's concept for the following reasons:

1. The formation rate of muo-atoms, a critical link in the catalyzing chain, was judged to be too slow at temperatures approaching the deuterium-tritium ignition temperature.
2. The stopping of muons in a small ICF pellet is very difficult.
3. The timing of μCF processes, which are limited to 2.2 μs, is incompatible with the compression time of an ICF pellet, which is less than 100 ns.

Seifritz and Goel[42] also examined Tan's scheme and concluded that μCF would not significantly influence the overall energy gain of an ICF pellet.

1. A pulse of muons is injected into a deuterium-tritium pellet (shown here with a tamper and an ablator) simultaneously with the application of an ablatively driven compression pulse.

2. The spark ignition condition is attained by μCF alpha particle heating of the central core of the compressed solid pellet.

3. The entire volume of deuterium-tritium fuel ignites and generates thermonuclear energy until the pellet dissembles.

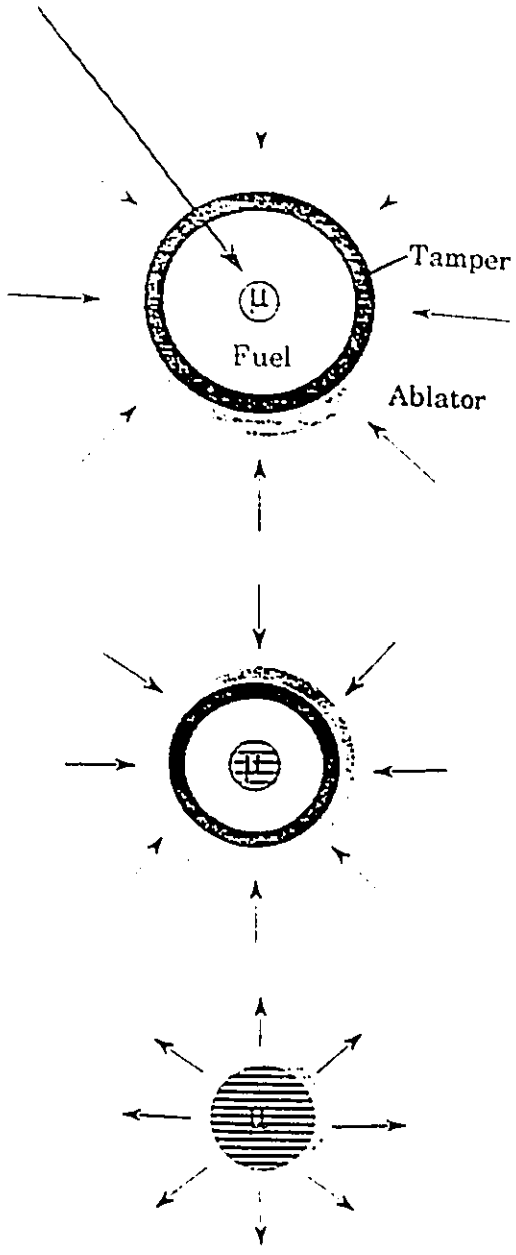

Figure 3.1 : Schematic of the μCF triggered ignition concept.

All of these papers are deficient in that they did not attempt to quantify the muon catalyzed fusion processes in the temperature and density ranges for ICF-like compression of deuterium-tritium. A more detailed analysis of the muon catalyzed fusion reaction rates approaching the ignition temperature in an ICF pellet would clarify whether muons could spark ignite a compressed pellet, and determine the energy costs to generate and deliver the requisite number of muons.

3.2.2 Introduction to High Density μCF

The second approach to μCF-ICF symbiosis considered in this work, the reaction rate enhancement of muon catalyzed fusion processes in a high density environment, is illustrated in Fig. 3.2. Here, a deuterium-tritium fuel pellet is compressed to an elevated density and then injected with muons. The determinant condition for the energetic viability of this scheme is the creation of an environment which will yield a long μCF reaction chain length and an overall energy gain within the hydrodynamic lifetime of the compressed fuel pellet.

Basically this scheme involves an deuterium-tritium pellet implosion; an energy system based on this approach will undergo the same primary course of events as an ICF scheme, except that a beam of moderated and focused muons are injected just at the average peak density of the pellet.

The idea of μCF in explosively compressed deuterium-tritium was initially alluded to by Jones[60] in the seventies. Since that time, there have been several studies of high density μCF reaction rate parameters and energy viability, including work by Kumar and Sahin[77], Menshikov and Somov[13],

1. A deuterium-tritium pellet (shown here with an ablator jacket) is compressed by means of an ablatively or explosively driven compression.

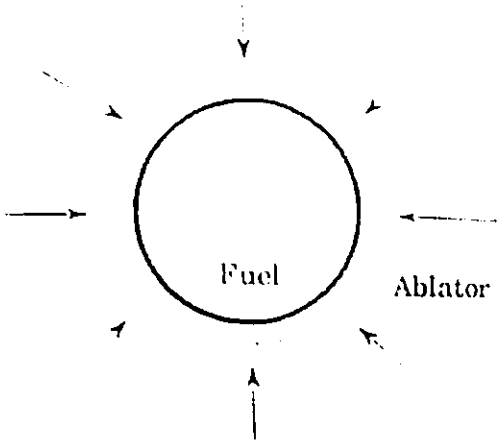

2. Muons are injected into the pellet just as the peak average density is reached.

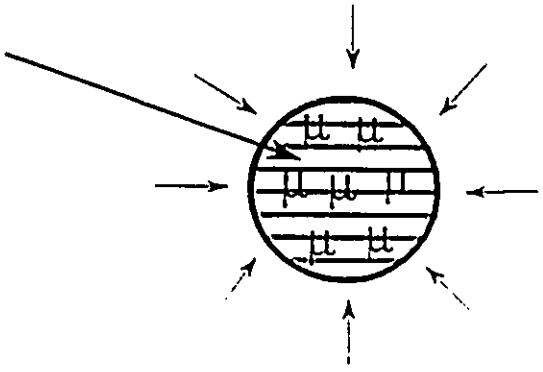

3. The μCF heated pellet disassembles.

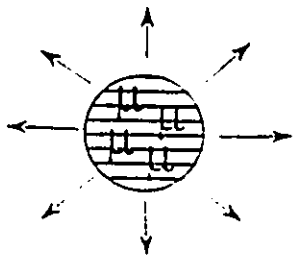

Figure 3.2 : Schematic of the high density μCF approach.

Takahashi[88] and Harley and Rafelski[24,87]. While each of these works made some contributions to the understanding of μCF processes at high density, none delved far enough into high density and temperature muon catalyzed fusion mechanisms to give convincing arguments for μCF-ICF synergism viability.

As in the μCF triggered ignition approach, an understanding of the temperature and density dependence of muon catalyzed fusion processes is key in determining the viability of using high density deuterium-tritium fuel and muons in an energy system.

3.3 Characteristics of a μCF-ICF Energy System

Figure 3.3 shows a schematic diagram of an energy production system based on a generic combination μCF and ICF technologies. The energy system is divided into the following components:

1. The compression driver.
2. The muon production, collection, moderating, focusing and injection devices.
3. The reactor, which includes the tritium breeding blanket, the blast chamber, the fuel pellet injectors, and the energy recovery and conversion facilities.

The muon production component and the compression driver component are characterized by E_{muon} and E_{driver}, their respective direct energy requirements, and also η_μ and η_d, their respective efficiencies in utilizing electrical energy. Analogously, the reactor component is characterized by the

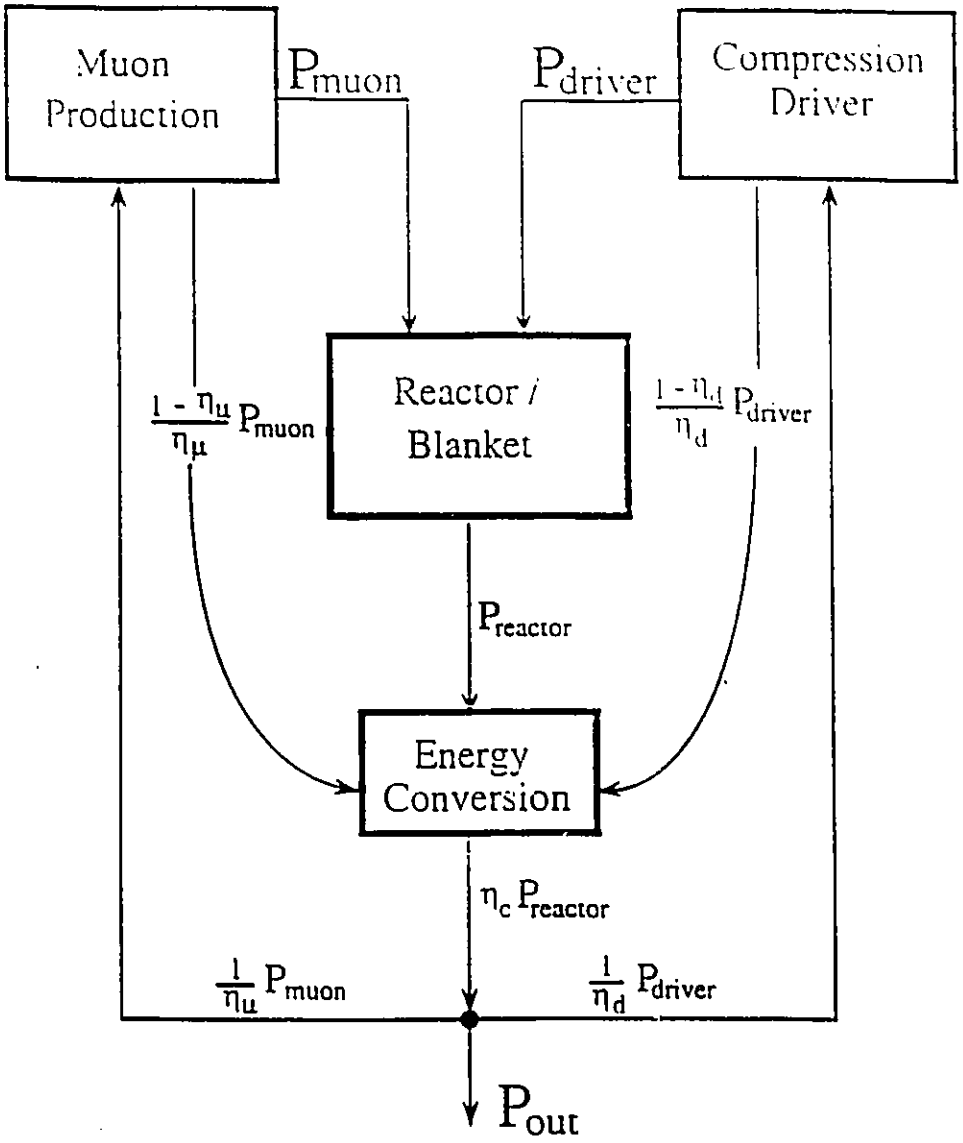

Figure 3.3 : An energy flow schematic of a general μCF-ICF energy system. Here P_{muon}, P_{driver}, $P_{reactor}$ and P_{out} represent power flows.

energy created within the reactor component represented by E_{fusion}, and the average conversion efficiency η_c.

In deuterium-tritium fusion, most energy is generated in the form of neutron kinetic energy, which can only be collected in a blanket as thermal energy. Thermal energy is then converted to electricity by a steam or gas turbine. Direct conversion of some of a pellet's blast energy may be possible, which would enhance the conversion efficiency. However, direct conversion of the charged particle energy fraction could play only a small role, and would probably not warrant the extra trouble and cost of installing direct energy converters within the blast chamber.

Recycling of the waste energy from the muon production and the compression driver components is included in Fig 3.3. Muons will be produced mainly by accelerated particles striking a solid target, as discussed further in Section 4.2. Energy not channelled into creating muons will heat the target as well as supporting material. Some of this heat can be recovered using a circulating coolant.

The compression driver may be a particle beam, a laser, or a chemical explosive. Waste thermal energy from the driver process can also be extracted and sent to a central thermal conversion unit.

3.4 μCF-ICF Energy System Approach Evaluation

In order to determine the optimal operating conditions for a μCF-ICF energy system, using either of the outlined approaches, expressions for the energy gain during the burning of a single deuterium-tritium pellet are

developed. From the generalized μCF-ICF energy system depicted in Fig. 2.4, and the energy gain expressions in Section 2.2.1, the single pellet energy gain in a μCF-ICF energy system is

$$G = \frac{E_{out}}{E_{in}} = \eta_c \left[1 + \frac{E_{reactor}}{\frac{E_{muons}}{\eta_\mu} + \frac{E_{driver}}{\eta_d}}\right] \tag{3.1}$$

where energy E is the integrated power delivered to or generated by the fuel pellet during the reaction time τ_r.

The viability of each of the approaches depends on the values of the parameters in Eq. 3.1. Following discussion of some of the technological requirements of a μCF-ICF energy system in Chapter 4 and discussion of key muon catalyzed fusion processes at elevated densities and temperatures in Chapter 5, the energetic viability of each approach is examined in Chapter 6.

CHAPTER 4

CRITICAL ASPECTS OF A μCF-ICF ENERGY SYSTEM

The components common to both μCF-ICF Energy Systems outlined in Chapter 3 are:

1. A compression driver that can generate an elevated density in a solid deuterium-tritium fuel pellet with minimum input energy.
2. A muon source that can deliver a very short duration pulse of muons into a very small volume of fuel.
3. A blast energy recovery system that will collect the energy of the exploding pellet and convert it to a useable form.

This chapter will discuss the issues surrounding each of the above components with a focus on their relevance to the overall energy gains of the two μCF-ICF energy systems.

4.1 High Density Attainment

In order to understand the general energetic and technological implications of fuel compression, it is important to determine the following:

1. the type of compression driver,
2. the fuel pellet design,
3. the driver energy required to compress to a given average fuel density of ϕ x LHD,
4. the optimal pressure pulse shape for compression of a spherical deuterium-tritium fuel pellet,
5. the compression driver power required,
6. the compression driver duration and
7. the energetic efficiency of the compression driver.

This analysis will assume ideal conditions. Phenomena such as compression driven instabilities and energy transfer inefficiencies at the compression driver-fuel pellet interface are not explicitly considered.

4.1.1 Compression Driver Type

A pressure pulse applied to compress a material may or may not be temporally shaped. By coating deuterium-tritium fuel pellets with a chemical explosive, a step, or unshaped, pressure pulse is generated when the explosive is ignited. The step pressure generated by a chemical explosion is limited by the energy of chemical bonds broken and cannot exceed 100 GPa.

If an ablative material coating is used, a temporally shaped pressure pulse can be obtained with a temporally shaped laser or ion beam. A thin surface layer is heated so vigorously by the beam that it "blows off" and generates an inwardly moving pressure wave by the rocket effect. The magnitude of the pressure wave, the velocity of the blow-off material, and the temperature at the surface are dependent upon the intensity of the energy

deposited at the body's surface. With maximum laser intensities reaching 10^{17} W/cm^2 and blow-off velocities of 10^8 cm/s, pressures of up to P = 10^6 GPa can be obtained, which can be utilized to achieve densities of over 1000 x LHD in a spherically convergent compression[46].

4.1.2 Fuel Pellet Design

The top diagrams in Figures 3.1 and 3.2 illustrate the basic fuel pellet designs for each of the approaches to a μCF-ICF energy system. In the μCF triggered spark ignition approach, the pellet design will be very much like a standard ICF pellet, with a tamper surrounding the central solid deuterium-tritium volume and an ablation or explosive layer surrounding the tamper. For the μCF triggered ignition approach, an additional feature is the high Z shell in the centre core of the pellet which will surround the spark region. This inner shell will slow incoming muons and ensure that they are preferentially stopped in the pellet centre.

It is anticipated that the high density μCF pellet will be much larger than the triggered ignition pellet because the operating temperature of μCF will be lower than for standard fusion, therefore more fuel is required in order to obtain the same output energy. As radiation must be allowed to escape, and also to reduce compression energy costs, there is no tamper on the high density μCF pellet. An ablation or explosive layer surrounds the solid fuel sphere.

4.1.3 Material Compression

Material mechanical stress limitations constrain the maximum static compression of deuterium-tritium to densities less than 2 or 3 times LHD. Such a maximum static compression requires a diamond anvil press where

pressures up to 50 GPa can be sustained[89,90]. Due to technical problems envisaged in compressing sufficient volumes of deuterium-tritium in such a device, it is not considered promising for a possible reactor environment. However, a diamond anvil could be used to perform experiments to confirm the propensity for enhanced μCF reactions as density increases[91]. In order to achieve higher densities, a dynamic compression must be contemplated.

The energy required to compress deuterium-tritium fusion fuel to an elevated density will depend upon the resistive forces within. The energy deposited in the pellet by the compression driver will transform into internal energy and kinetic energy of the molecules, atoms, ions and electrons within the fuel pellet. The fuel constituents' relative fractions will depend upon the temperature and density of the fuel, as discussed in Appendix A.

The total energy within the pellet at the end of an applied pressure pulse will be

$$E(\phi,T) = E_i^P(\phi) + E_e^P(\phi) + E_i^K(\phi,T) + E_e^K(\phi,T) , \qquad (4.1)$$

where $E_i^P(\phi)$ and $E_e^P(\phi)$ represent the stored potential energies and $E_i^K(\phi,T)$and $E_e^K(\phi,T)$ are the kinetic energies of an assemble of molecules, atoms, ions (subscript i) and free electrons (subscript e). The resistive pressure of the pellet to any applied pressure is then

$$\begin{aligned} P(\phi,T) &= \left(\frac{dE}{dV}\right)_T \\ &= P_i^P(\phi) + P_e^P(\phi) + P_i^K(\phi,T) + P_e^K(\phi,T) , \end{aligned} \qquad (4.2)$$

where V is the specific volume, $P_i^P(\phi)$ and $P_e^P(\phi)$ represent the internal pressures and $P_i^K(\phi,T)$and $P_e^K(\phi,T)$ the kinetic pressures of the assemble of molecules, atoms, ions and free electrons.

The potential energy contributions of the possible mixtures of deuterium and tritium molecules, atoms and ions is very complex. Indeed much is unknown about the many-body interactions among the various possible constituents to be encountered at elevated densities. However, in the following analysis it will be assumed that the kinetic pressure from the ideal gas approximation or the resistive pressure of degenerate electrons, or a combination of both, will provide conservative estimates of the energy required to overcome the internal energy.

The ideal gas model can be used to describe the kinetic pressure for molecules, atoms, ions and free electrons. For a fully ionized plasma of deuterium-tritium, the kinetic pressure is

$$P^K \sim 16\,\phi\,T \ (GPa) \ , \tag{4.3}$$

where T is the temperature in eV.

From Appendix B, electrons are considered degenerate when

$$T_e < 5.1\,\phi^{2/3} \ \ (eV) \ , \tag{4.4}$$

and the degenerate electron pressure is

$$P_{fermi} = \frac{2}{5} E_f N_0 \phi \sim 16.3\,\phi^{5/3} \ \ (GPa), \tag{4.5}$$

Compression along the density-temperature line dividing electron non-degeneracy and electron degeneracy is optimal. Along this compression route, the ideal gas model may be assumed, and the energy to compress a volume V_0 of fuel to a density ϕ in LHD units is the degenerate electron energy of the volume given by the following expression:

$$E_{compression} = E_d \phi^{2/3} V_0 N_0 \sim 0.17\,(MJ)\,\phi^{2/3} r_0^3\,, \tag{4.6}$$

where E_d = 5.1 eV and r_0 is the fuel volume radius in cm.

This model only breaks down at low temperatures where the degenerate electron or ideal gas models do not apply, for example, for solid deuterium-tritium (T = 20 Kelvin, ϕ = LHD) where the true resistive pressure is represented by

$$P_o = \rho_o c_s^2 \sim 0.8 \quad (GPa)\,. \tag{4.7}$$

Here, ρ_o = g/cm^2 is the mass density at LHD and c_s, the sound speed in solid deuterium-tritium at LHD, is approximated using the following solid deuterium sound speed[92]:

$$c_s \sim 2.0 \times 10^5 \quad (\frac{cm}{s})\,. \tag{4.8}$$

The degenerate electron gas approximation overestimates this initial pressure at low temperatures and densities. The degenerate electron or ideal gas models along the compression route can be used once electrons become free, i.e., unbound to molecules or atoms, by pressure or temperature ionization.

4.1.4 Explosive Compression

In order to analyze an explosive compression, consider Fig. 4.1, which depicts a slab of deuterium-tritium at LHD impinged on one side by a very strong constant pressure. The strong pressure gradient at the surface will generate a shock front that moves into the material. A shock front will move with a velocity u_s and partition the material into a compressed side and an undisturbed side. The mass density, pressure, specific volume, and temperature are represented by ρ, P, V and T, respectively. Subscripts 0 and 1 denote the undisturbed and compressed sides. The pressure P_1 is the pressure of the compression driver P_d. As the shocked material is compressed, it will be set into motion with a velocity u_p. The equations for conservation of mass and momentum across the shock front are:

$$\rho_o u_s = \rho_1 (u_s - u_p) \tag{4.9}$$

$$P_d - P_o = \rho_o u_s u_p \tag{4.10}$$

For most materials, the following linear relation between the shock speed u_s and the particle speed u_p in the shocked region can be assumed[92],

$$u_s = c_s + s u_p \tag{4.11}$$

and therefore the density increase, $\phi = \rho_1/\rho_o$, can be calculated by

$$\phi = \left(\frac{1}{s} + \frac{P_o}{2P_d}\right) - \sqrt{\left(\frac{1}{s} + \frac{P_o}{2P_d}\right)^2 - \frac{1}{s^2}} \; . \tag{4.12}$$

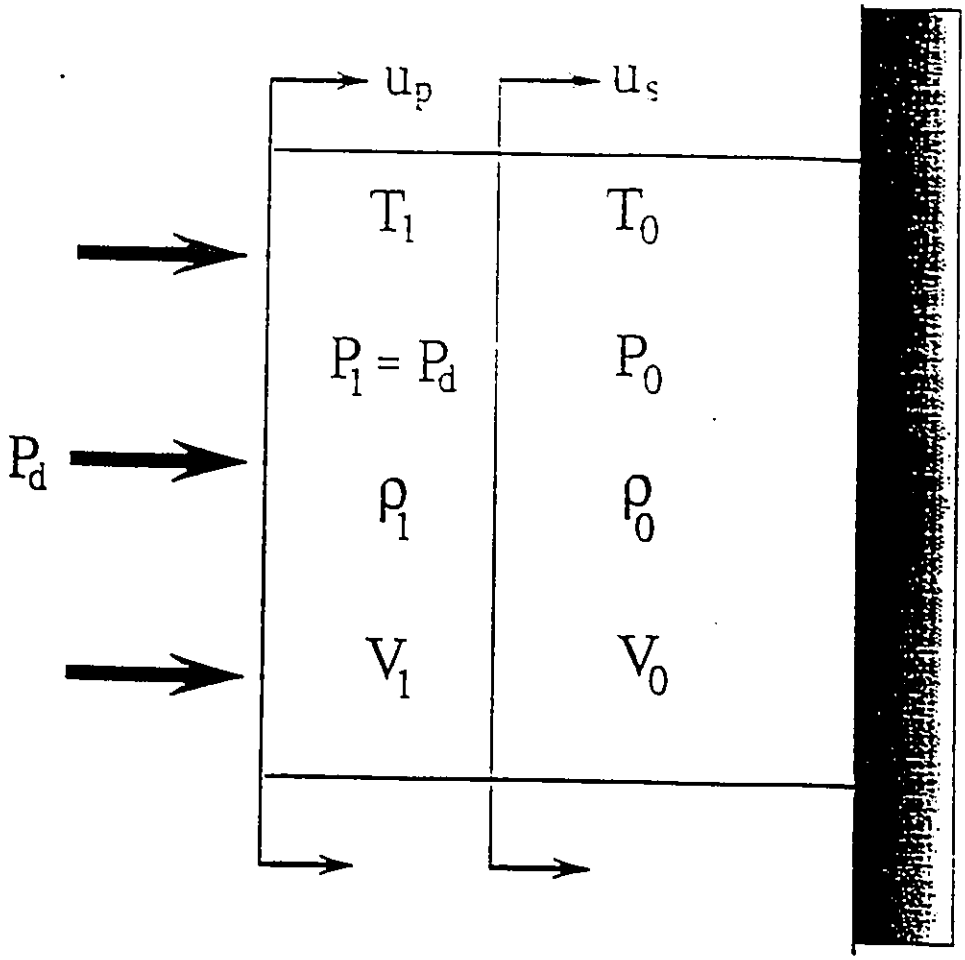

Figure 4.1 : Depiction of a strong pressure pulse generating a shock wave in a solid slab. Here T is temperature, P is pressure, ρ is mass density and V is the specific volume where the subscript 0 represents the unshocked region and 1 represents the post-shocked region. P_d is the driver pressure at the slab's surface.

As the driving pressure P_d, increases it can be seen from Eq. 4.12 that the density increase will saturate to $\phi = 1/s$, where

$$s = \frac{\gamma - 1}{\gamma + 1} . \tag{4.13}$$

and γ is determined by

$$\gamma = \frac{c_p}{c_v} , \tag{4.14}$$

the ratio of specific heats. The ideal gas or degenerate electron gas value of $\gamma = 5/3$ leads to a maximum density increase of $\phi = 4$.

A constant strong shock compression will significantly heat the post-shocked material and the temperature calculated using the ideal gas model (note: N_1 has units particles per volume) is

$$E^K = kT_1 = \frac{P_d}{N_1} . \tag{4.15}$$

An explosive pressure pulse, like one generated from a chemical charge implosion or by the impact of a large accelerated mass, will compress material as described above. For strong shock compressions, accounting for the possibility of a single shock reflection, density increases above 10 times LHD are not likely and the temperature rise during these compressions will be significant. Experimental compression of frozen deuterium with explosives and impact pressure devices yields the following rough density-temperature relationship during compression[93],

$$\frac{T}{T_o} \sim \left(\frac{\phi}{\phi_o}\right)^{4.6} . \tag{4.16}$$

The size of the exponent shows how far this compression is away from the ideal isentropic case. For an ideal gas, the exponent would be γ-1 = 2/3.

It is clear that a constant pressure pulse is not efficient for compressing fuel because the compression magnitude is limited and much of the applied energy will be diverted into undesirable heating.

4.1.5 Isentropic Compression

In order to maximize the final density attained, it is important that the driving energy be channelled into overcoming the internal pressure and not lost to kinetic energy of fuel particles. In other words, the entropy of the compression should be kept at a minimum. An isothermal compression is impossible in a dynamic compression because of the strong pressure gradients created, however an isentropic compression is attainable.[37,38,46,94,95]

Consider the following thermodynamic relation:

$$T dS = c_v dT + T(c_p - c_v)\frac{dV}{V} = 0 , \qquad (4.17)$$

where c_p and c_v are the specific heats of a material. Setting the change in entropy to zero leads to the isentropic relationship between the temperature and the specific volume of the material in question. The specific volume is related to the density by the following relationship:

$$\frac{V}{V_o} = \frac{1}{\phi} \qquad (4.18)$$

The isentropic temperature-density relation is then

$$\frac{T}{T_i} = \phi^{<\gamma>-1} = \phi^{2/3} \tag{4.19}$$

where T_i is the temperature at the beginning of the isentropic process and the value of $<\gamma>$ is the logarithmic average of $\gamma(\phi)$ over the density range encountered,

$$<\gamma> = \frac{\int_1^{\phi} \frac{\gamma(\phi')\, d\phi'}{\phi'}}{\ln(\phi)} . \tag{4.20}$$

It is true that γ will depend on the physical structure of the fuel and may change dramatically for various phase transitions possible, however it is thought that the average value of γ will be close to the ideal gas and degenerate electron gas value. Therefore a value of $<\gamma> \approx 5/3$ is assumed.

A derivation of the requisite isentropic pressure pulse for isentropic compression of a spherical deuterium-tritium fuel pellet follows.

The time history of a pellet's surface is illustrated in Fig 4.2. The distance of the pellet's surface from the pellet's centre is represented by r and the velocity at which the surface moves towards the pellet's centre is u. The radius of the pellet will then follow

$$\frac{dr}{dt} = -u \ . \tag{4.21}$$

Since u is a linear function of the shock speed in the pellet material, u_s (see Eq. 4.11), Eq. 2.68 may be used to express the velocity as

$$u \sim \kappa\sqrt{T + \phi^{2/3}} \ . \tag{4.22}$$

Using the isentropic density - temperature relationship from Eq. 4.18, and

$$\phi \propto r^{-3} \ , \tag{4.23}$$

the radius of the pellet can be described by

$$\frac{dr}{dt} \propto -u \ll r^{-\frac{3(<\gamma> - 1)}{2}} \ . \tag{4.24}$$

Solving the above with the following ideal boundary conditions:

1. $r(t=0) = r_o$,
2. $r(t=t_c) = 0$,

where t_c is defined as the compression time, yields the following expression for temporal history of the pellet radius,

$$r = r_o\left(1 - \frac{t}{t_c}\right)^{\beta} \tag{4.25}$$

where

$$\beta = \frac{2}{3<\gamma> - 1} \ . \tag{4.26}$$

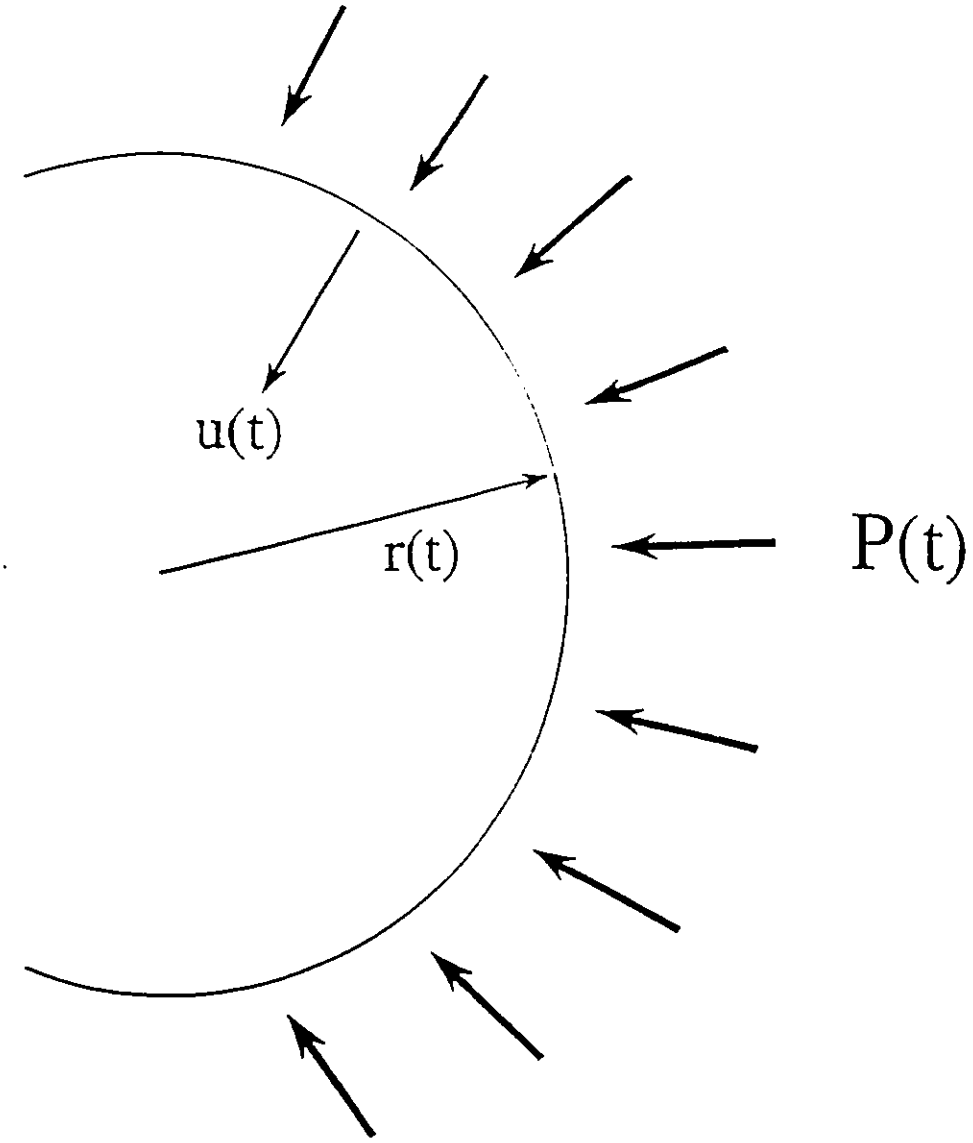

Figure 4.2 : Depiction of an isentropic compression of spherical pellet. Here r(t) is the radius of the spherical pellet, u(t) is the pellet surface velocity and P(t) is the applied surface pressure.

Using Eq. 4.25, the pellet's surface velocity is

$$u(t) = u_i \left(1 - \frac{t}{t_c}\right)^{\beta - 1} \tag{4.27}$$

directed towards the pellet centre, where u_i is the initial velocity.

Recalling that the ideal gas model temperature-pressure relationship is used to determine the pressure pulse shape, and the total internal energy is calculated from the degenerate electron energy, the pressure pulse applied to achieve the ideal isentropic compression is

$$P(t) = P_i \left(1 - \frac{t}{t_c}\right)^{-(\beta + 2)}, \tag{4.28}$$

where P_i is the initial pressure of the compression driver pulse. The power density, I(t), required to achieve the pressure necessary for an ideal isentropic compression is

$$I(t) = P(t)\,u(t) = \frac{P_i u_i}{1 - \frac{t}{t_c}}. \tag{4.29}$$

The total energy spent applying an isentropic pulse, not including the compression efficiency, is

$$E_{isentropic} = \int_0^{t_b} W_{isentropic}(t)\,dt \tag{4.30}$$

where

$$\begin{aligned} W_{isentropic}(t) &= 4\pi r^2(t)\,P(t)\,u(t) \\ &= 4\pi r_o^2\,P_i u_i \left(1 - \frac{t}{t_c}\right)^{2\beta - 3} \end{aligned} \tag{4.31}$$

is the work performed on the pellet and t_b is the time that the pressure pulse is applied. Substituting $\langle\gamma\rangle \approx 5/3$ into Eq. 4.26 gives $\beta \approx 1/2$ and evaluation of Eq. 4.30 yields

$$E_{isentropic} \approx 4\pi r_o^3 P_i \frac{t_b/t_c}{1 - t_b/t_c} . \tag{4.32}$$

Using the following expression for the initial velocity with Eqs. 4.27 and 4.28 into 4.32,

$$u_i \approx \frac{c_s}{\sqrt{P_o}} \sqrt{P_i} , \tag{4.33}$$

and using $P_0 \approx 0.8$ GPa and $c_s = 2.0 \times 10^5$ cm/s (Eq.4.8) yields

$$E_{isentropic} \sim 1.9 r_o^3 \sqrt{P_i} I_{max}^{1/3} \quad (MJ) , \tag{4.34}$$

where P_i is the initial pressure of the compression pulse in GPa and $I_{max} \approx I(t_b)$ is the maximum power density applied at $t = t_b$ in TW/cm^2.

4.1.6 Energy Requirement for Isentropic Compression

It is assumed that the energy in the isentropic pulse will be converted primarily into internal energy of the deuterium-tritium fuel, which has been assumed to be the energy of the degenerate electrons. The pressure pulse energy needed to compress material to an average density of ϕ is expressed by Eq. 4.6. Substitution of this expression into Eq.4.34 yields the following equation for the maximum density obtainable with a compression power source having a maximum intensity of I_{max} in TW/cm^2 and an initial pressure of P_i in GPa,

$$\phi \sim 2.0 P_i^{3/4} I_{max}^{1/2} , \tag{4.35}$$

Maximizing the density enhancement in an isentropic compression requires maximization of the peak power intensity I_{max} or the initial pressure of the compression pulse P_i, or both. The largest existing compression driver, the NOVA laser at Lawrence Livermore National Laboratories in the US, can generate a peak power nearing 10^5 TW/cm^2 (Ref.49), but efficiencies are low. Lasers and ion beams which will deposit laser or ion energy with focused peak power intensities up to 10,000 TW/cm^2 with maximum efficiencies can be expected in the near future[46,47].

With limited values of I_{max}, higher densities are achieved by using larger initial pressures. This results in a higher final fuel temperatures and also requires much more energy in the compression pulse. A high initial pressure in the compression pulse will behave as a strong shock and generate an initial temperature, immediately before the isentropic pressure pulse begins to compress, of

$$T_i \sim \frac{P_i}{N} . \tag{4.36}$$

Using N = 4.81 x10^{22} cm^{-3} for deuterium-tritium and Eq.4.35 yields the following expression for the initial temperature:

$$T_i \sim \frac{\phi^{4/3}}{21\, I_{max}^{\,2/3}} \quad (eV) \tag{4.37}$$

From Eq.4.18, the final temperature of an isentropically compressed spherical fuel pellet may be calculated as.

$$T_f \sim \frac{\phi^2}{21\, I_{max}^{\,2/3}} . \tag{4.38}$$

Limitations of the isentropic compression model include the following:

1. An ablative pulse that exactly fits the pulse shape desired may not be technically feasible. A series of pulses which fit the desired pulse in a step wise fashion are technically more realistic.
2. It is thought that irregularities in the fuel pellet surface and/or the pressure pulse over the pellet's surface of more than 1% cannot be tolerated. Also, hydrodynamic instabilities may disrupt the compression of the pellet and effectively reduce the final pellet density.

From Eq. 4.35, 4.37 and Eq. 4.18, it is evident that it is possible to have low final fuel temperatures after large isentropic compressions with reasonable driver power intensities. Table 4.1 presents some likely isentropic compression scenarios.

4.1.7 Compression Timing

The duration of an ideal isentropic compression can be calculated from

$$t_c = \frac{r_o}{u_i} \sim 7087\, r_o \frac{I_{max}^{1/3}}{\phi^{2/3}} \quad (ns)\,. \tag{4.39}$$

Typical values of given in Table 4.1.

4.1.8 Compression Efficiency

The efficiency at which a compression driver can take electrical energy and transform it to internal energy of the compressed deuterium-tritium is an important part of the energy balance of an energy system. An analysis of the

o (LHD)	E_c/r_0^3 (MJ/cm^3)	I_{max} (TW/cm^2)	P_i (GPa)	T_i (eV)	T_f (eV)	t_c/r_o (ns/cm)
10	0.8	100	0.40	0.05	0.22	7086.0
		1000	0.09	0.01	0.05	15266.0
100	3.7	100	8.55	1.03	22.10	1526.6
		1000	1.84	0.22	4.76	3289.0
		10,000	0.40	0.05	0.98	7086.0
1000	17.0	1000	39.67	4.76	476.19	708.6
		10,000	8.55	1.03	102.59	1526.6
		100,000	1.84	0.22	22.10	3289.0

Table 4.1 : Characteristics of an isentropic compression using Eqs. 4.35, 4.37, 4.38 and 4.39. E_c/r_0^3 is the energy density of degenerate electrons (Eq.4.6) in the compressed deuterium-tritium, I_{max} is the maximum power intensity, P_i is the initial pressure of the isentropic pressure pulse, T_i is the temperature generated by the initial pressure pulse, T_f is the temperature after the isentropic pressure pulse reaches the pellet centre and t_c/r_0 is the duration of the isentropic pressure pulse per centimetre of pellet radius.

efficiencies of all processes, from the internal workings of the compression driver, to energy transfer to the fuel pellet is presented here. Based on Table 2.3, the following are typical efficiencies for laser and ion beam drivers in the ICF designs:

1. Heavy Ion Beams $\eta_d = 30\%$,
2. Light Ion Beams $\eta_d = 25\%$,
3. LASERs (KrF) $\eta_d = 7\%$.

The efficiency η_d is assumed to be the ratio of energy stored by degenerate electrons in the fuel pellet at the end of the compression pulse to the electricity supplied to the compression driver during the pulse. For chemical explosives, the efficiencies are unknown but are assumed to be high, with $\eta_d > 0.5$.

4.2 Muon Production Concepts

This section will first give an overview of some of the various muon production methods with a focus upon the energy cost per muon. Then, a system consisting of materials, electric fields and magnetic fields arranged to concentrate a high energy, high velocity phase space muon pulse and focus it into a small fuel pellet will be discussed. The analysis in this section provides insight into the technological requirements of a muon production and injection system.

4.2.1 Muon Pulse Requirements

For the μCF triggered spark ignition concept, a short duration muon pulse must be precisely deposited into a small central spark region which could be less than 0.1 mm in radius. In this scheme it is desirable to have the muons

deposited quickly so that they can heat the pellet core. An approximation to an acceptable pulse duration would be the travel time for a shock wave through the spark region prior to ignition. This time period is estimated to be less than 10 ns.

In the high density μCF concept, it is desirable to deposit muons evenly throughout the deuterium-tritium pellet. Therefore, the muon beam width should correspond roughly to the pellet diameter and the average range of the muons should be less then the pellet's radius. It is possible that this approach could use fuel pellets with greater than 1 cm radius. Hence, focusing of the muon pulse is not as difficult as it is for μCF triggered spark ignition. The muons will be injected into the fuel pellet at the point when the peak average density is achieved. The reaction time for this approach is the disassembly time of the compressed pellet; this is anticipated to be much greater than 10 ns.

Because a shorter, smaller muon pulse will be required, it is evident that the technological effort required for the high density μCF system is much less than for the μCF triggered ignition.

4.2.2 Muon Production Facility Components

Figure 4.3 illustrates the linkage of the following components of the two approaches to a μCF-ICF energy system:

1. LINear ACcelerator and Pion Production Target
2. Pion Converter
3. Muon Damper

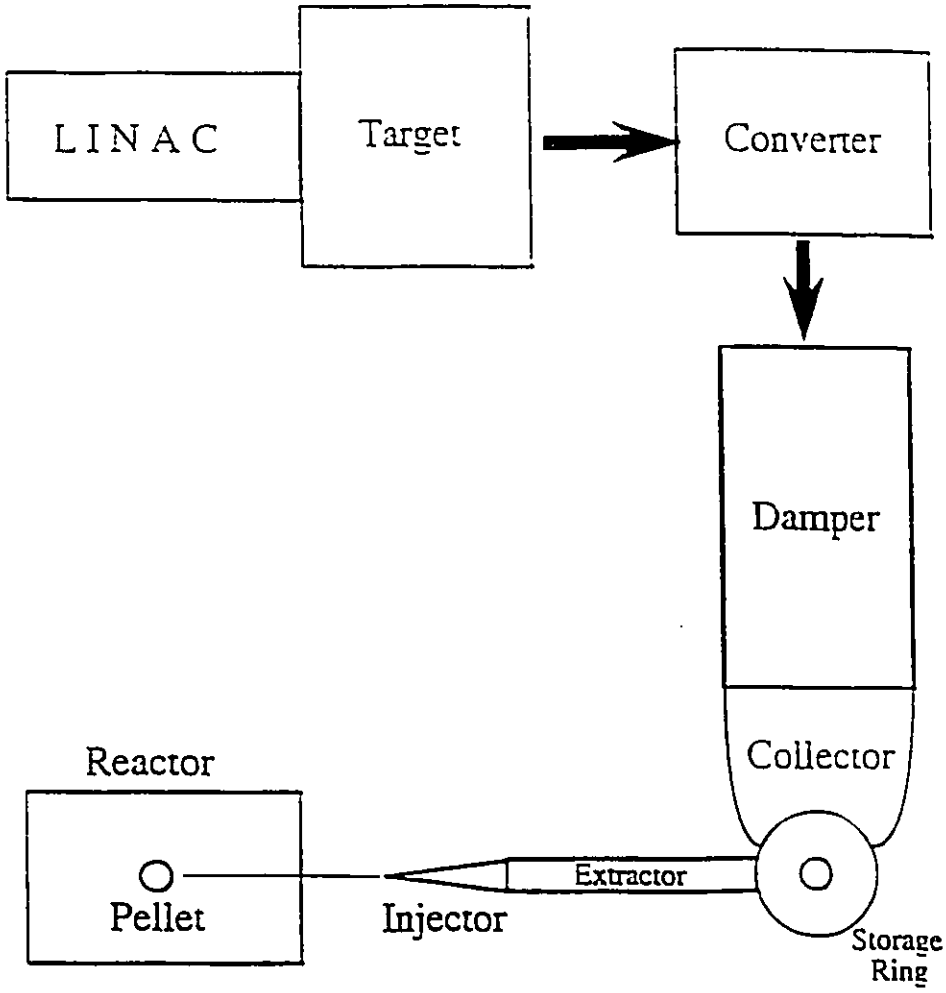

Figure 4.3 : Schematic of the components of a muon production facility.

4. Muon Collector
5. Muon Extractor and Injector.

The following factors must be considered, to evaluate a muon production and injection scheme: the energy cost of a single muon E_μ; the energy efficiency, η_{LINAC}, of creating pions in the LINAC/Target stage; the efficiency of converting pions to muons, $\eta_{convert}$; the probability of muon energy reduction and muon energy compression, η_{decel}; the efficiency of collection of the slowed muons and injection into a muon storage ring, $\eta_{collect}$; and the efficiency of extraction and injection of a muon pulse from the storage ring into a waiting fuel pellet, η_{inject}.

4.2.3 Pion Production

At the present time, muons are most efficiently produced by firing high energy (E > 1 GeV), neutron rich nuclei at neutron rich target material, which leads to the following high energy inelastic scattering interactions between protons, p, and neutrons, n, to produce negative pions:

$$pn \rightarrow pp + \pi^- \tag{4.40}$$

$$nn \rightarrow pn + \pi^- \tag{4.41}$$

Negative pions decay to muons:

$$\pi^- \rightarrow \mu^- + \bar{\nu}_\mu \,, \tag{4.42}$$

The pion decay half-life is about 26 ns.

The real picture is much more complex. The yield of pions from a single energetic particle will depend on a complex interaction of the primary particle with the target nuclei to generate pions and secondary particles. These may

also collide and yield further pions.

The largest cross-section for negative pion creation occurs for neutron-neutron collisions[60]. When pions are created they can be re-absorbed by the surrounding material. Reabsorption by protons is preferred; thus, the target and beam with the highest neutron to proton ratio is best.

Table 4.2 lists estimates of the energy cost of producing a pion by inelastic collisions of accelerated particles, not including the accelerator efficiencies. From this survey, a conservative estimate of the minimum negative pion energy cost is

$$E_{\mu} \sim 4\,GeV \tag{4.43}$$

The accelerator efficiency, the ratio of energy in emergent pions to the electrical energy used by the particle accelerator, will have a range of $\eta_{LINAC} \approx$ 0.6 - 0.9. The lower bound is possible with current state-of-the-art technology[96] and the upper bound is likely to be feasible as a result of future technological advances[97].

4.2.4 Pion to Muon Conversion

Containment of energetic pions until they decay into muons is a significant technological problem. In a pion converter, pions are confined to an evacuated volume by a strong magnetic field. This allows them to decay to muons with little chance of absorption by surrounding material. Once all the pions have decayed to muons, the muons are directed to the muon decelerator. The probability that the pions will survive the conversion phase has been estimated by various sources, as listed in Table 4.3.

Reference	Value (GeV)	Comments
Petrov and Shabelski[98]	≈ 2	1 GeV triton beam on tritium
	≈ 4	1 GeV deuteron beam on Li or Be
Takahashi[99]	≈ 4	2 GeV deuteron on Be
Ottewitte[100]	≈ 1	4 GeV deuteron beam on neutron rich target
Chapline and Moir[101]	≈ 4	900 MeV triton beam on tritium
	= 1.8	Colliding 600 MeV triton beams
Shin and Rafelski[102]	2.7	5 GeV proton beams on Be
	3.4	5 GeV proton beam on Pb/Be
Jändel[103]	3.8	3.8 GeV deuteron beam on tritium
Lewis et. al.[104]	280 - 28,000	Proton - anti-proton annihilation
Daniel[105]	3	Proton beam on deuterium-tritium
A.P. Cheplakov et.al.[106]	16.5 ± 1.1	Deuterons on carbon target
	14.8 ± 1.3	Deuterons on beryllium target

Table 4.2 : A survey of the energy cost to produce a negative pion.

Reference	$\eta_{convert}$
Petrov and Shabelski[98]	≈ 0.8
Petrov and Sakhnovsky[107]	0.69 - 0.83
Chapline and Moir[101]	≈ 0.8
Jändel[103]	≈ 0.77

Table 4.3 : A survey of the estimated values of the conversion efficiency of pions to muons, $\eta_{convert}$.

The emergent pion energy range from the LINAC/target stage will depend upon the initial particle energy, the particle type and the thickness of the target. As an example, Fig. 4.4 illustrates Petrov and Shabelski's calculated angular and the energetic distributions of emergent pions from an 800 MeV deuteron beam on a 4 cm radius and 2 m long Be target[98]. The energy peak of the pion flux is about 75 MeV but some pions will have energies up to almost 500 MeV. The angular spread of the pions coming out of the target will be fairly wide and a strong magnetic field along the axis of the particle beam is required to confine the pions within the converter. In such a magnetic field, the pions will be confined to a helical path with radius

$$r_{\pi} = \frac{c\,p_{\perp}}{e\,B} \tag{4.44}$$

where $p_{\perp}$ is the pion momentum perpendicular to the magnetic field, c is the speed of light and e is the electronic charge. Assuming that $p_{\perp} < 500$ MeV and a cylindrical converter cavity with an average magnetic field B = 10 Tesla, the minimum radius of the converter cavity such that the pion trajectories will not touch the converter walls is $R_{convert} > r_{\pi} \approx 17$ cm.

Once all pions have decayed to muons, these are transferred by a combination of diverting magnetic fields and electric fields to the mouth of the muon decelerator. The energy range of the muons going into the muon decelerator will be approximately E ≈ 0 MeV - 500 MeV.

4.2.5 Muon Deceleration and Collection

A key requirement of the muon source in a μCF-ICF energy system is the ability to deposit muons into a small volume. High energy muons exiting the pion converter will have an unsuitably long range in deuterium-tritium and

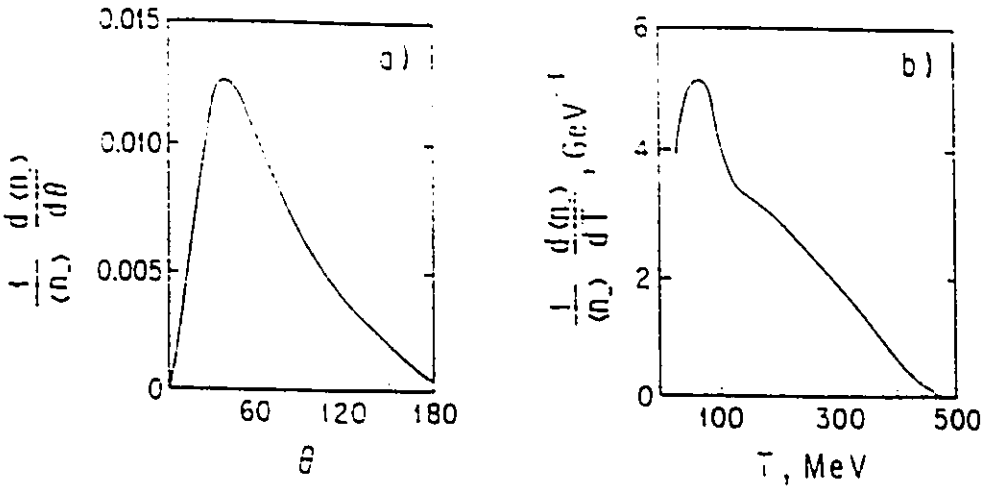

Figure 4.4 : Calculated emergent pion differential angular distribution ($d\langle n\rangle/d\theta$) versus emergent angle θ (a) and the differential energy distribution ($d\langle n\rangle/dT$ versus pion energy T in MeV (b) from a 800 MeV deuteron beam on a 4 cm radius X 200 cm long Be target (taken from Ref.107).

large energy spread for use in either of the outlined μCF-ICF energy system approaches. The created muons within the converter must be slowed and the energy spread must be narrowed to allow for precise spatial deposition.

Reduction of the energy distribution of the muon pulse without unacceptable muon losses is performed by a muon decelerator, which will be characterized by an efficiency η_{decel}. The value of η_{decel} will indicate the fraction of the muons which pass from the convertor, through the energy conditioning phase, to a storage ring where the "high quality" muons are stored waiting to be extracted and injected into a waiting pellet.

The muon decelerator device will consist of a series of thin foils along the axis of an applied magnetic field beginning at the end of the muon converter. As the muon beam exits the convertor, a transverse magnetic field will act as a diverter for low energy muons. The higher energy muons, the fraction not diverted, will be allowed to pass through a thin foil in which their energy will be reduced. On the other side of this foil, subsequent series of foils and diverters will allow for the moderation of the entire muon energy range.

The diverted muons will be collected and inserted into the final section of the decelerator, a gas chamber with a confining magnetic field and an electric field applied across it. In this chamber, the applied fields and the gas will act together to cause the muons to accelerate to a single energy.

4.2.6 Muon Injection

The final consideration in the moderation of muons is the desired energy. Muons are to be injected into a cold, solid deuterium-tritium pellet prior to

compression, or a compressed plasma. In Figure 4.5, energy loss models, described in Appendix D, have been used to plot the muon range versus energy for solid molecular deuterium-tritium and deuterium-tritium plasmas of various temperatures and densities. In both the cold solid and the plasma cases, muon kinetic energies must be efficiently reduced to energies less than 10 MeV, if fuel pellet radii of 0.01 to 1 cm are to be contemplated.

When the muons have attained the desired energy they are collected and stored in a cyclotron ring. Muons can accumulate within the storage ring for a time period of an average muon lifetime. Upon accumulation of the desired number of muons, initiation of an electric field parallel to the cyclotron magnetic field will empty the muon storage ring. The intense slow muon pulse will be focused and directed to the fuel pellet. The efficiency in which muons can be collected and stored in the storage ring is $\eta_{collect}$.

The extraction, focusing and injection of muons from the muon storage device into a fuel pellet will likely present the greatest opportunity for muon losses from the system.

Because of the space charge effect, compensation of the muon beam will be required to focus the intense muon pulse onto the fuel pellet at the centre of a blast shield within the reactor volume[108]. The beam may be compensated by using a low density background gas within the reactor chamber, or by neutralizing the muon beam with tritium ions or positrons.

It is difficult to estimate the efficiency with which a large pulse of muons may be injected into a small pellet volume. A much more detailed analysis of muon focusing and injection is required to estimate realistic values. For the

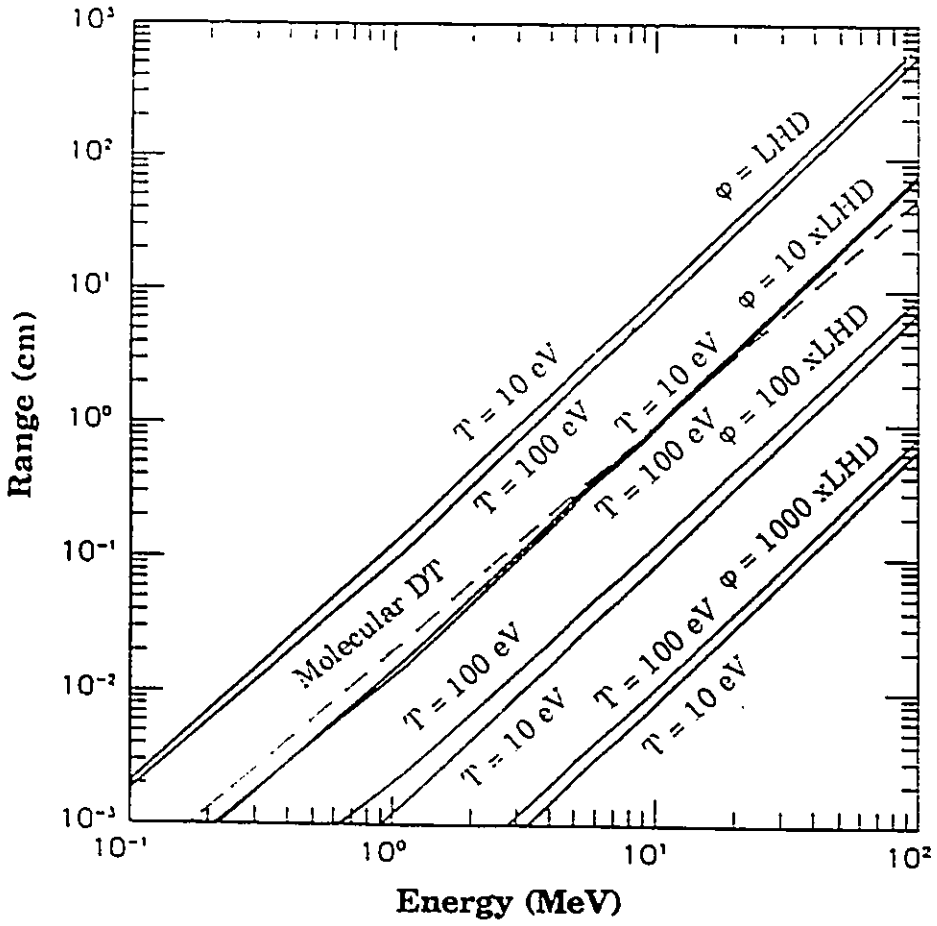

Figure 4.5 : The energy dependent muon range in cold molecular deuterium-tritium (20 Kelvin,LHD) and the muon range in a deuterium-tritium plasma with temperature and densities labelled.

purposes of this study, the limiting values of $\eta_{collect} = \eta_{extract} \approx 100\%$ are assumed. However, energy calculations will leave the muon production related efficiencies as free parameters. Values will only be assumed for the purposes of final calculations, so that the impact of lower, more realistic efficiencies can be examined.

4.2.7 Muon Production Efficiency Summary

The overall efficiency of creating a single muon is

$$\eta_{\mu} = \eta_{condition}\,\eta_{LINAC} \tag{4.45}$$

where

$$\eta_{condition} = \eta_{inject}\,\eta_{collect}\,\eta_{decel}\,\eta_{convert} \cdot \tag{4.46}$$

Upper limit of values of $\eta_{condition} \approx 0.8$ and $n_{LINAC} \approx 0.9$ yield an absolute upper limit value of $\eta_{\mu} \approx 0.7$.

4.2.8 Particle Current Requirement

In each of the outlined approaches, muons must be injected into a fuel pellet from the muon storage ring. The muons can be manufactured prior to injection into the pellet and stored. The particle current required in the LINAC to generate the necessary muon inventory must be determined.

It is assumed that the particle current is constant, the pions and muons travel rapidly through the convertor and decelerator, and the only muon losses in the storage device are due to muon decay. Using a muon pulse duration, into the storage ring, of approximately $\tau_{\mu} \approx 2.2$ μs minimizes both the particle current and the total energy needed. Then, the particle current required in

2.2 μs is

$$I_p \sim \frac{S_\mu}{\eta_\mu} \sim \frac{0.63\,\lambda_\mu N_\mu}{\eta_\mu} \sim 7.0\,N_\mu[10^{14}]\ (A) \qquad (4.47)$$

where $N_\mu[10^{14}]$ is the number muons required x 10^{14}.

4.3 μCF-ICF Reactor Characteristics

In both of the conceptualized approaches to a μCF-ICF energy system, a pulse of energy is generated in the form of an exploding pellet blast and a burst of neutrons. Thus, a conceptual design for a μCF-ICF energy plant will have requirements similar to those for an ICF design, as regards the blast chamber, the tritium breeding blanket, the energy extraction and the energy conversion systems.

Reviewing the latest designs of an ICF plant summarized in Table 2.3, the following represent the optimal values and design characteristics for a μCF-ICF energy system:

1. Liquid Flibe is used as coolant, blast shield and tritium breeding material. Flibe is safe and sufficiently effective for all three of the these purposes[35,36].
2. The first wall, i.e., blast shield, and blanket are constructed of woven carbon fibre and ceramic. This material yields good strength and low neutron activation[54]. At the first wall, liquid Flibe bleeds through the fibre weave creating a layer that vaporizes at the impact of the exploding pellet. The energy absorbed by this layer is removed from the blast chamber long before a new pellet is exploded.

3. The neutron energy multiplication of a Flibe blanket is about 1.15, yielding a total energy $E_f \approx 20$ MeV per fusion (Ref.35).
4. The frequency at which deuterium-tritium pellets are exploded is F = 1 - 10 Hz, and higher rates can be contemplated.
5. The thermal conversion efficiency is $\eta_c \approx 0.4 - 0.5$.
6. The overall electrical output of a fusion power plant is required to be 1000 MW. Therefore, the energy generated from a single deuterium-tritium pellet,

$$E_{pellet} = \frac{1000\ (MW)}{F\,\eta_c} \tag{4.48}$$

results in a required range of $E_{pellet} \approx 200 - 2500$ MJ.

Having established the characteristics of a reactor system, the conditions for energy generation from a single deuterium-tritium pellet, and the viability of the energy system, must be examined.

CHAPTER 5

HIGH DENSITY MUON CATALYZED FUSION

5.1 Introduction

In this chapter, temperature and density dependent muon catalyzed fusion reaction rate models will be developed which can be utilized to evaluate the two previously outlined approaches to a μCF-ICF energy system. The temperatures and densities to be considered encompass the possible conditions necessary for μCF triggered spark ignition as well as those which may lead to a viable pulsed μCF energy system. Muon catalyzed fusion via resonant muo-molecular ion formation as well as μCF processes were previously discussed in Section 2.4; the models introduced in this section are used for temperatures and densities where molecular formation is possible. For both μCF-ICF approaches, it is anticipated that the temperature will be $T > 1$ eV. Accordingly, the temperatures considered in this section range from 1 to 10^4 eV, with fuel densities varying from LHD to 1000 times LHD.

Figure 5.1 illustrates the network of possible muon catalyzed fusion reactions in high density deuterium-tritium fuel. The processes of muon capture to form a muo-atom, muon transfer, muo-molecular ion formation, fusion and muon sticking and regeneration are all important in calculating the efficiency with which a muon can induce fusions in elevated density and

temperature deuterium-tritium. The differences between this high density and temperature μCF network and the one employed in the study of muon catalyzed fusion processes in molecular fuel lie in that: 1) reverse transfer from μd to μt is possible, 2) hyperfine transitions are not important, 3) three body reactions are important, and 4) the break-up of the μdt_{11} muo-molecule is significant.

In the development of analytic models to describe the overall controlling processes, it is assumed that all processes work in a local thermodynamic and hydrodynamic equilibrium, i.e., the local temperature and density are considered relatively stable over the duration of a given reaction. This assumption allows for a point kinetic analysis of the reaction dynamics. In addition, the electron and ion temperatures are assumed to be equal.

Models of the fraction of molecules represented by f_m, the fraction of atoms represented by f_a and the fraction of ions represented by f_i in hydrogenic material are developed in Appendix A. Since μCF depends upon the existence of muo-atoms, the fraction of muo-atoms ionized f_μ is also calculated.

5.2 Muo-atom Formation

As injected muons slow in deuterium-tritium they will be captured by molecules, atoms or ions and form muo-deuterium (μd) and muo-tritium (μt). The specific mechanisms of formation are:

1. molecular and atomic formation,
2. radiative formation and,
3. three-body formation.

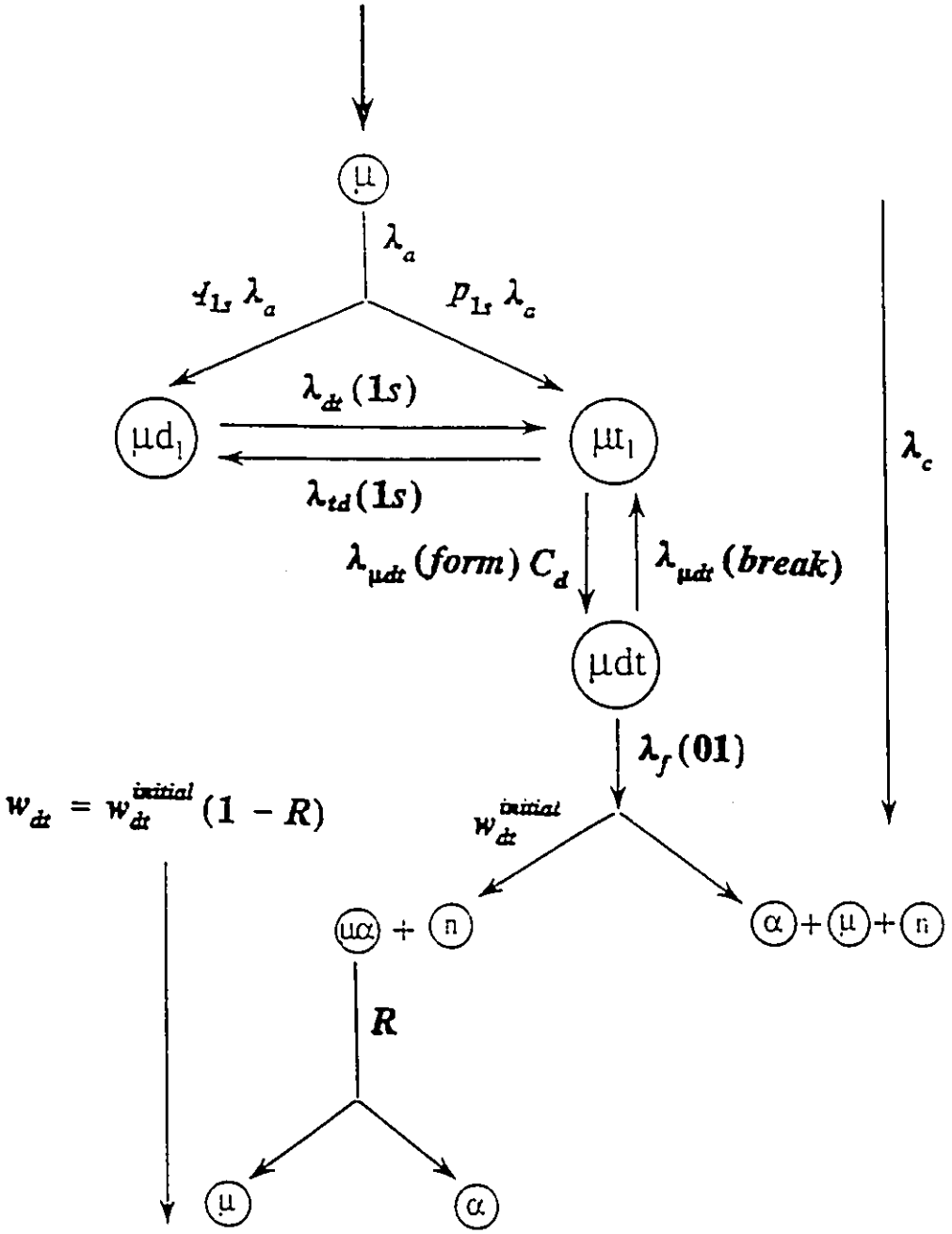

Figure 5.1 : Reaction network for muon catalyzed fusion in a high density deuterium-tritium mixture.

Muo-atom formation reactions through muon-atom interaction,

$$\mu + D \rightarrow \mu d + e, \tag{5.1}$$

$$\mu + T \rightarrow \mu t + e. \tag{5.2}$$

are analogous to the muon-molecule interaction reactions previously discussed in Section 2.4.3.1.. The cross-section for these reactions is approximated by

$$\sigma_{atom} \sim \pi a_e^2 \tag{5.3}$$

where $a_e \approx 0.53$ Å is the electronic Bohr radius.

The reaction rate for atomic muon capture is calculated as $\lambda = \langle \sigma v_\mu \rangle N$ where the atomic density is $N = 4.8 \times 10^{22} \phi f_a$ (cm^{-3}) and f_a is the atomic fraction at temperature T and density ϕ defined in Appendix A. The atomic reaction rate is then calculated as

$$\lambda_a(atomic) \sim 7.5 \times 10^{13} \phi f_a f_\mu \quad (s^{-1}), \tag{5.4}$$

where f_μ represents the fraction of muo-atoms in the ground state.

At elevated fuel temperatures and densities, where ions begin to exist, the following radiative capture reactions can occur:

$$\mu + D^+ \rightarrow \mu d, \tag{5.5}$$

$$\mu + T^+ \rightarrow \mu t. \tag{5.6}$$

The threshold distance of muon capture by an ion can be approximated by

$$r_{imp} \sim \frac{a_\mu I_\mu}{kT} = \frac{a_e I_e}{kT} = \frac{e^2}{2kT} \tag{5.7}$$

where r_{imp} is the minimum distance of approach of the muon, a_μ,I_μ and a_e,I_e are the Bohr orbits and ionization potentials for muo-hydrogen and electro-hydrogen respectively, and kT is the fuel temperature[28,77]. Using this model the rate of radiative muon capture is calculated as,

$$R_{radiative} \sim N_\mu v_\mu \pi r_{imp}^2 N_+ \tag{5.8}$$

where N_+ is the concentration of ions, N_μ is the concentration of muons and v_μ is the muon velocity. The muon velocity is approximately the thermal velocity, therefore,

$$v_\mu \sim \sqrt{\frac{3kT}{m_\mu}} . \tag{5.9}$$

Upon substitution, the radiative muon capture rate becomes,

$$\lambda_a(radiative) \sim \frac{1.8\times10^{15}}{T^{3/2}} \phi \, f_i \, (s^{-1}) \tag{5.10}$$

where T is the temperature in eV.

During muon capture by an ion, some of the energy of the muon can be transferred to a third particle and the following set of three-body or non-radiative reactions can occur:

$$\mu + D^+ + X \rightarrow \mu d + X^*, \tag{5.11}$$

$$\mu + T^+ + X \rightarrow \mu t + X^* . \tag{5.12}$$

The third body, X, can be an ion, electron or neutral particle. The three-body formation rate can be approximated by multiplying the muon capture rate of an ion, from Eq. 5.8, by the probability of an energy transition due to a third body-muon collision within a reaction sphere around the ion.

The probability that a third body and a muon are both within a sphere of diameter equal to the radiative impact distance r_{imp} (Eq. 5.7) is

$$P_1 = \frac{4\pi}{3} r_{imp}^3 N_X \tag{5.13}$$

where N_X is the concentration of particles that are acting as third bodies and τ_X and τ_{muon} are the transit times of particle X and the muon within the reaction volume. The probability that sufficient energy is transferred to the third body and that the muon loses sufficient energy to be caught by the ion is approximated by

$$P_2 \sim 1 . \tag{5.14}$$

The above analysis corresponds to a classical trajectory approximation and is insufficient to predict the behaviour when a tritium or deuterium ion is the third body. Indeed, the rate of muo-atom formation with the third body as a nucleus is very small because muon energy transitions via nuclear collisions are highly improbable[13]. When electrons are the third body, the above classical trajectory approximation can be used. However, when the electrons become degenerate, only those electrons near the fermi surface can act as third bodies because of the nature of the fermi distribution. The effective number of available electrons N_e can be approximated as

$$N_e \sim N f_{deg} f_i \tag{5.15}$$

Using the results of Appendix B:

$$\begin{aligned} f_{deg} &= 1 \quad , \quad T > E_f \\ &= \left(\frac{T}{E_f}\right)^{3/2} , \quad T \le E_f \end{aligned} \tag{5.16}$$

where T is the temperature in eV and $E_f \approx 5.1\ \phi^{2/3}$ eV.

Using Eqs. 5.13 - 5.15, the three body (electron) muo-atom formation reaction rate is

$$\begin{aligned} R_{three-body} &\sim N_\mu v_\mu f_\mu \pi r_{imp}^2 N_e P_1 P_2 \\ &\sim N_\mu \frac{4\pi^2}{3} v_\mu r_{imp}^5 N^2 f_i^2 f_\mu f_{deg} . \end{aligned} \tag{5.17}$$

Equating all the known parameters, the temperature and density dependant three-body muon capture rate parameter is described by

$$\lambda_a(three-body) \sim \frac{3.2 \times 10^{17}\ \phi^2}{T^{9/2}} f_{deg} f_i^2 f_\mu \quad (s^{-1}) . \tag{5.18}$$

The atomic muon capture mechanisms are similar to the molecular capture mechanism in Eqs. 2.110 - 2.113 in the sense that they lead to an initial muon-atomic energy level of about $n = (m_\mu/m_0)^{1/2} \approx 15$. Muo-atom formation from radiative and three-body capture will result in a variety of initial bound-muon energy states, but it is assumed that they are all greater then n=3. The muo-atoms are assumed to reach the n=3 state very quickly with no significant muon transfer occurring. The μd_3:μt_3 ratio is C_d:C_t.

The rate at which muons are captured into the n=3 state of muo-deuterium and muo-tritium, referred to as λ_a in Fig. 5.1, is a sum of the

molecular formation rates discussed in Section 2.4.3.1. and the muo-atom formation rates described by Eqs. 5.4, 5.10 and 5.18. Figures 5.2a and 5.2b plot λ_a for a density range of LHD to 1000 LHD and temperature ranges of 1 eV to 10^4 eV. Fig. 5.2b shows the large magnitude of the formation rate, $\lambda_a > 10^8\ s^{-1}$, in the regime of interest. The abrupt nature of the pressure ionization approximation is evident in Figs. 5.2a at $\phi \approx 37$ LHD. The change in λ_a is not great, and is thought not to affect these calculations adversely. Also, it is likely that the real transition is smoother.

5.3 Muon Transfer

The possibility of muon transfer from μd to μt was introduced in Section 2.4.3.2, where it was demonstrated that the 48 eV lower binding energy of the μt leads to an irreversible exchange reaction in Eq. 2.118. By a detailed balance argument, at elevated temperatures, the following reverse reactions can proceed,

$$\mu t_n + d \rightarrow \mu d_n + t - \frac{48.1}{n^2}\ eV. \tag{5.19}$$

Figure 5.3 illustrates the possible collisional cascade routes of a muon from the n=3 muo-deuterium and muo-tritium state[73,74], with the muon transfer routes in high density deuterium-tritium. For energy levels of n > 2, transfer can occur when the deuterium-tritium fuel is dissociated or ionized. At temperatures greater than approximately 5 eV, no net muon transfer results, because dissociation of hydrogen molecules competes with muon transfer.

The probability of formation of μd_3 and μt_3 is assumed to follow the ratio C_d:C_t, and the ground state populations, μd_{1s} and μt_{1s}, will depend on the

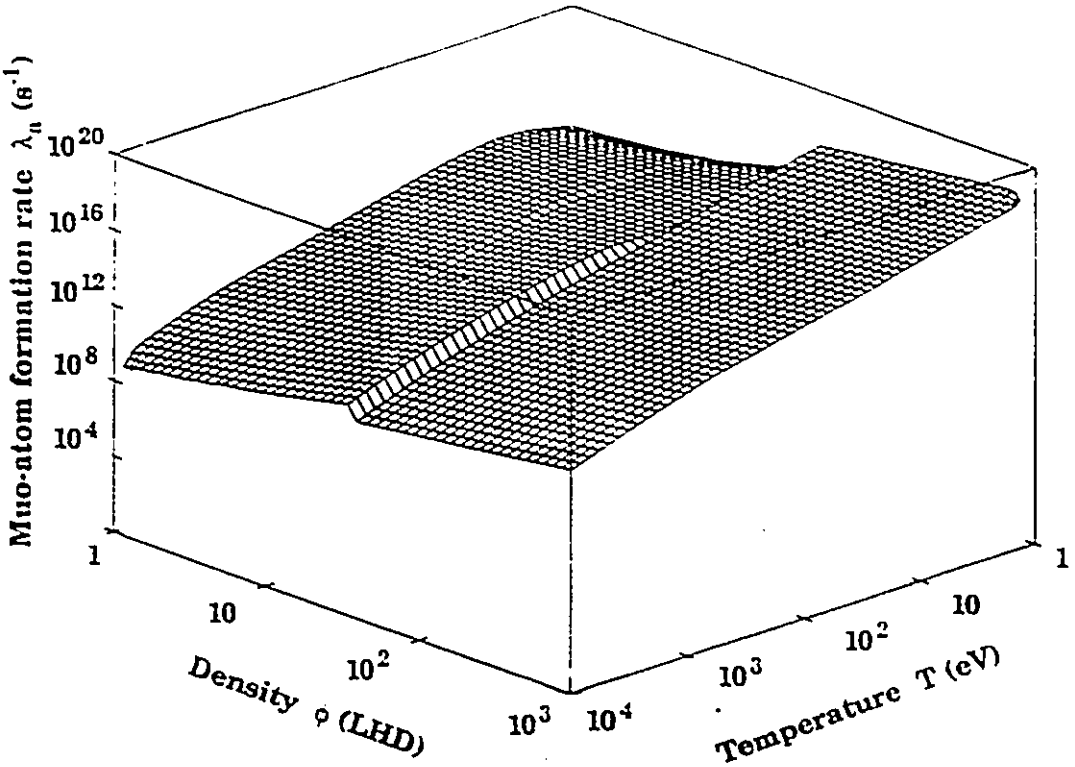

Figure 5.2a : Muo-atom (μd,μt) formation rate in deuterium-tritium versus temperature and density.

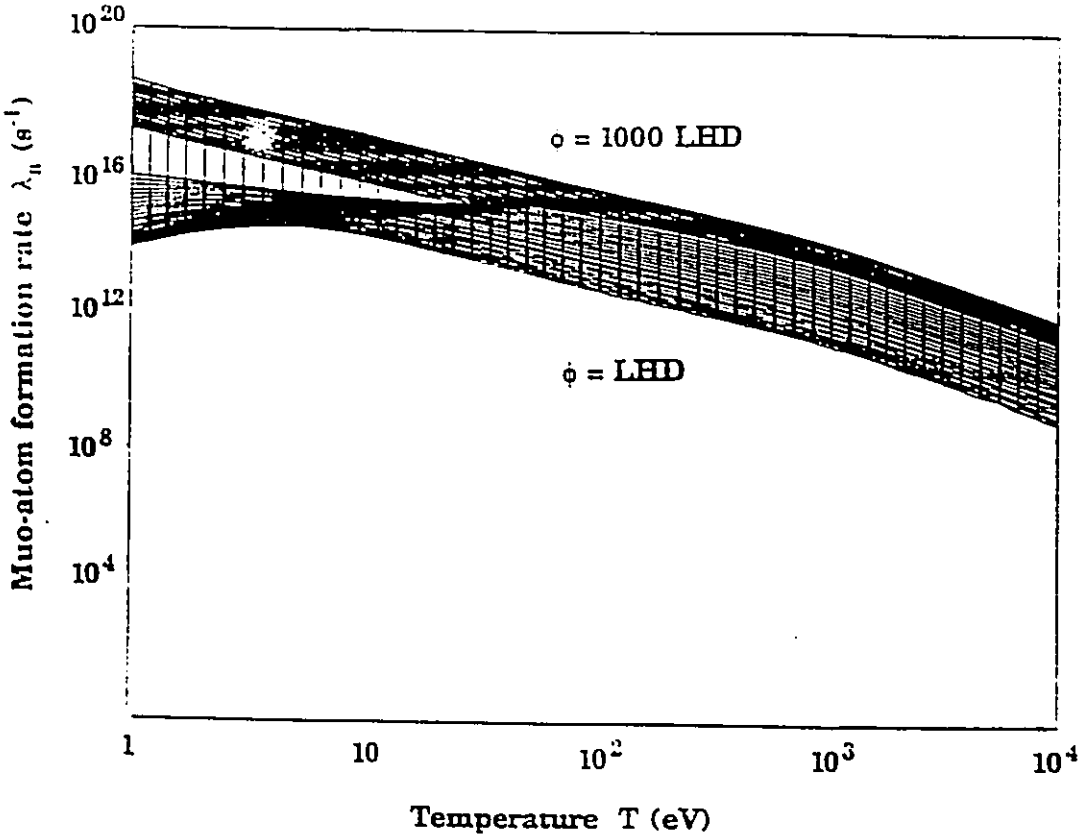

Figure 5.2b : Projection of the muo-atomic formation rate of Fig. 5.2a on to the temperature axis illustrating the range of λ_{μ} for the density range $\phi = 1 \rightarrow$ 1000 LHD.

relative strengths of the cascade reactions outlined in Fig. 5.3. We assume that the competing de-excitation reactions and the transfer reaction, $\mu d + t \rightarrow \mu t + d$ vary only weakly with temperature; thus, only the temperature dependence of the reverse transfer reaction must be included in the model.

The de-excitation reactions and the transfer reaction for $n > 1$ occur quickly (from n=3 to n=1s in < 10 ps). Therefore, modelling of the final μd_1:μt_1 ratio from an initial C_d:C_t ratio suffices.

Figure 5.4 displays p_{1s}, the fraction of muons that end up as μt_1 as a function of the fuel temperature and tritium concentration. The fraction of muons that end up as μd_1 is q_{1s}, where $p_{1s} = 1-q_{1s}$. Radiative transitions are ignored in Figs. 5.3 and 5.4 in order to be able to calculate the limiting behaviour of q_{1s} and p_{1s} at elevated densities.

In Fig. 5.4, as the temperature increases past 50 eV, the muon transfer rate at excited states from the triton approaches the muon transfer rate from the deuteron and μd_1:μt_1 approaches C_d:C_t. Once the muo-atoms are in the ground state, transfer may occur but muo-molecule formation may also proceed. The ground state transfer reaction is assumed to be the same as that for the molecular fuel case, Eq. 2.120, yielding

$$\lambda_{dt}(1s) \sim 3 \times 10^8 \phi f_\mu \quad (s^{-1}) . \tag{5.20}$$

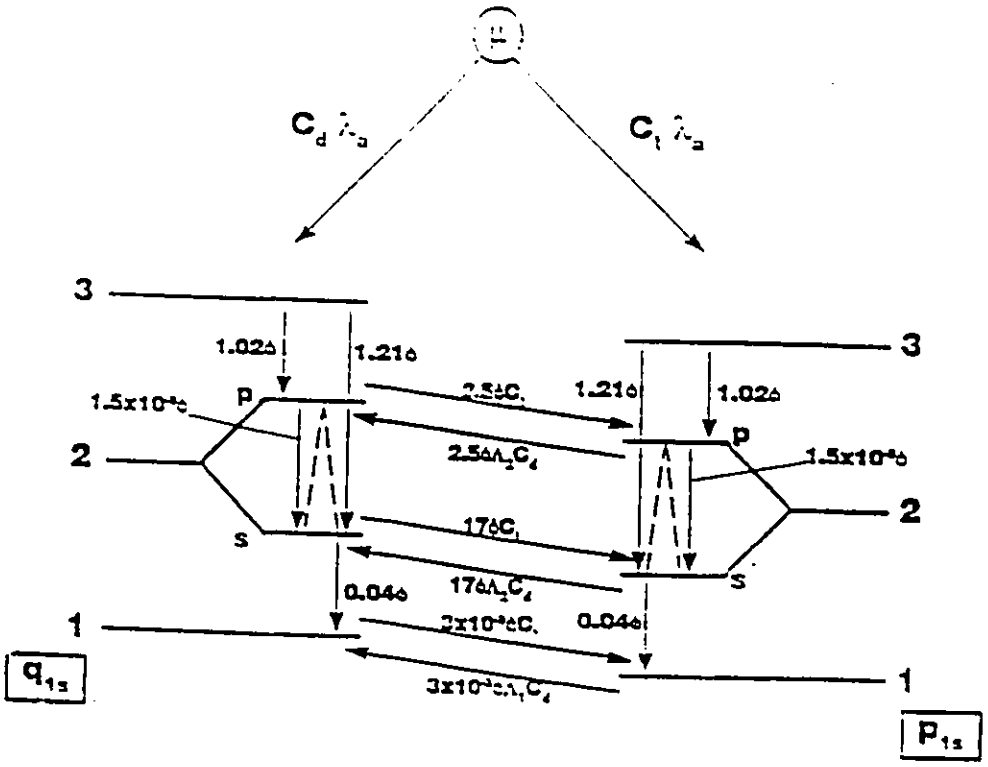

Figure 5.3 : Schematic of the μd and μt cascade in high density deuterium-tritium stressing the collisional de-excitation and transfer processes[73]. All numerical values above are in units of 10^{11} s^{-1} and $\Lambda_2 = \exp(-12.03/T)$ and $\Lambda_1 = \exp(-48.1/T)$ where T, the fuel temperature, is in eV.

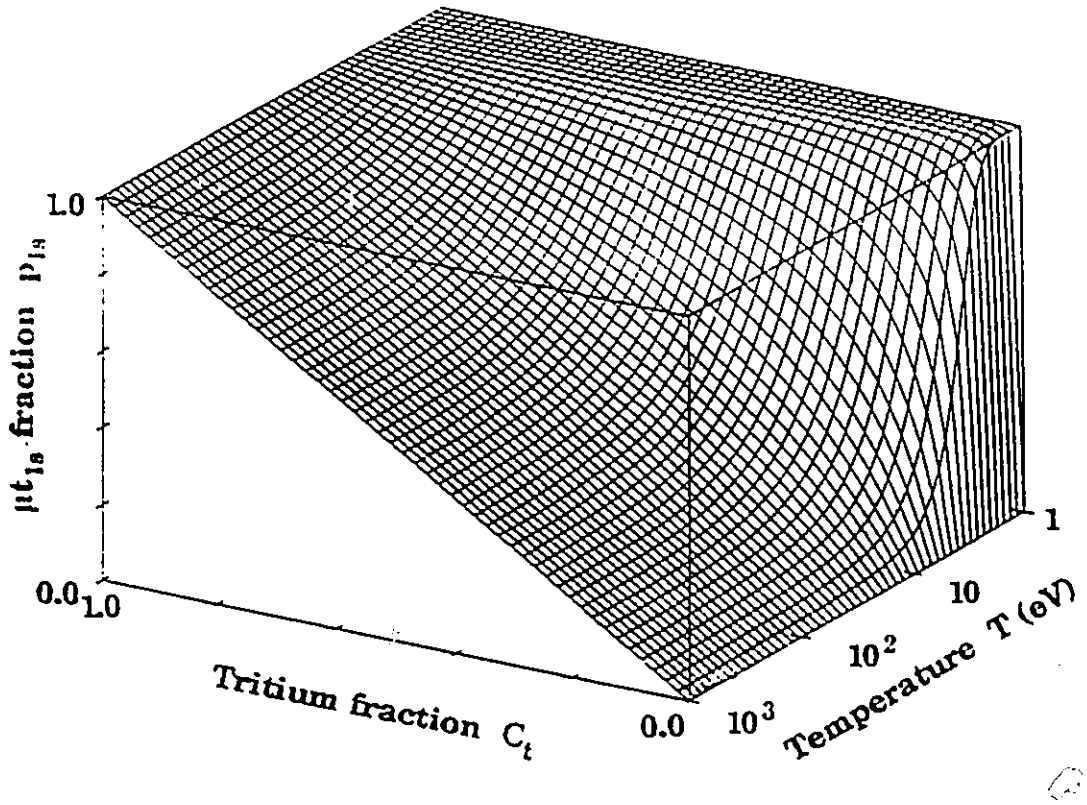

Figure 5.4 : Fraction of initially excited muo-atoms that cascade to the μt ground state, p_{1s}, versus temperature and tritium fraction.

Using a detailed balance argument, the reverse transfer is

$$\lambda_{td}(n) = \lambda_{dt}(n)\, e^{-\frac{48.1}{n^2 T}} \quad (s^{-1}) . \tag{5.21}$$

Muon transfer from μd and μt to nuclei with Z > 1 nuclei can be significant; therefore, deuterium-tritium fuel pellets must be highly pure initially, but contamination by the following Helium impurities will be impossible to avoid:

1. ^{4}He (α particle), which is produced in μdt and μtt fusion,
2. ^{3}He (h), which is produced in μdd fusion and also by tritium decay,

$$t \rightarrow {}^3He + e + \bar{\nu}_e \tag{5.22}$$

Although the dynamics affecting muon transfer to helium are not fully understood, a number of recognized processes can be identified[109]. Muon transfer is most effective by the following molecular charge exchange reactions,

$$\mu d + He \rightarrow d\mu He \rightarrow \mu He + d + \gamma , \tag{5.23}$$

$$\mu t + He \rightarrow t\mu He \rightarrow \mu He + t + \gamma . \tag{5.24}$$

The molecular charge exchange will cease to function once the He atom begins to ionize, at temperatures greater than 10 eV. The transfer mechanisms for ionized helium are:

$$\mu d + He^{++} \rightarrow \mu He^{+} + d . \tag{5.25}$$

$$\mu t + He^{++} \rightarrow \mu He^{+} + t \ . \tag{5.26}$$

The ionized helium transfer reaction rate is slow with ground state μd and μt, but may be rapid in excited state muo-deuterium and muo-tritium. It has been suggested that He concentrations must be less than 0.01% (Ref.8), in order to avoid helium "poisoning", analogous to Xenon poisoning in a fission reactor.

5.4 Muo-molecular Ion Formation

In this section, the processes relevant to the formation of the μdt_{11} muo-molecular ion at high deuterium-tritium densities and temperatures are analyzed. Once ground state muo-tritons exist, formation of and fusion via μdt_{11} muo-molecular ions can proceed. When a μdt_{11} is formed it may break-up, de-excite to a lower muo-molecular energy state, or undergo a fusion reaction. Since fusion within a μdt muo-molecule is dominant in the J=0 state ($\lambda_{fdt}(J=0,v=1) \approx 10^{12}\ s^{-1}$), de-excitation from the μdt_{11} to the μdt_{01} state predicates the overall μdt fusibility.

Figure 5.5 illustrates a reduced portrait of the energy level structure[25] associated with a μdt muo-molecular ion, showing only the parts significantly affecting the overall muon induced fusion rate. At high temperatures, muo-molecular ion breakup competes with formation and de-excitation of the μdt_{11} state. As a reaction equilibrium is established, a detailed balance of the reaction rates yields the following expression for the breakup rate of the μdt_{11} molecule $\lambda_{\mu dt}$(break),

$$\frac{\lambda_{\mu dt}(form)}{\lambda_{\mu dt}(break)} = 3N\left(\frac{2\pi}{M_{\mu t,d}T}\right)^{3/2} e^{\epsilon_{11}/kT} \tag{5.27}$$

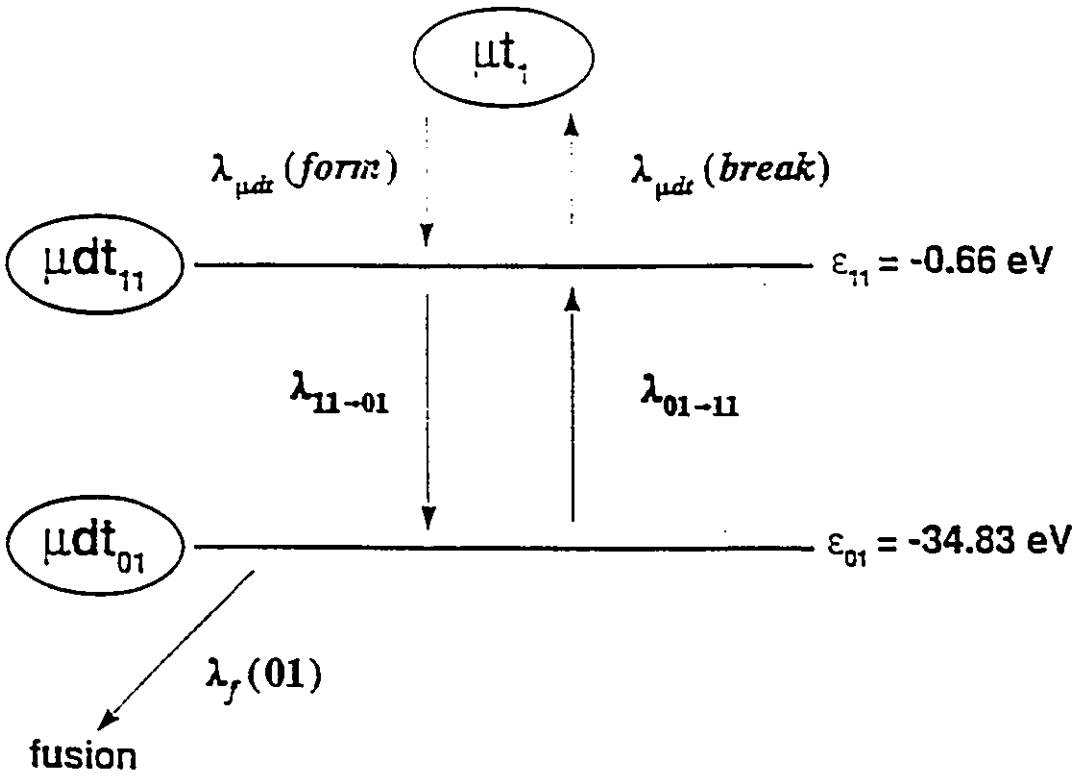

Figure 5.5 : Schematic of the reduced energy structure of μdt muo-molecular ion[24].

where $\lambda_{\mu dt}$(form) is the μdt_{11} formation rate, ε_{11} = 0.66 eV is the energy difference between μt_{1s} and μdt_{11}, $M_{\mu t,d}$ is the reduced mass of the μdt muo-molecule and N = 5 x10^{22} ϕ cm^{-3} is the fuel density. When the μdt_{11} muo-molecular ion breaks up it is assumed that a μt_{1s} muo-atom results.

For μdt_{11} formation via the molecular resonance mechanism, it was assumed that the μdt_{11} break-up rate was small relative to the $\mu dt_{11} \rightarrow \mu dt_{01}$ de-excitation. At elevated temperatures the break-up of the 0.66 eV μdt_{11} state must be considered. As well, at high temperatures (T > 35 eV), it is possible that re-excitation of the μdt_{01} can happen before fusion occurs. It is assumed that the direct formation and break-up of μdt_{01} is slow, and that the μdt_{01} re-excitation returns to the μdt_{11} state. A detailed balance argument is used to calculate the re-excitation rate from μdt_{01} to μdt_{11} giving specifically,

$$\lambda_{01\rightarrow 11} = \lambda_{11\rightarrow 01} e^{-|\varepsilon_{01}-\varepsilon_{11}|/kT} \tag{5.28}$$

where $|\varepsilon_{01}-\varepsilon_{11}|$ = 34.17 eV.

Formation of the μdt_{11} from μt_{1s} can occur by several mechanisms:

1. resonance,
2. non-resonance,
3. ionic capture, and
4. capture via three body reactions.

Low temperature muon catalyzed fusion in deuterium-tritium fuel, dominated by the resonance formation of μdt, was discussed in Section 2.4.3.3. When the density increases past the molecular dissociation point, the resonance formation mechanism becomes less important as a μdt_{11} formation

process. Therefore, at temperatures greater than 1 eV and densities greater than LHD, three-body formation processes begin to compete with the resonance formation rate. Modelling of the complex dynamics leading to the resonance formation, including μt spin dynamics and epithermal μt formation, is not needed and the following model derived from Eq. 2.125 suffices,

$$\lambda_{\mu dt}(resonance) \sim 4 \times 10^8 \, T^{-3/2} \, e^{-\frac{0.64}{T}} \, \phi f_m f_\mu \quad (s^{-1}) \, . \tag{5.29}$$

As the density increases, the total μdt_{11} formation rates will increase as a function of ϕ^2. Menshikov, with Ponomarev[11], and with Somov[13], investigated three-body formation and found that the reaction rates are highest when the third body is an electron or a neutral particle, when a muon and an ion interact, or an ion when a muon and a neutral particle interact. The possible reactions are:

the electronic (i-e)

$$\mu t + d + e \rightarrow \mu dt + e^* \, , \tag{5.30}$$

the ionic - neutral (i-n)

$$\mu t + de + X \rightarrow \mu dt + e^* + X \, , \tag{5.31}$$

$$\mu t + d + Xe \rightarrow \mu dt + X + e^* \, , \tag{5.32}$$

and the neutral-neutral (n-n)

$$\mu t + de + Xe \rightarrow (\mu dt)e + X + e^* \, , \tag{5.33}$$

where X = {d,t}.

All of these three-body reactions involve the excitation of an electron to remove the excess binding energy in the μdt_{11} formation. Deuterium or tritium ions are not effective third bodies in the muo-molecular ion formation for the same reasons that they are not effective for muo-atom formation, i.e.,

provide a route for an energy transition. The effect of degenerate electrons is also similar to the three-body muo-atom formation mechanism. When the third body is a degenerate electron, only those electrons close to the fermi level can take part in an energy transitions. Electron degeneracy will also affect the μdt collisional de-excitation and excitation rates because an electron is the mediating particle in these reactions. A factor of f_{deg} is also applied to the reaction rates $\lambda_{11\to01}$ and $\lambda_{01\to11}$.

Analytic models of the reactions Eqs. 5.30 - 5.33 from Men'shikov and Ponomarev[11], and Men'shikov and Somov[13] are:
for the electronic three-body formation

$$\lambda_{\mu dt}^{i-e}(three\text{-}body) \sim \frac{1.9\times10^{10}\ \phi^2 f_i^2 f_{deg} f_\mu}{T^2}\ (s^{-1}), \tag{5.34}$$

for the neutral-ionic formation

$$\lambda_{\mu dt}^{i-n}(three\text{-}body) \sim \frac{6.0\times10^{10}\ \phi^2 f_i f_a f_\mu}{T^{3/2}}\ (s^{-1}), \tag{5.35}$$

and for the neutral-neutral formation

$$\lambda_{\mu dt}^{n-n}(three\text{-}body) \sim \frac{1.6\times10^{10}\ \phi^2 f_a^2 f_\mu}{T^{3/2}}\ (s^{-1}). \tag{5.36}$$

The other possible mechanisms of μdt_{11} formation are ionic capture and non-resonance formation. These are always dominated by the resonance or three body formation[77] and are therefore neglected. The sum of the reaction rates from the resonance mechanism and the three-body mechanisms yields

$$\lambda_{\mu dt}(form) = \lambda_{\mu dt}(resonance) + \sum_j \lambda_{\mu dt}^{j}(three\text{-}body), \tag{5.37}$$

where j = {i-e,i-n,n-n} and $\lambda_{\mu dt}(form)$ is the total formation rate of the μdt_{11} muo-molecular ion.

Considering Fig. 5.5, the temporal evolution of the number density of μdt_{11} and μdt_{01} at a given equilibrium temperature and density can be represented by the following point kinetic rate equations:

$$\frac{dN_{11}}{dt} = \lambda_{\mu dt}(form)\, C_d N_{\mu t} + \lambda_{01\text{-}11} N_{01} - (\lambda_{\mu dt}(break) + \lambda_{11\text{-}01} + \lambda_{\mu}) N_{11}\,, \tag{5.38}$$

$$\frac{dN_{01}}{dt} = \lambda_{11\text{-}01} N_{11} - (\lambda_f(01) + \lambda_{01\text{-}11} + \lambda_{\mu}) N_{01}\,. \tag{5.39}$$

Here, N_{11} represents the number density of μdt_{11} and N_{01} represents the number density of μdt_{01}.

It is assumed that the rates of change of the number density of μdt_{11} and μdt_{01} are small, i.e., that the rate determining processes such as breakup and fusion are more rapid than any other processes. Eqs. 5.38 and 5.39 are set to zero and an effective muo-molecular ion formation rate can be calculated which reflects the number of muo-molecular ions that are formed and lead to a fusion event. The fusion rate will then be

$$R_{fusion} = \lambda_{\mu dt} C_d N_{\mu t} \tag{5.40}$$

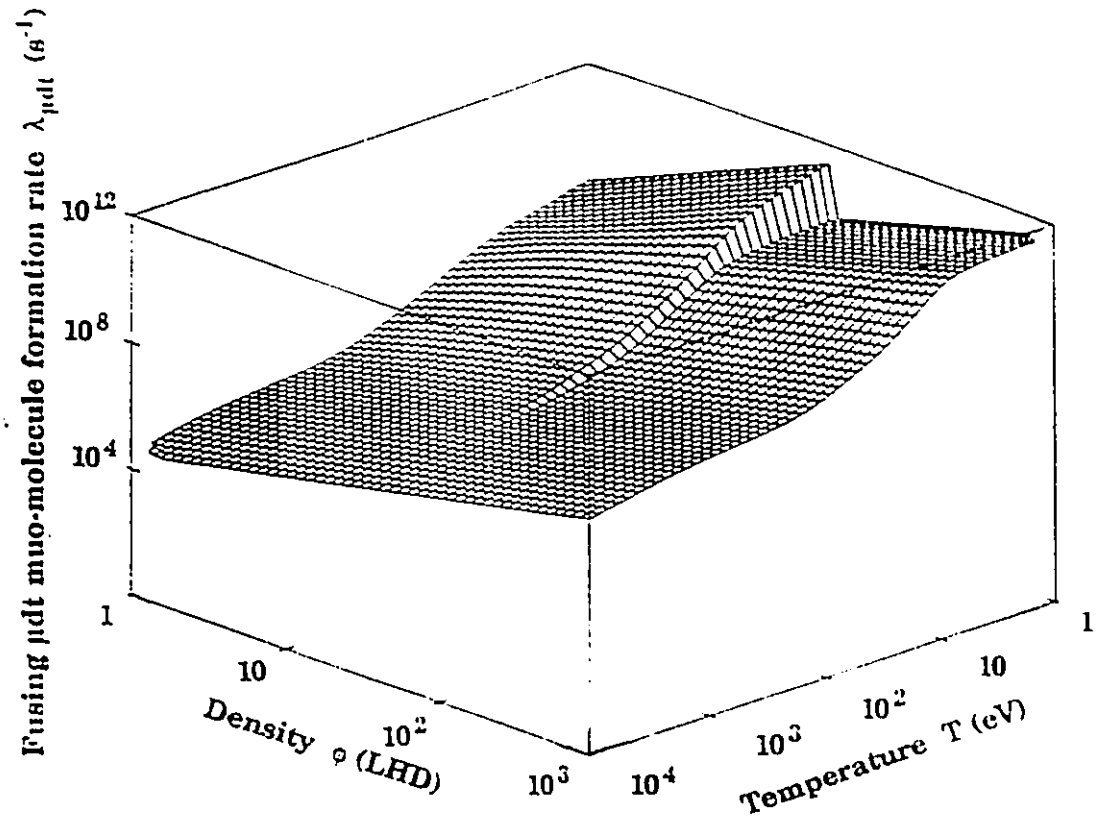

Figure 5.6a : Plot of the temperature and density dependent formation rate of μdt_{11} that lead to fusion plus the direct μdt fusion rate.

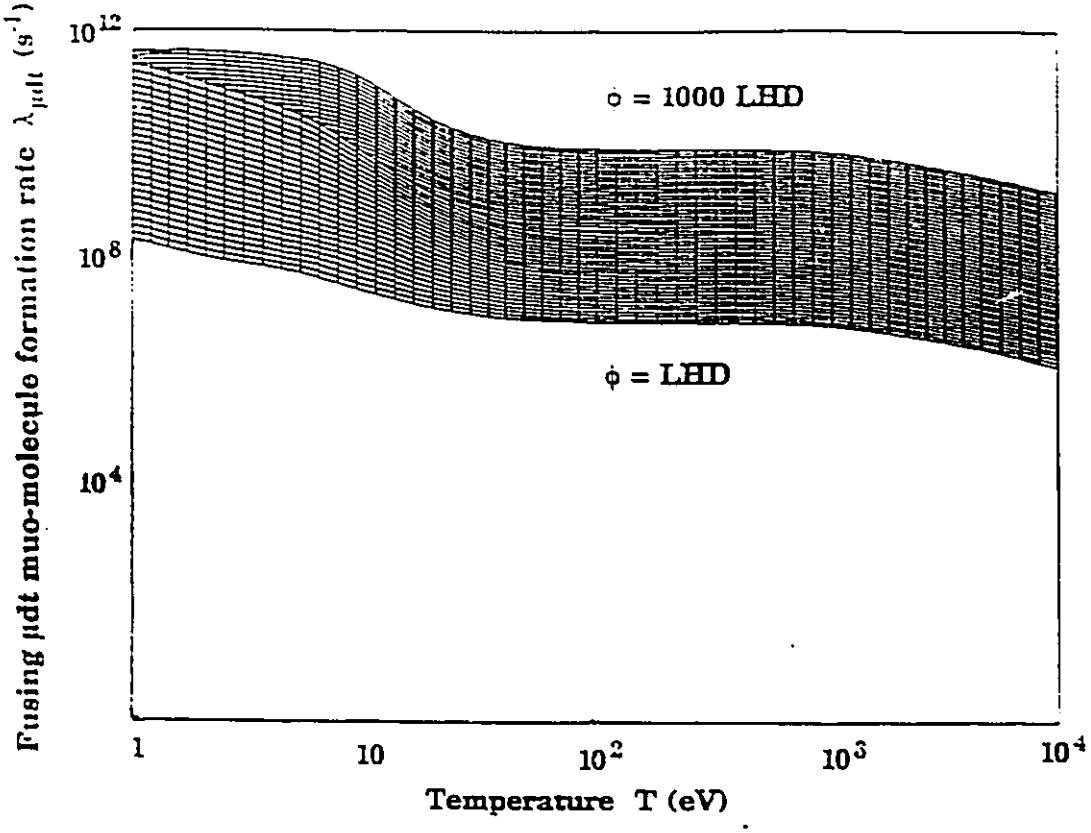

Figure 5.6b : Projection of the formation rate of Fig. 5.6a on to the temperature axis illustrating the range of values of $\lambda_{\mu dt}$ for fuel densities from $\phi = 1 \rightarrow 1000$ LHD.

where

$$\lambda_{\mu dt} = \frac{\lambda_{\mu dt}(form)}{1 + \frac{\lambda_{\mu dt}(break)}{\lambda_{11-01}}\left(\frac{\lambda_{01-11}}{\lambda_f(01)} + 1\right)} + \lambda_{\mu dt}(direct) \,. \tag{5.41}$$

Direct fusion via μd or μt and d or t atoms collisions, having a reaction rate (see Eq. 2.35)

$$\lambda_{\mu dt}(direct) = 1.13 \times 10^5 \, \phi f_\mu \quad (s^{-1}) \tag{5.42}$$

is insignificant compared to the fusion rate via muo-molecule formation as long as muo-molecules exist for sufficient durations to allow fusion. Since the direct fusion mechanism is not dependent upon the existence of an intermediate state that can be affected by the local temperature and density of surrounding fuel molecules, atoms, ions and electrons, the direct mechanism can be much faster than the muo-molecular ion mechanism at high temperatures and densities.

Figures 5.6a and 5.6b show the dependence of $\lambda_{\mu dt}$ on fuel temperature and density, including muo-molecular and direct fusion mechanisms (Eq. 5.41 plus Eq.5.42). It is apparent that muo-molecular fusion reactions are severely limited for fuel temperatures greater than 50 eV, because of the re-excitation of μdt_{01} and the highly probable subsequent breakup of μdt_{11}. The direct fusion rate is significant only at densities greater than 100 times LHD.

5.5 Muon Sticking and Regeneration

The problem of muon sticking in the muon catalyzed fusion chain in molecular fuel was presented in Section 2.4.3.4. As was mentioned earlier, the unexpected density dependence of the sticking probability measured at

deuterium-tritium densities of less than 1.3 LHD was, in part, the initial impetus behind the pursuit of μCF-ICF symbiosis. The purpose of this section is to elucidate the basic mechanisms behind muon sticking in deuterium-tritium, in conditions ranging from the LHD molecular case to a high density plasma. Once a basic understanding of muon sticking is achieved, some mechanisms of muon sticking reduction in compressed deuterium are discussed and a temperature and density muon sticking model will be advanced.

5.5.1 Initial Muon Sticking

As is illustrated in Fig. 5.1, nuclear fusion in the μdt molecular ion usually results in the release of a free muon which can catalyze further fusion reactions. However, there is a small probability (< 1%) that, after fusion, the muon will be bound to the by-product α particle and therefore lost from the catalyzing chain. This initial sticking probability is the sum of the probabilities of muon sticking at all muo-alpha (μα) energy levels,

$$w_{dt}^{initial} = \sum_{nl} w_{dt}^{initial}(nl) \ . \tag{5.43}$$

Table 5.1 shows typical analytic values of the energy level distribution of the initial sticking probabilities from the fusioning μdt_{01} state[110]. These values are a function only of the quantum mechanical decay of the μdt_{01} muo-molecular ion, and the fuel conditions (i.e density or temperature) have no effect upon their value. The muon catalyzed fusion chain length, considering only the initial sticking will be limited to

$$X_{\mu} < \frac{1}{w_{dt}^{initial}} < 114 \ . \tag{5.44}$$

Although the initial sticking can not be altered by an external mechanism, a stuck muon may be regenerated by muon stripping (ionization) or by muon transfer leading to the resumption of the catalyzing chain. It is by the various excitation processes leading to muon stripping and transfer that external influences, such as the local fuel density and temperature, can play a role in the muon sticking probability. The density and temperature dependent effective muon sticking can be expressed as

$$w_{dt}(\phi,T) = w_{dt}^{initial}\,(1 - R(\phi,T)) , \tag{5.45}$$

where $R(\phi,T)$ is the density and temperature dependent regeneration probability. A closer examination of the dynamics of muon regeneration will provide a clearer view of possible mechanisms leading to a decrease in the muon sticking loss.

5.5.2 Muon Regeneration Mechanisms

The $\mu\alpha$ exiting the fusion event will have a kinetic energy of $E_{\mu\alpha} = 3.5$ MeV, about 1/5 of the total fusion energy. As the $\mu\alpha$ travels through the surrounding deuterium-tritium fuel, the bound muon will experience various excitation and de-excitation processes and at the same time the $\mu\alpha$ itself will dissipate energy mainly to the surrounding electrons and eventually stop. Muon stripping (collisional ionization) reactions and, to a lesser degree, muon transfer from the ^{4}He (α particle) to a deuterium or tritium molecule, atom or ion are the mechanisms for muon regeneration.

The following excitation and de-excitation reactions compete with the stripping reactions and $\mu\alpha$ energy loss:

1. inelastic collisions,

nl	$P_{nl}(0)$	$w_{dt}(nl)$
1s	77.3 %	0.006803
2s	11.1 %	0.000973
2p	2.7 %	0.000237
3	4.3 %	0.000382
4	1.9 %	0.000164
5	0.9 %	0.000079
6	0.5 %	0.000046
≥ 7	2.3 %	0.000116
Total	100.0 %	0.008800

Table 5.1 : The distribution of initial muon sticking probabilities versus energy level[110].

2. radiative transitions.
3. auger transitions and.
4. stark transitions.

By analyzing this competition, the population of excited μα states can be determined where,

$$\frac{dP_i(E,\phi,T)}{dt} = \nu_{\mu\alpha}(E)\left(\sum_k \left(\sigma_{k\to i}(\phi)\, P_k(E,\phi,T) - \sigma_{i\to k}(\phi)\, P_i(E,\phi,T)\right) - \sigma_i^{strip}(\phi)\, P_i(E,\phi,T)\right). \tag{5.46}$$

Here, $P_i(E,\phi)$ represents the muon energy level populations at a given fuel density and a μα kinetic energy E, $\sigma_{k\to i}(\phi)$ represents all possible excitations and de-excitations to a given energy level, $\sigma_{i\to k}(\phi)$ represents all the possible excitations and de-excitations from that energy level and $\sigma_i^{strip}(\phi)$ is the density dependent muon stripping rate. The expression $S(E,\phi,T)$ is the stopping power, defined as the μα energy loss per unit distance in deuterium-tritium with a temperature T and a density ϕ.

The most important excitation mechanism in muon regeneration is muon stripping. The muon stripping rate for excited states will have the following approximate dependence,

$$\sigma_{strip}^{n} \sim \sigma_{strip}^{1s}\, n^2 . \tag{5.47}$$

It is apparent that exciting muons to high energy states will maximize muon stripping reactions. For muon regeneration, muons must attain these higher energy levels before the μα loses its kinetic energy by electronic stopping.

The stopping time of the μα is determined by

$$t_{stop}(\phi,T) = \int_{3.5MeV}^{0MeV} \frac{dE}{v_{\mu\alpha}\, S(E,\phi,T)} \tag{5.48}$$

with

$$v_{\mu\alpha} = \sqrt{\frac{2E}{m_{\mu\alpha}}} \tag{5.49}$$

where E is the μα's kinetic energy and $m_{\mu\alpha}$ is its mass.

The overall regeneration rate can calculated by solving Eqs. 5.46 to 5.49 for P_i, the population of muon energy levels on the α particle at time $t=t_{stop}$, yielding,

$$1-R = \sum_i P_i(t_{stop}) \; . \tag{5.50}$$

The longer the stopping time, the greater the opportunity for muon excitations to lead to stripping reactions.

5.5.3 Mechanisms for Enhanced Muon Regeneration

Enhancement of muon regeneration through background temperature and density effects may occur by:

1. Muon excitation to higher energy levels, where muon stripping reaction rates are greater.
2. Reduction of the medium stopping power S(E,ϕ,T).

A qualitative investigation of these effects will lead to a better understanding of regeneration probability enhancement in increased density fuel.

5.5.4 Enhancement of Muon Excitation

The effects of the following two muon excitation - de-excitation processes will be discussed:

1. radiative de-excitation, and
2. non-linear processes.

Some of the muon de-excitation processes are radiative transitions; at low densities these will dominate over density dependent collisional excitations or de-excitations. As the fuel density increases, collisional de-excitation and excitation processes compete and then dominate the radiative de-excitation. The solid line in Fig. 2.15 illustrates the theoretical density dependence of muon sticking in molecular deuterium-tritium. For this theoretical dependence, it was assumed that enhanced stripping takes place at only one excited level. As density increases and collisional excitations become appreciable, the advent of multi-step collisional, or "ladder", excitations yields a mechanism for enhanced muon regeneration. This mechanism may explain the discrepancy between the theoretical and experimental results, shown in Fig. 2.15.

First approximations of non-radiative excitation and de-excitation processes have a linear density dependence and little temperature dependence for fuel temperatures less than about 2 keV (Ref.111-113). It is probable that more complicated three-body and/or collective mechanisms would result in more complex, non-linear temperature and density dependencies, both for the excitation and de-excitation rates, and the regeneration and sticking probabilities. Further experimental investigation of the specific excitation and

de-excitation processes is required to determine whether these effects would favour excitation rather than de-excitation so that enhanced populations in high energy states can occur.

5.5.5 Stopping Power Reduction

The stopping power in molecular fuel at elevated densities may be reduced by the pressure-induced continuum lowering effect upon the ionization and dissociation potentials of molecules and atoms[115]. The Bethe stopping model for bound electrons is presented in Appendix C. Initially, molecular deuterium-tritium will have the Bethe ionization potential of molecular hydrogen, I ≈ 20 eV. As the density increases and molecules dissociate to atoms, the value of I will approach the atomic value I ≈ 15 eV (Refs.110,114). As the density continues to increase, the continuum lowering effect causes the Bethe ionization potential to be further reduced[115]. From Eq. C.2, reduction in the average value of the ionization potential will result in a reduction in the stopping power.

As the temperature increases past about 15 eV or if the density is greater than the full pressure ionization value, deuterium-tritium will be in a plasma state. A charged particle slowing in a plasma is best modeled using the dielectric approach discussed in Appendix C. Because the velocity of the plasma electrons plays a direct role in the charged particle energy loss, the deuterium-tritium plasma stopping power will be dependent upon the plasma electron temperature. In addition, when the plasma electrons are degenerate and the velocity of electrons is determined by the fermi velocity, the stopping power will be dependent on the density [12,13,88,117-120].

For temperatures less than 10 keV, nuclear elastic scattering (NES) is much less than electronic scattering. Therefore, the energy loss of a moving charged particle (i.e. μα) is due mainly to excitation of electrons[116].

5.5.6 Regeneration in Intense Electric and Magnetic Fields

One novel way to decrease the stopping power is to introduce an electric or magnetic field, or both, which would accelerate the μα and counteract the energy loss of the μα due to collisions. Effectively, the E and B fields would re-accelerate the μα after every de-accelerating collision. This mechanism is included in the analysis because it is possible to have large magnetic and electric fields in compressing ICF-like pellets[6].

The electric field necessary to re-accelerate a μα and increase the possibility of regeneration was investigated by Bracci and Fiorentini[121]:

$$\vec{E} = \frac{[dE/dx]_{\mu\alpha}}{e} . \qquad (5.51)$$

where dE/dx is the medium stopping power at the initial μα energy and e is the electron charge. The electric field required is approximately 15 kV/cm, which is impractically large.

There also exists the possibility of muon regeneration from a μα in a magnetic field where a large vxB force between the muon and the alpha effectively strips the muon[60]. The magnitude of the field necessary to ionize the muon from the alpha can be calculated by equating the attractive coulomb and the maximum repulsive vxB force:

$$\frac{1}{4\pi\varepsilon}\frac{3e}{r^2} = 3e\,|v\times B| \qquad (5.52)$$

Assuming that the magnetic field and the $\mu\alpha$ velocity are perpendicular, and substituting $v \approx 1.28 \times 10^7$ m/s, $E_{\mu\alpha} = 3.46$ MeV, $r \approx a_e/207 \approx 256$ fm and $\varepsilon \approx \varepsilon_0 = 8.85$ pF/m, the size of the magnetic field necessary to separate the muon from the alpha exceeds 10^9 Tesla. The largest known magnetic fields, generated by laser irradiation inside a solid deuterium-tritium shell, do not exceed 10^2-10^3 Tesla. Even if compression of the shell is considered, maximum fields of approximately 10^6 Tesla could be created for very brief periods of time[6,7].

5.5.7 Muon Sticking Model

From the above qualitative analysis it is clear that the physics of muon regeneration in dense fuel is very complicated and provides fertile ground for future experimental work. In the mean time, simplified models of the muon excitations and alpha stopping must suffice in a muon regeneration model. Such a simple simulation of density and temperature dependent muon regeneration has been performed by Jändel et.al.[12]. This model, henceforth referred to as the Jändel model, uses Cohen's linear muon excitation models[111] and the stopping power uses Maynard and Deutsch's RPA dielectric formalism[120]. Whereas this model does not include possible molecular and atomic fuel effects or non-linear effects upon the excitation and de-excitation mechanisms, it does include plasma and degenerate electron effects.

A simple temperature and density dependent regeneration expression is extracted by a fit to the available output of the Jändel model, yielding

$$R(T,\phi) \sim 0.33 + 0.66 \cdot \frac{\phi}{\phi+\beta(T)}, \qquad \beta(T) = e^{-(a+b\ln(T))}, \tag{5.53}$$

for

$$T < 30\ eV, \quad a = -3.06, \quad b = 0.0318,$$
$$\geq 30\ eV, \quad a = -5.36, \quad b = 0.713\ .$$

Eq. 5.53 assumes a regeneration probability of 33% at molecular deuterium-tritium temperatures and densities of LHD. Including an initial sticking probability, $w_{dt}^{initial} = 0.088$, Jändel's model yields $w_{dt} = 0.0058$ at low temperatures (T < 500°C) and LHD. This value is somewhat larger than measured values of the sticking probability; this discrepancy between theory and experiment is a subject of interest[60-68].

While there may be some concerns at the appropriateness of extending Eq. 5.53 to large fuel densities ($\phi > 10$ LHD) and non-plasma conditions, it is thought that this sticking model is conservative for most of the temperature and density regime of interest. However, the above fit to the Jändel model neglects an expected increase in the stopping power for temperatures between 1 and 20 eV. This results in an effective increase in sticking probability for these temperatures, compared with the sticking probability at the same density but lower temperatures. The maximum deviation between the true model values and the fit in Eq. 5.53 will be approximately 25%.

The muon sticking model will be most useful in comparing the muon sticking contribution to other muon catalyzed fusion processes in the overall muon catalyzed fusion dynamic. In Figure 5.7a, w_{dt} from Eq. 5.53 is shown as function of temperature and density.

Fig. 5.7b depicts the isoclines of w_{dt}^{-1}. Considering that w_{dt}^{-1} represents the maximum possible number of fusions per muon, Jändel's model suggests a sufficiently large number of fusions per muon, i.e., $X_\mu > 1000$, at

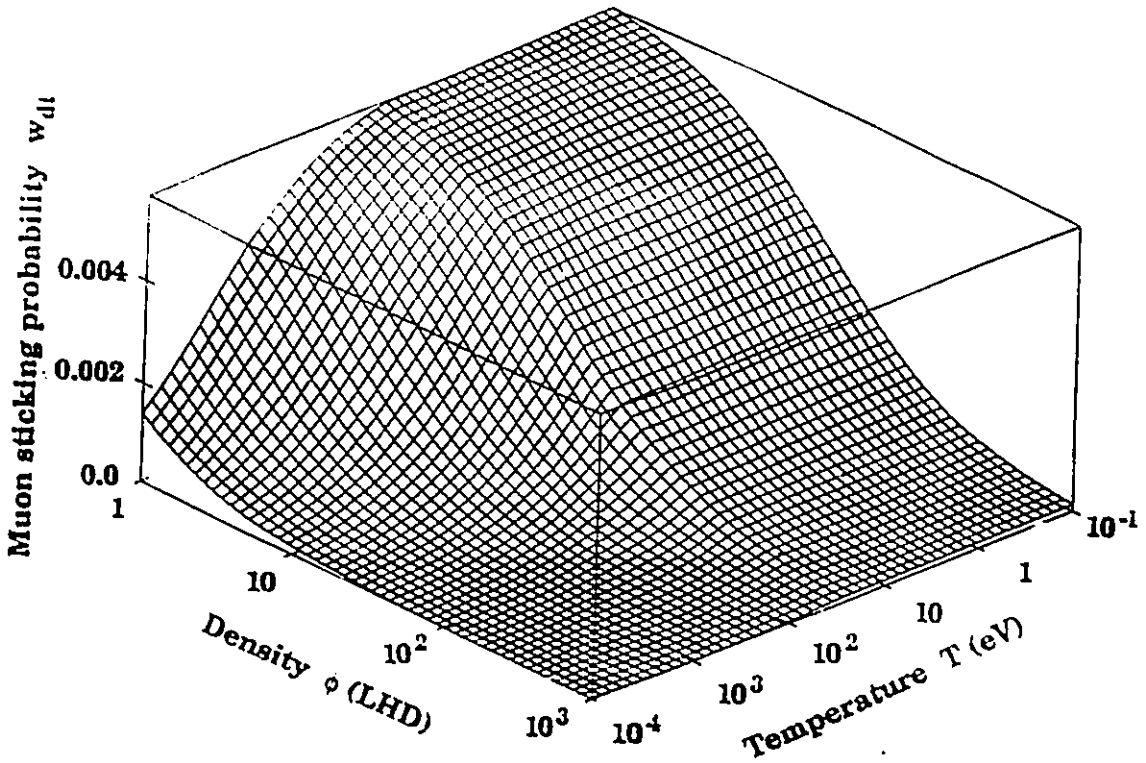

Figure 5.7a : A smooth fit to the density and temperature dependent muon sticking model of Jändel et.al (Ref.12).

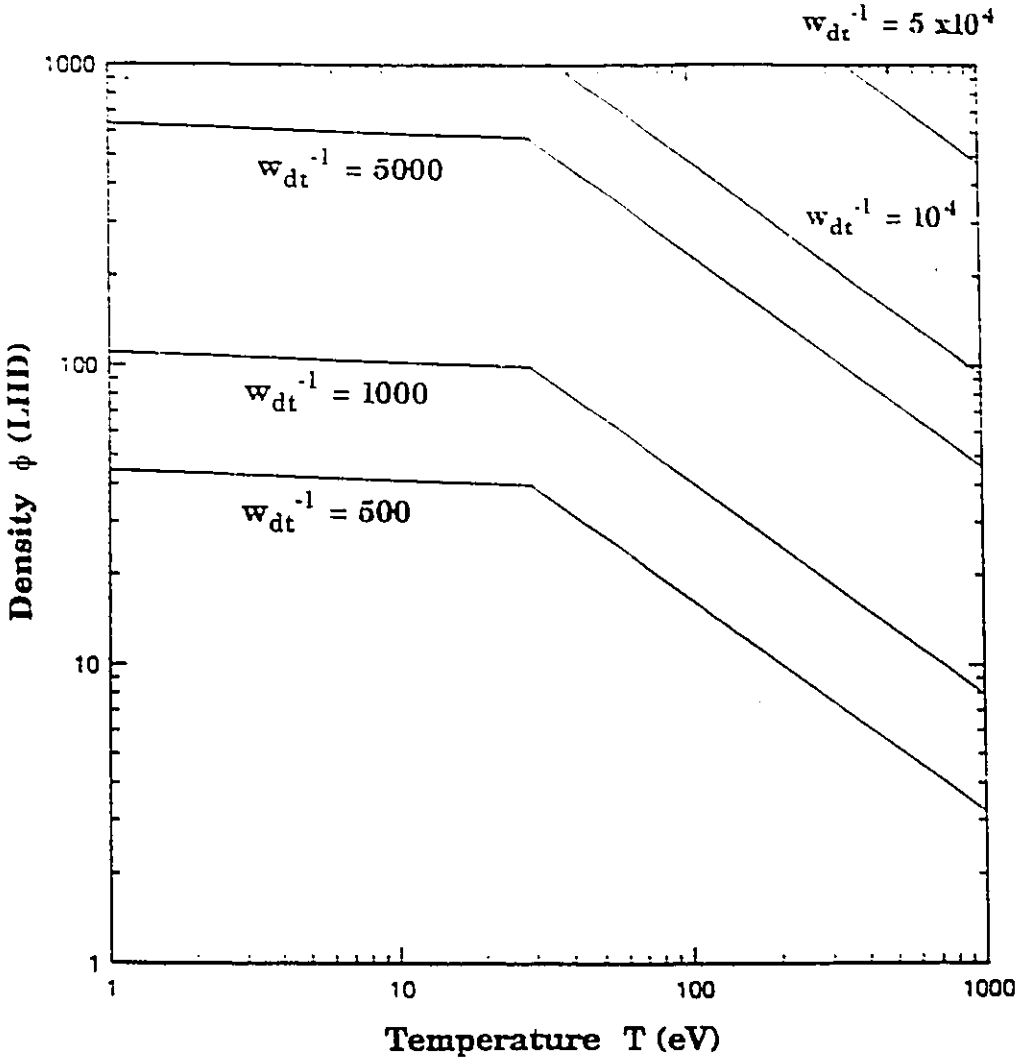

Figure 5.7b : Isoclines of w_{dt}^{-1} calculated from a smooth fit to Jändel's model (Eq.5.53).

temperatures less then 50 eV for densities of approximately 100 times LHD.

5.6 Muon Catalyzed Fusion Network

In Section 5.4, it was decided that the concentrations of the muo-molecular ions μdt_{11} and μdt_{01} would quickly equilibrate because the μdt_{11} and μdt_{01} break-up, de-excitation and fusion reactions are very rapid. Setting the time rates of change of the μdt_{11} and μdt_{01} concentrations, N_{11} and N_{01} respectively, to zero yields the following static values:

$$N_{01} = \frac{\lambda_{\mu dt} C_d N_{\mu t}}{\lambda_f(01)}, \tag{5.54}$$

$$N_{11} = \frac{\lambda_f(01) + \lambda_{01-11}}{\lambda_f(01)\,\lambda_{11-01}} \lambda_{\mu dt} C_d N_{\mu t}, \tag{5.55}$$

where $\lambda_{11\to 01}$, $\lambda_{01\to 11}$, $\lambda_f(01)$ and $\lambda_{\mu dt}$ are defined in Section 5.4.

From the μCF reaction network depicted in Fig. 5.1, assuming the fast equilibration of the μdt_{11} and μdt_{01} concentrations in Eqs. 5.54 and 5.55, the following set of point kinetic equations describe the evolution of the network reaction constituents:

$$\frac{dN_\mu}{dt} = -(\lambda_a + \lambda_\mu) N_\mu + \lambda_{\mu dt} C_d (1 - w_{dt}) N_{\mu t}, \tag{5.56}$$

$$\frac{dN_{\mu d}}{dt} = \lambda_a q_{1s} N_\mu - (\lambda_{dt}(1s) C_t + \lambda_\mu) N_{\mu d} + \lambda_{td}(1s) C_d N_{\mu t}, \tag{5.57}$$

$$\frac{dN_{\mu t}}{dt} = \lambda_a(1 - q_{1s})N_\mu - \lambda_{dt}(1s)C_t N_{\mu d} - (\lambda_{td}(1s)C_d + \lambda_{\mu dt}C_d + \lambda_\mu)N_{\mu t}, \quad (5.58)$$

where N_μ, $N_{\mu d}$ and $N_{\mu t}$ represent the concentrations of muons, muo-deuterium and muo-tritium, respectively.

In a dynamic compression of a deuterium-tritium fuel pellet, density and temperature will have a spatial dependence, as well as a temporal dependence. Assuming that the entire dynamic compression can be represented by an average temperature and density for an average reaction duration τ_r, the above point kinetic equations can be solved and the effective muon cycling rate, the effective muon sticking probability and the average number of fusions can be calculated. The averaged μCF parameters, while not exactly the same as calculating the full spatial and temporal solution for a compression of a spherical fuel pellet, will provide an estimate of the average temperature and density required to achieve sufficiently high muon catalyzed fusion rates and low muon sticking losses.

The number of fusions that occur during a given reaction time in a unit volume of deuterium-tritium with muons is

$$N_f(\phi,T,t) = \int_o^t \lambda_{\mu dt}(\phi,T)C_d N_{\mu t}(\phi,T,\tau)\,d\tau . \quad (5.59)$$

Assuming that all the muons are injected into the compressed deuterium-tritium at t = 0, then the muon catalyzing efficiency, defined as the total number of fusions induced per muon during the fuel pellet reaction time, is

$$X_\mu(\phi,T) = \frac{N_f(t=\tau_r,\phi,T)}{N_\mu(0)} = \frac{\int_o^{\tau_r} \lambda_{\mu dt}(\phi,T)\, C_d N_{\mu t}(\phi,T,\tau)\, d\tau}{N_\mu(0)} \tag{5.60}$$

The reaction time of the deuterium-tritium fuel, τ_r, should be contrasted with the time required for the bulk of the μCF reactions to occur, $\tau_{\mu CF}$. An expression of $\tau_{\mu CF}$ is developed in Section 5.6.2. For present purposes, we will consider the consequences of assuming $\tau_\mu > \tau_r > \tau_{\mu CF}$. Then, τ_r in the integral in Eq. 5.60 can be replaced with

$$\tau_r = \infty \tag{5.61}$$

and using the solution of the reaction equations 5.56 - 5.58, described in Appendix D, the integration of $N_{\mu t}$ gives,

$$\int_0^\infty N_{\mu t}(\phi,T,\tau)\, d\tau = \frac{N_\mu(0)}{\lambda_\mu^3 + A(\phi,T)\,\lambda_\mu^2 + B(\phi,T)\,\lambda_\mu + C(\phi,T)} . \tag{5.62}$$

Substitution of the above expression into Eq. 5.60 yields the following expression for the muon catalyzing efficiency,

$$X_\mu(\phi,T) = \frac{\lambda_{\mu dt}(\phi,T)\, C_d}{\lambda_\mu^3 + A(\phi,T)\,\lambda_\mu^2 + B(\phi,T)\,\lambda_\mu + C(\phi,T)} , \tag{5.63}$$

where the density and temperature dependent values of A, B and C are defined as:

$$A(\phi,T) = \lambda_a(\phi,T) + \lambda_{dt}(1s)(\phi)\, C_t + \lambda_{td}(1s)(\phi,T)\, C_d + \lambda_{\mu dt}(\phi,T)\, C_d , \tag{5.64}$$

$$B(\phi,T) = \lambda_a(\phi,T)\,(\lambda_{dt}(1s)(\phi)\,C_t - \lambda_{td}(1s)(\phi,T)\,C_d) + \lambda_{\mu dt}(\phi,T)\,C_d\,(q_{1s}(T,C_t)\,\lambda_a(\phi,T) - \lambda_{dt}(\phi,T)\,C_t)\,, \tag{5.65}$$

$$C(\phi,T) = \lambda_a(\phi,T)\,\lambda_{dt}(1s)(\phi)\,C_t\,\lambda_{\mu td}(\phi,T)\,C_d\,w_{dt}(\phi,T)\,. \tag{5.66}$$

5.6.1 Muon Cycling Rate

Comparing Eq. 5.63 to the simplified muon catalyzing efficiency expression of Eq. 2.127, the effective cycling rate λ_c can be extracted yielding:

$$\frac{1}{\lambda_c(\phi,T)} = \frac{1}{\lambda_a(\phi,T)} + \frac{q_{1s}(T,C_t)}{C_t\,\lambda_{dt}(1s)(\phi)} + \frac{1}{\lambda_{\mu dt}(\phi,T)}\left(\frac{1}{C_d} + \frac{\lambda_{td}(1s)(\phi,T)}{C_t\,\lambda_{dt}(1s)(\phi)}\right). \tag{5.67}$$

Using the density and temperature dependent models developed previously for λ_a, $\lambda_{dt}(1s)$, $\lambda_{td}(1s)$ and $\lambda_{\mu dt}$, the muon cycling rate can be calculated.

Considering the simple formula for the number of fusions per muon in Eq. 2.127, if the muon sticking probability were zero then the number of fusions induced per muon would be

$$X_\mu(zero\text{-}sticking) = \frac{\lambda_c}{\lambda_\mu} \tag{5.68}$$

where λ_μ is the muon decay rate. In Figure 5.8a, Eq. 5.68 has been used to plot zero-sticking muon efficiency versus temperature and density. The isoclines of Eq.5.68, referred to as the zero-sticking μCF chain length isoclines, are plotted in Fig. 5.8b for values of X_μ(zero-sticking) = 500, 1000, 5000 and 10^4. It appears that, in the ideal zero muon sticking case, more than 1000 fusions per muon occur when the fuel density is greater than approximately 40 x LHD, for fuel temperatures less than T ≈ 20 eV.

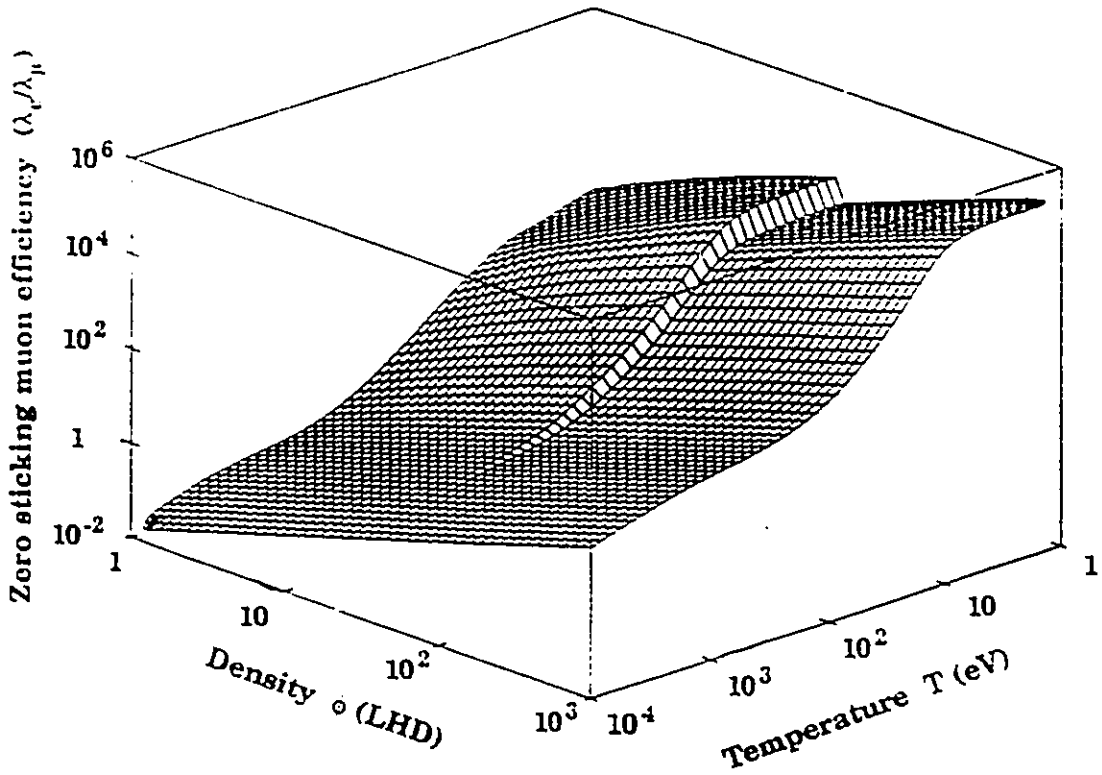

Figure 5.8a : Plot of the muon catalyzing efficiency assuming zero sticking, X_u(zero-sticking) (λ_c/λ_u) versus temperature and density using the expression of λ_c in Eq. 5.61.

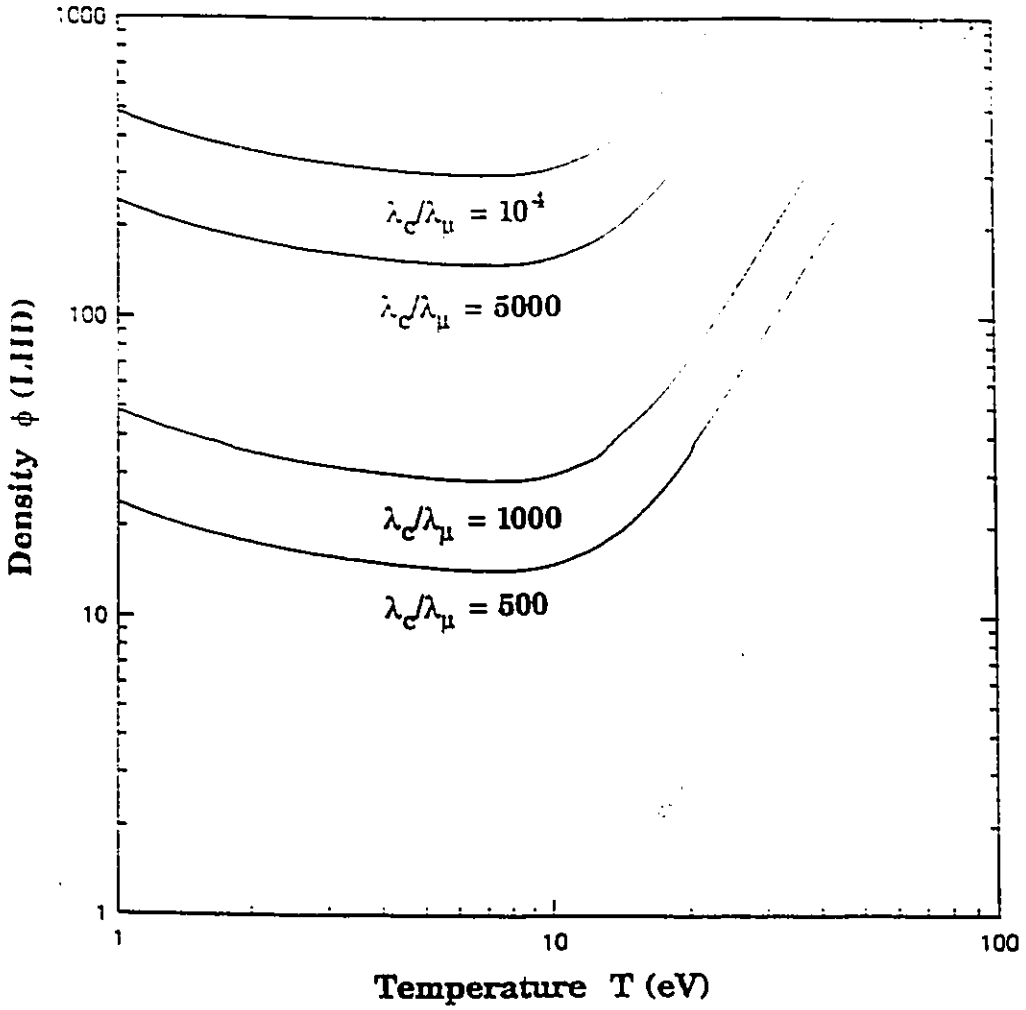

Figure 5.8b : Isoclinic plot of the zero-sticking muon efficiency, X_μ(zero-sticking).

5.6.2 μCF Reaction Timing

The magnitude of $\tau_{\mu CF}$ can be expressed as the total number of fusions induced per muon, divided by the rate at which the muon cycles through the μCF reactions yielding

$$\tau_{\mu CF} = \frac{X_\mu}{\lambda_c} = \frac{1}{\lambda_\mu + \lambda_c w_s} . \tag{5.69}$$

The limiting value of $\tau_{\mu CF}$ is determined by the time it takes for injected muons in deuterium-tritium fuel to be lost by decay, represented by τ_μ, or stuck to helium, represented by $\tau_{all\text{-}stuck}$. The parallel combination of the muon loss processes yields the following expression for $\tau_{\mu CF}$,

$$\tau_{\mu CF} = \frac{1}{\frac{1}{\tau_\mu} + \frac{1}{\tau_{all\text{-}stuck}}} . \tag{5.70}$$

Equating Eq. 5.69 and 5.70 yields

$$\tau_{all\text{-}stuck} = \frac{1}{\lambda_c w_{dt}} . \tag{5.71}$$

Even though the μCF reaction chain lifetime is ultimately limited by the mean muon lifetime $\tau_\mu \approx 2.2$ μs, the time in which all injected muons are lost from the catalyzing chain due to muon sticking may rival, or even be less than, τ_μ. Indeed, in LHD molecular deuterium-tritium the value of $\tau_{all\text{-}stuck}$ is measured to be approximately 2 μs, such that $\tau_{\mu CF}$ is slightly greater than 1 μs. If the muon cycling rate is high and the muon sticking probability is low, i.e., X_μ is large, the time in which all the muon catalyzed fusions occur could be less than 1000 ns. This is certainly desirable in our scheme where we want all possible muon catalyzed fusion reactions to occur within the lifetime of the fuel. Figure 5.9 shows the $\tau_{\mu CF}$ = 500 ns, 750 ns, and 1000 ns isoclines.

From analysis of Fig. 5.9, in order to take advantage of the full catalyzed fusion chain-length in the temperature and density regions of interest here, it is necessary that the reaction time of a deuterium-tritium fuel τ_r be in the neighbourhood of 500 ns. Because the fuel reaction time τ_r decreases with increasing temperature and density, as indicated by Eqs. 2.66 and 2.68, the operating point will restricted by the muon catalyzed fusion reaction time $\tau_{\mu CF}$.

5.6.3 Muon Catalyzing Efficiency Calculations

Using the density and temperature model of the cycling rate in Eq. 5.67 and the muon sticking model in Eq. 5.53, and assuming that the majority of possible muon catalyzed fusion reactions occur within the reaction duration (i.e $\tau_r > \tau_{\mu CF}$), then the average muon catalyzing efficiency can be calculated using the simplified model expressed in Eq. 2.127. Figure 5.10a depicts the temperature and density average muon catalyzing efficiency and Fig. 5.10b plots the X_μ = 500, 1000, and 5000 isoclines. Figure 5.10c is an overlay of the w_{dt}^{-1}, the λ_c/λ_μ and the X_μ isoclinic plots which clearly demonstrates the parallel effect that the muon cycling and the muon sticking have on the muon efficiency. Figure 5.10d is an overlay of the μCF reaction time $\tau_{\mu CF}$ isoclines and the muon catalyzing efficiency X_μ isoclines illustrating the reaction duration requirements for maximum output.

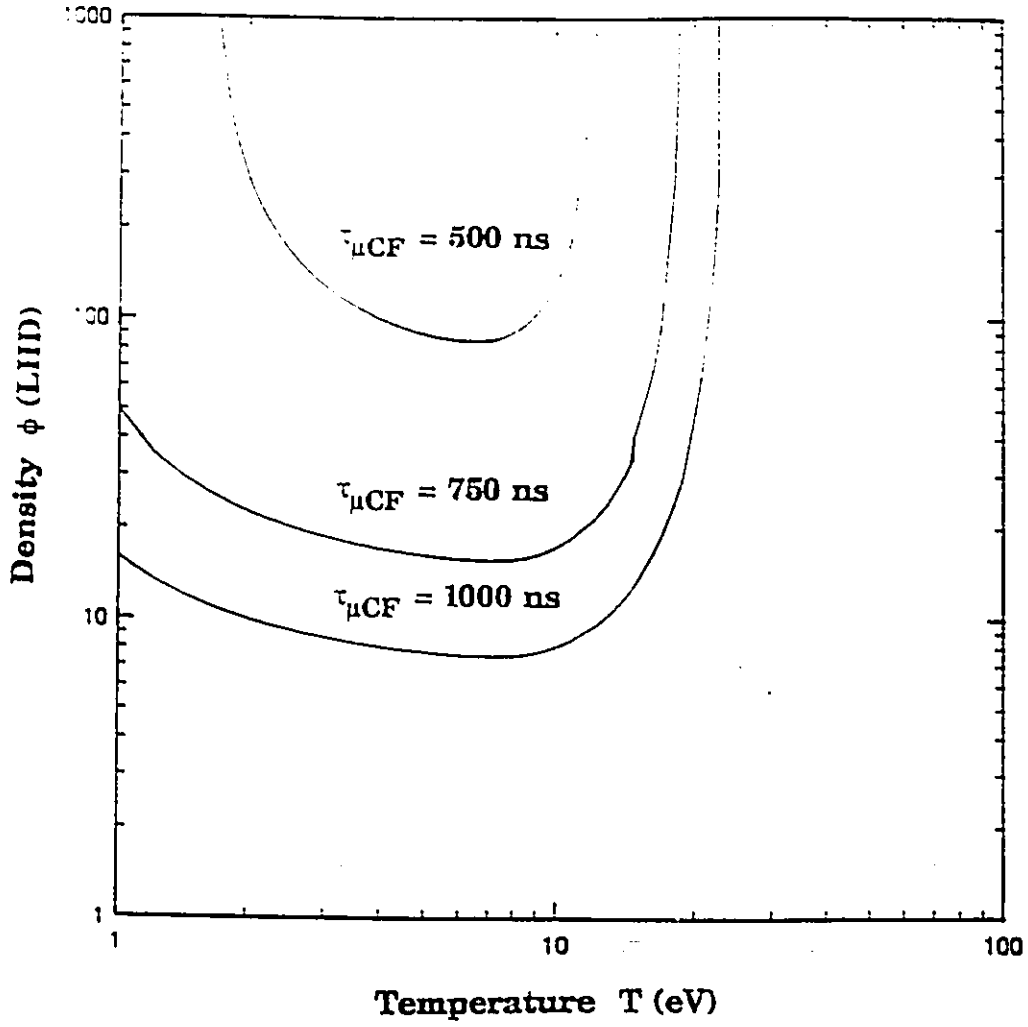

Figure 5.9 : Isoclinic plots of the μCF reaction time $\tau_{\mu CF}$.

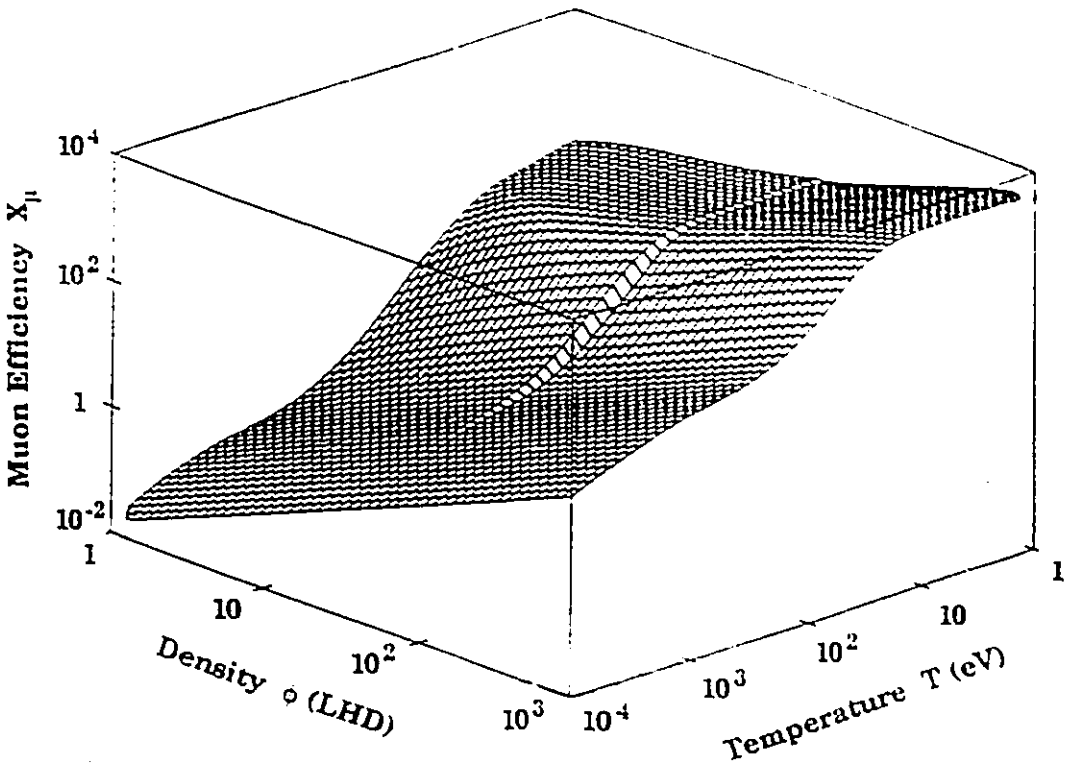

Figure 5.10a : Plot of muon catalyzing efficiency X_μ versus deuterium-tritium density and temperature.

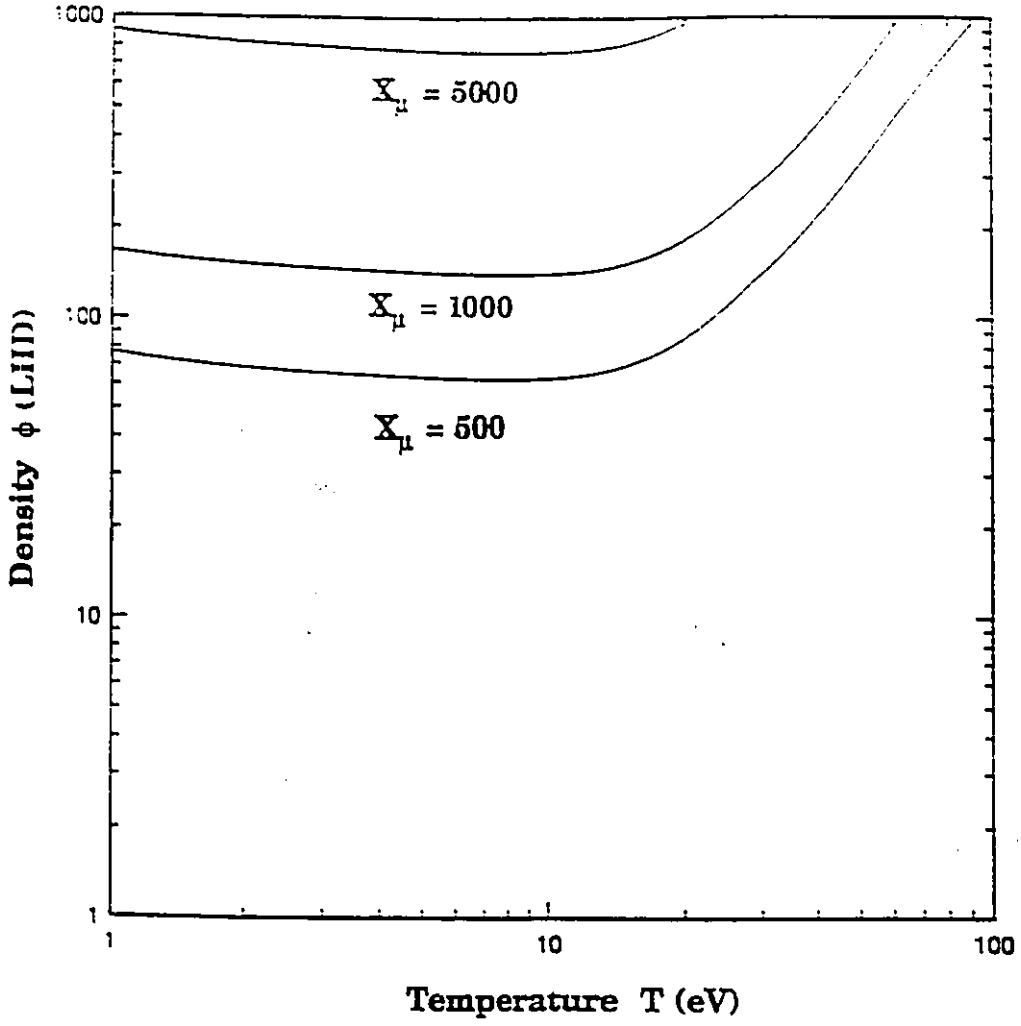

Figure 5.10b : Isoclinic plots of the muon catalyzing efficiency X_μ.

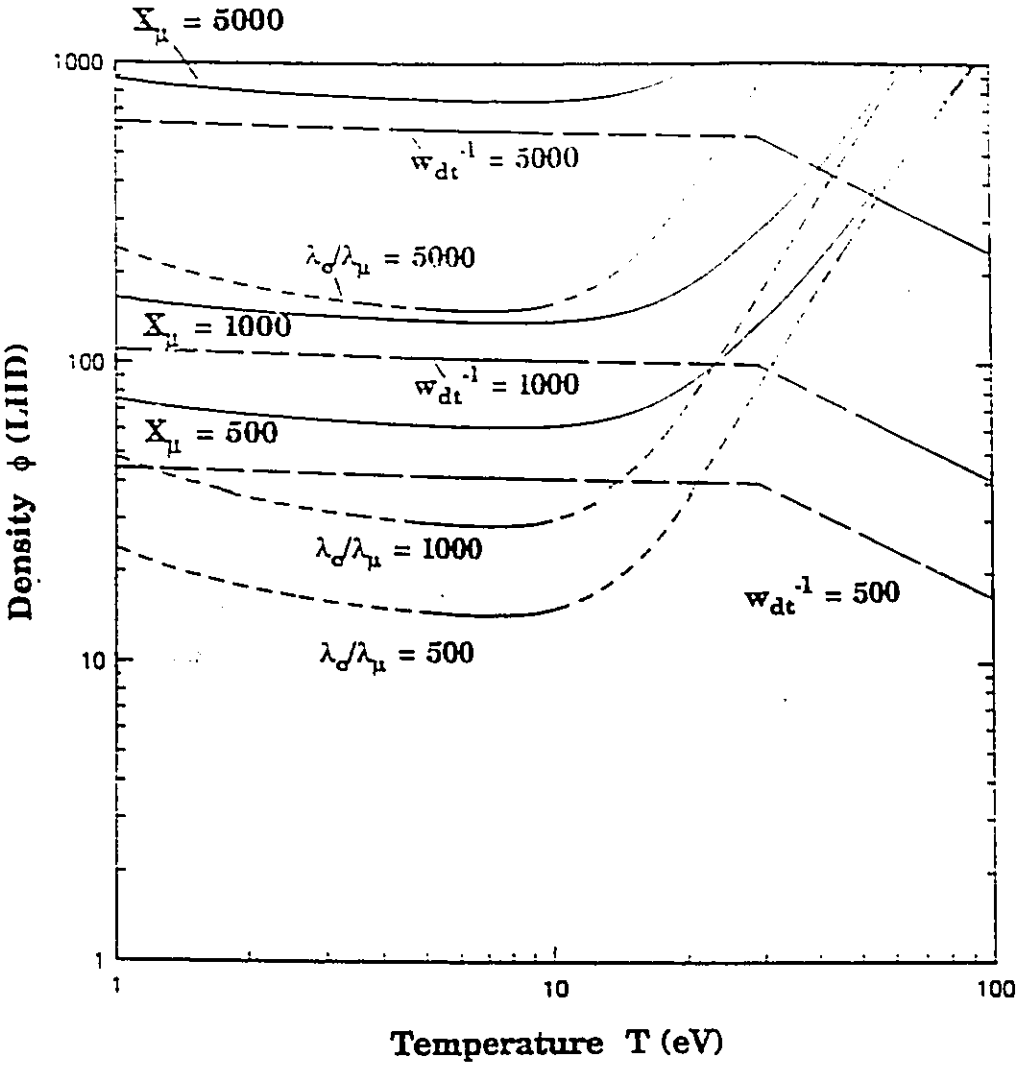

Figure 5.10c : Isoclinic plot of the muon catalyzing efficiency X_μ (solid) compared to λ_d/λ_μ (small dash) and w_{dt}^{-1}(long dash).

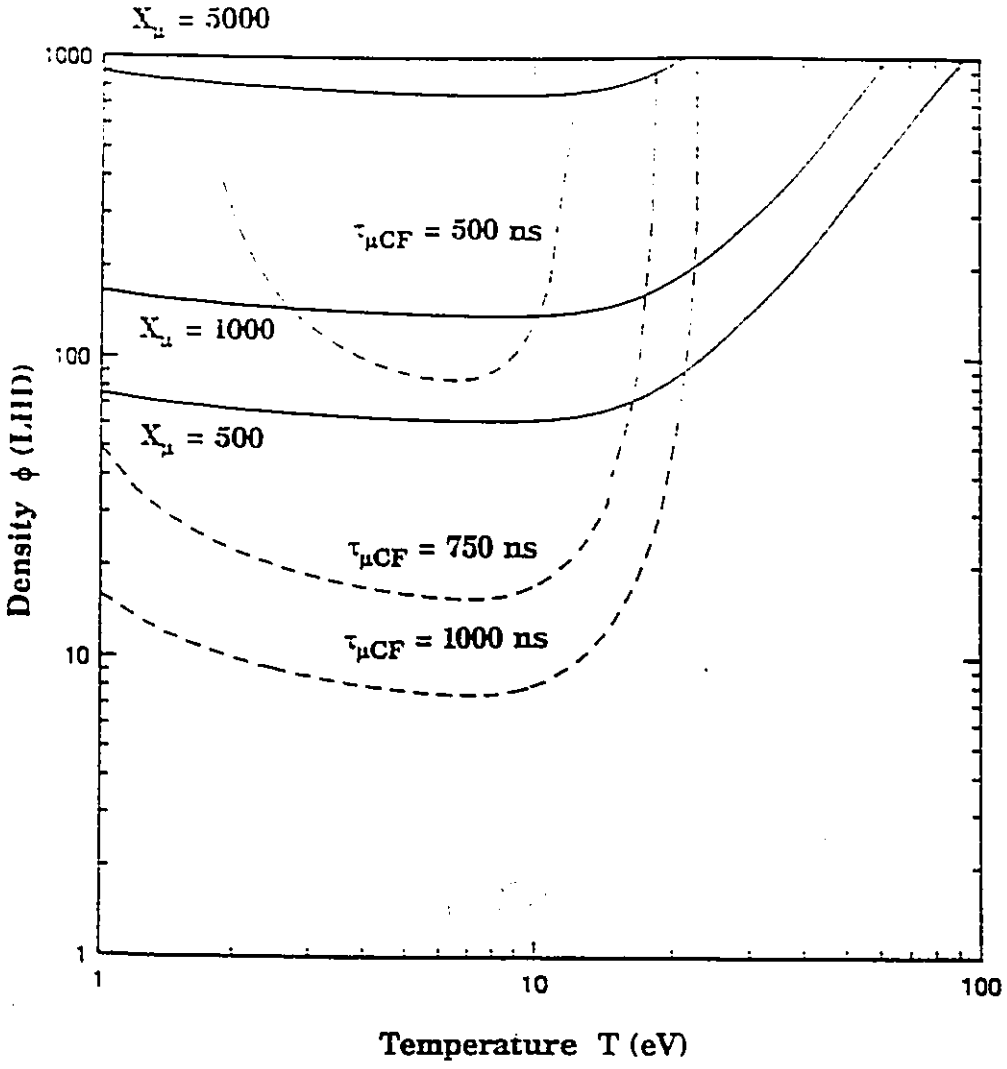

Figure 5.10d : Isoclinic plots of the muon catalyzing efficiency X_μ (solid) with the μCF reaction time $\tau_{\mu CF}$ (small dash).

CHAPTER 6

DISCUSSION

6.1 μCF-ICF Energy System Viability Evaluations

The viability of energy systems based upon the μCF triggered ignition concept and the high density μCF reactor concept are determined in this chapter by evaluating the critical parameters relevant to the energy gain of a single deuterium-tritium pellet.

The assumptions to be used in the energy gain calculations for both approaches are summarized below:

1. The energy generated per fusion is $Q_{dt} \approx 20$ MeV, which assumes a neutron energy multiplication of approximately 1.15 in the breeding blanket.
2. The alpha particle energy represents approximately 1/5 of the total deuterium-tritium fusion energy, yielding $Q_{\alpha} \approx 3.5$ MeV.
3. The maximum conversion efficiency for fusion and breeder blanket thermal energy is $\eta_c \approx 0.5$, using He or Flibe as a coolant.
4. The energy to compress a volume of fuel is determined by the degenerate electron pressure, as expressed in Eq. 4.6.

5. The maximum driver efficiency range of lasers and ion beams is $\eta_d \approx 7\% - 30\%$.
6. The minimum electrical energy cost of a single muon is E_μ = 4000 MeV.
7. The maximum efficiency of muon production by an accelerator beam - target system, followed by injection into a specific volume of deuterium-tritium fuel is $\eta_\mu = 0.7$.
8. The ignition temperature of deuterium-tritium is $T_{ign} = 4$ keV.

6.2 Evaluation of the μCF Triggered Spark Ignition Concept

The μCF triggered spark ignition concept hinges on the successful heating of a specific central deuterium-tritium fuel volume to the ignition temperature. Achieving the ignition condition in the spark region using muon catalyzed fusion reactions will depend upon the following conditions:

1. the deposition of muons within the required spark volume in a brief duration, and
2. the ability of muon catalyzed fusion reactions within the spark region to generate the necessary ignition temperature.

Once the ignition condition is satisfied, i.e., a central core volume with a fuel areal density of $\rho_s r_s \approx 0.22$ attains the ignition temperature, the fusion energy generated is calculated from the spark ignition energy gain models in Eq. 2.105 - 2.108.

The feasibility of injecting a sufficient number of muons into a small central volume of a pellet is not yet known. In Section 4.2, a general

description of the material, electric and magnetic field configuration was provided. It appears that a suitable system could be developed with a reasonable amount of cost and effort.

The optimal time for muon injection into the central core region is an important concern. The following possible scenarios for muon injection can be considered:

Case 1. Muons are injected into the fuel pellet core just as compression begins; the core density and temperature will increase when compressive pressure waves coalesce at the centre.

Case 2. Muons are deposited into the central volume when the pellet core reaches maximum density.

The advantage of the first case is that muon injection is relatively simple. However, muons present in the pellet prior to compression may generate sufficient energy to disrupt the pellet compression. At cryogenic temperatures the μCF reaction rates are very slow, so this problem can be avoided by using initially frozen deuterium-tritium fuel. This solution assumes that the pellet is comprised only of D_2 and T_2 molecules and no DT molecules (see Section 2.3) and that there is little preheat of the pellet core during compression.

The final spark region radius, in order to satisfy the spark ignition requirement, must be

$$r_s > \frac{1.1}{\phi} \ (cm) . \tag{6.1}$$

Using the Case 1 muon injection scenario, the radius of the spherical volume in which muons must be deposited in order to have a final spark region radius of r_s is

$$r_\mu = \phi^{1/3} r_s = \frac{1.1}{\phi^{2/3}} \ (cm) . \tag{6.2}$$

The number of muons needed to ignite the spark region can be calculated by analyzing the increase in temperature of the spark region when muons are injected. Once muons are present in the deuterium-tritium pellet core, a series of μCF reactions generate 3.5 MeV alpha particles. The range of alpha particles at the ignition temperature is

$$r_\alpha (ignition) \sim \frac{0.08}{\phi} \ (cm) \tag{6.3}$$

Comparing with Eq. 6.1, we see that it is valid to assume that initially, alpha particles created in the spark region deposit all of their 3.5 MeV within the spark region. For temperatures less than the deuterium-tritium ignition temperature, most of the alpha particle's energy is first transferred to electrons, but it is assumed that the electron and ion temperatures quickly equilibrate and $T_e=T_i=T$ (see Eq. 2.41).

A simple power balance in the spark region may be used to determine the temperature, if we assume that the energy gained by the fuel is due to deposition of alpha particles from muon induced fusion and the energy loss is due to bremsstrahlung radiation. The bremsstrahlung radiation is assumed

to be totally transparent in the spark region. Thus, the power balance in the spark region is

$$P_{spark}(t) = \frac{d}{dt}\{N_s(t)\, V_s(\phi)\, T_s(t)\}$$
$$= \lambda_c(T_s)\, N_\mu(t)\, Q_\alpha - A_{brems}\, N_s^2(t)\, \sqrt{T_s(t)}\, V_s(\phi)\,, \tag{6.4}$$

where $N_s(t)$ is the deuterium-tritium number density in the spark region, $T_s(t)$ is the spark region temperature in keV, $V_s(\phi)$ is the spark region volume and the required number of muons in the spark region is expressed as

$$N_\mu(t) = N_\mu(0)\, e^{-\{\lambda_\mu + \lambda_c(T(t),\phi)\, w_{st}(\phi,T(t))\}}\,, \tag{6.5}$$

This equation is derived in Appendix D.

Several additional simplifying assumptions are appropriate during the period of temperature increase to the ignition temperature within the spark region:

1. There is little fuel burn-up as the temperature increases to the ignition temperature, and the density within the spark region is the same as the maximum average density of the fuel pellet, therefore $N_s(t) \approx N_0 = 5 \times 10^{22}\, \phi\ cm^{-3}$,
2. The spark region heating time is much less than $\tau_{all\text{-}stuck}$ or τ_μ and muon losses can be neglected, thus $N_\mu(t) \approx N_\mu(0)$.
3. At elevated temperatures, the kinetic pressure within the fuel pellet determines the shock speed.

Using the above assumptions in Eq. 6.4, the spark region temperature rise is determined by

$$\frac{dT_s(t)}{dt} = \frac{Q_\alpha N_\mu(0)}{N_0} \lambda_c(\phi, T_s) - A_{brems} N_0 \sqrt{T_s(t)}\, V_s(\phi) . \qquad (6.6)$$

It is required that the temperature increase to the ignition temperature be attained within the duration of a single shock transit time across the spark region. Utilizing the transformation,

$$dt = \frac{dr}{u_s(T)} , \qquad (6.7)$$

where the kinetic pressure dominant shock speed $u_s(T)$ is described by Eq. 2.69, yields the following expression for the spark region temperature rise,

$$\int_{T_i}^{T_f} \frac{dT_s\, u_s(T_s)}{\lambda_c(\phi, T_s) \frac{N_\mu(0)}{N_0} Q_\alpha - A_{brems} N_0 \sqrt{T_s}\, V_s(\phi)} = r_s(\phi) . \qquad (6.8)$$

where T_i and T_f are the initial and final temperatures of the spark region. Substitution of known parameter values yields the following expression in which the muon cycling rate and the initial number of muons are components:

$$\int_{T_i}^{T_f} \frac{dT_s}{\frac{\lambda_c(\phi, T_s)}{\sqrt{T_s}} \frac{N_\mu(0)\,\phi}{1.45 \times 10^{21}} - 1} = 8.25 \times 10^{-6} . \qquad (6.9)$$

The number of muons required for spark ignition depends primarily upon the muon cycling rate up to the ignition temperature. With the assumption that the fuel disassembly time is much less than $\tau_{\mu CF}$, the muon sticking probability has little effect.

As the temperature increases to greater than approximately 40 eV, muon induced fusion via the μdt_{11} muo-molecule formation reduces drastically due to the high probability of the μdt_{01} re-excitation to the μdt_{11} state and subsequent break-up of the muo-molecule (see Fig. 5.6). At temperatures

higher than approximately 40 eV, muon induced fusion occurs predominantly by the direct fusion process, described by Eq. 2.35. However, even these reactions begin to slow as the fuel temperature exceeds T ≈ 2 keV because the population of ground state μt muo-atoms abates, as discussed in Appendix A.

It is assumed that the pellet core temperature quickly reaches 40 eV by a combination of μdt_{11} muo-molecular ion fusion and isentropic pressure pulse heating. When the compression waves coalesce at the pellet centre, the ignition temperature of 4 keV must be realized by the direct fusion process. For temperatures greater than 40 eV the cycling rate can be represented by

$$\lambda_c^{-1} = \frac{1}{1.5 \times 10^5 \phi f_\mu(T)} + \frac{T^{3/2}}{1.8 \times 10^{15} \phi f_\mu(T)} . \qquad (6.10)$$

Considering Eq. 6.10, for temperatures less than 4 keV, the cycling rate is limited not by the formation of muo-atoms as was suggest by Hincks et.al.[81] in their criticism of Tan's original μCF triggered ignition concept[80], but by the direct fusion reaction. Substituting into Eq. 6.9 the expression of $f_\mu(T)$ from Appendix A, $T_i \approx 40$ eV and $T_f \approx 4$ keV, the number of muons required for spark ignition is

$$N_\mu(0) \sim \frac{3.12 \times 10^{20}}{\phi^2} \qquad (6.11)$$

and the energy needed to create these muons is

$$E_{muon} = E_\mu N_\mu \sim \frac{12.6 \times 10^6}{\phi^2} \ (MJ) . \qquad (6.12)$$

Once the spark region is ignited, the burning pellet behaves identically to the standard ICF spark ignited pellet described in Section 2.3.2.7; the fusion energy generated is described by Eq. 2.95. A tamper with M_{tamp}/M_{fuel}

Once the spark region is ignited, the burning pellet behaves identically to the standard ICF spark ignited pellet described in Section 2.3.2.7; the fusion energy generated is described by Eq. 2.95. A tamper with M_{tamp}/M_{fuel} = 2 is assumed. The deuterium-tritium fuel burn-up fraction with a tamper $f_{burn}(ICF)$, is illustrated in Fig. 2.9.

Using the general energy gain formula of Eq. 3.1, and assuming that the energy to compress a deuterium-tritium fuel pellet and tamper is due only to the degenerate electron pressure, the energy gain of a single deuterium-tritium pellet of initial pellet radius r_o compressed to an average final density of ϕ (LHD) is

$$G_1 \sim \frac{\eta_c f_{burn} V_o^3 N_0 Q_{dt}}{\frac{E_\mu N_\mu(0)}{\eta_\mu} + \frac{3 E_d \phi^{2/3} V_0 N_0}{\eta_d}} \sim \frac{\eta_c 6.7 \times 10^5 (MJ) r_0^3 f_{burn}}{\frac{12.6 \times 10^6 (MJ)}{\eta_\mu \phi^2} + \frac{0.51 (MJ) r_0^3 \phi^{2/3}}{\eta_d}} \tag{6.13}$$

Assuming that the ρr value of the final compressed fuel pellet is less than 10 g/cm^2, the energy required to generate the requisite number of muons will always be greater than the energy required to compress the fuel and the energy gain can be reduced to

$$G_1 \sim \frac{\eta_c \eta_\mu f_{burn}(ICF) \phi^2 r_0^3}{18.5} \sim \eta_c \eta_\mu 6.6 (\rho r)^3 f_{burn}(ICF) . \tag{6.14}$$

It appears that μCF triggered ignition could be a successful method of spark igniting a deuterium-tritium pellet, provided that sufficient muons could be injected into a very small volume and efficient powerful compression drivers are available. High densities will reduce the number of muons required to be injected into the spark region and also the accelerator current required for muon generation. However, the spark radius decreases with increasing density (Eq 6.2). The required particle current in the muon production system, calculated using Eqs. 4.47 and 6.11, is very large even for large fuel densities. Considerable technological development will be necessary before GeV deuteron accelerators with currents greater than 10 Amperes are available[122].

6.3 Evaluation of the High Density μCF Concept

With $X_\mu \approx 1000$ for densities greater than 200 x LHD and $T < 30$ eV, it appears from Figures 5.10a and 5.10b that high muon efficiencies can be attained in high density deuterium-tritium fuel. Whereas this result suggests that elevated densities could result in a viable energy production system, this simple analysis does not represent the complete picture. The previous time independent model did not address the dynamics of energy generation in a disassembling fuel pellet. A more thorough derivation of the energy gain of the high density μCF energy system follows.

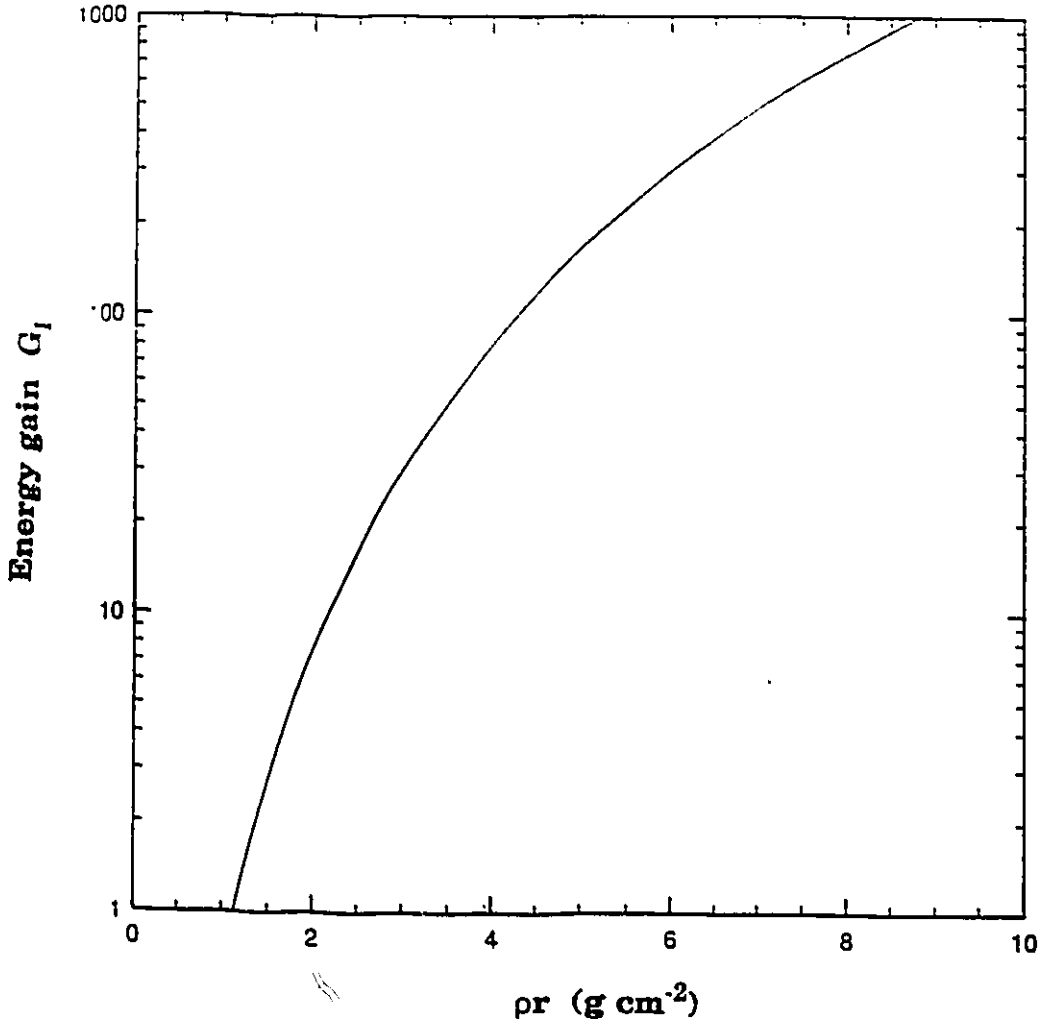

Figure 6.1 : Single pellet energy gain plot of the μCF triggered spark ignition concept G_1 (not including efficiencies).

Consider a deuterium-tritium pellet at its peak average density. The temperature at the peak density is determined using the post-isentropic compression/temperature relationship from Eq. 4.38; this temperature determines the initial operating point of muon catalysis. Muon catalyzed fusion reactions will produce energetic neutrons and alpha particles that may be locally deposited and heat the deuterium-tritium fuel. The heated fuel will cool by radiation emission. The energy gain will be maximized if the optimum temperature and density for muon catalysis can be sustained. In the energy gain calculation, the following simplifying assumptions will be used:

1. The 3.5 MeV alpha particle energy is always deposited within the fuel. This appears reasonable because large fuel pellets will be considered and extreme temperatures are not expected.
2. Heating due to the 14.1 MeV fusion neutrons will be appreciable only if the fuel pellet has a $\rho r > 3$ g/cm^2.
3. Energy is lost from the pellet only by bremsstrahlung radiation.

Using these assumptions, the power balance within the disassembling pellet can be described by,

$$\frac{\lambda_c N_\mu Q_\alpha \phi}{V_0} = P_{brems}(\phi, T) = A_{brems} N_0^2 \phi^2 \sqrt{T}, \qquad (6.15)$$

where Q_{dep} is the energy deposited in the fuel per fusion reaction and N_μ represents the muon population within the compressed fuel pellet. The value of Q_{dep} ranges from 3.5 to 17.6 MeV, depending on the extent of neutron heating. Assuming that the reaction time of the compressed fuel pellet is of the order of the muon catalyzed reaction time $\tau_{\mu CF}$, the muon population will be time dependent and can be represented by Eq. 6.5.

After the muons are injected, the compressed and heated deuterium-tritium sphere will disassemble by a rarefaction wave that moves from the surface of the pellet to the centre. The reaction time of the disassembling pellet can be calculated by assuming that the velocity of the rarefaction wave is dependent on the pressure within the fuel, as follows:

$$\tau_r \sim \frac{r}{u_s} = \frac{r_0}{\phi^{1/3} u_s(\phi,T)}, \qquad (6.16)$$

where $u_s(\phi,T)$ is the sound speed and r_0 is the initial deuterium-tritium fuel radius. For highly compressed deuterium-tritium in the relatively low temperatures expected in high density μCF ($T < 100$ eV), the velocity of the rarefaction wave must include the internal pressure. Therefore, from Eq. 2.68:

$$u_s(\phi,T) \sim 1.13 \times 10^6 \sqrt{T + 1.07\,\phi^{2/3}} \quad (\frac{cm}{s}), \qquad (6.17)$$

From the definition of the muon catalyzed fusion reaction time in Section 5.6.2, the minimum $\tau_{\mu CF}$ for a density less than 1000 times LHD is always greater than 500 ns. The disassembly time of a compressed deuterium-tritium sphere with muons represented by the reaction time τ_r will always be shorter than the $\tau_{\mu CF}$ as long as the initial pellet radius is $r < 5$ cm. For pellets smaller than 5 cm in radius, it can be assumed that the muon concentration

within the pellet remains steady during the pellet's lifetime, and that the temperature will also remain constant. From the power balance in Eq. 6.15, the number of muons required to achieve a given operating temperature is determined by the following:

$$N_\mu(0) = \frac{P_{brems}(\phi,T)\,\frac{4\pi}{3}\,r_0^3}{\lambda_c(\phi,T)\,Q_{dep}} \tag{6.18}$$

Figure 6.2 shows the initial muon concentration requirement represented by $N_\mu(0)/r_0^3$ as a function of the operating temperature for fuel densities of ϕ = 1, 10, 100 and 1000 x LHD and for alpha particle deposition energies of Q_{dep} = 3.5 MeV and alpha particle and neutron deposition energies of Q_{dep} = 17.6 MeV.

The salient feature of this plot is that the fuel temperature changes drastically for very small increases in the muon concentration at temperatures below 20 eV; however, as the operating temperature increases past 20 eV, the required muon concentration increases considerably. This effect is a result of the abatement of the muo-molecular fusion process as the temperature approaches 35 eV.

It is desirable to achieve a maximum operating temperature using a minimum quantity of muons. Examining Fig. 6.2, the optimal muon requirement appears to be about 10^{20} muons per r_0^3 which would provide for a constant temperature near 30 eV.

The instantaneous fusion power generated by muon catalyzed fusion reactions is calculated by

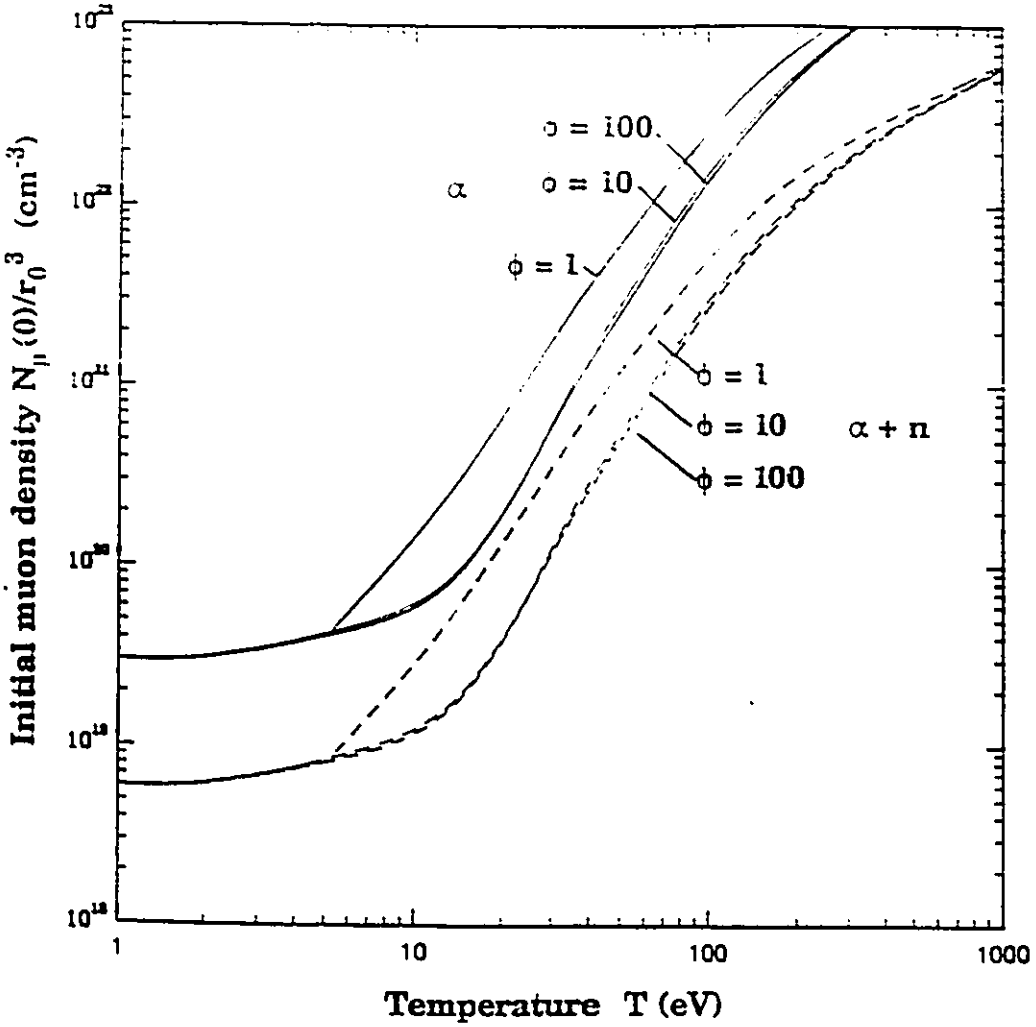

Figure 6.2 : Plot of the number of muons per r_0^3 required to heat a compressed deuterium-tritium sphere to a temperature T for fuel densities of ϕ = 1, 10 and 100 LHD. The solid lines use Q_{dep} = 3.5 MeV (alphas only) and the dashed lines use Q_{dep} = 17.6 MeV (alphas and neutrons).

$$P_{fusion}(t) = \left(\frac{r_0}{\phi^{1/3}} - u_s t\right)^3 \lambda_c \frac{N_\mu(t)\,\phi}{V_0} Q_{dt} \tag{6.19}$$

where V_0 is the initial volume, $u_s(\phi,T)$ is the speed of the rarefaction wave in the disassembling pellet and $N_\mu(t)$ is the number muons at time t.

Integrating the fusion power over the lifetime of the pellet $\tau_r = r/u_s = r_0/(\phi^{1/3}u_s)$ results in

$$\begin{aligned} E_{fusion}(\phi,T) &= \int_0^{\frac{r}{u_s}} P_{fusion}(t,\phi,T)\,dt \\ &\sim V_0 \frac{r_0}{u_s(\phi,T)} \frac{N_\mu(0)\,\lambda(\phi,T)}{\phi^{4/3}} Q_{dt}\,. \end{aligned} \tag{6.20}$$

The energy required to supply muons will always exceed the compression energy and thus the energy gain is,

$$\begin{aligned} G_2 &= \eta_c \eta_\mu \frac{r_0}{4\,u_s(\phi,T)} \frac{Q_{dt}}{E_\mu} \frac{\lambda_c(\phi,T)}{\phi^{1/3}} \\ &\sim \eta_c \eta_\mu \frac{\lambda_c(\phi,T)}{8.77\times10^8} \frac{r_0}{\phi^{1/3}\sqrt{T + 1.07\,\phi^{2/3}}}\,. \end{aligned} \tag{6.21}$$

At the optimal temperature of T ≈ 30 eV, the energy gain without efficiencies per pellet radius $G_2/\eta_c\eta_\mu r_0$ is depicted as a function of density in Fig. 6.3. The energy gain does not break-even even when extremely high fuel densities and pellet radii are considered. Also the effect of alpha particle build-up, which poisons the muon catalyzed fusion chain, is not considered in this analysis and would limit the energy gain further.

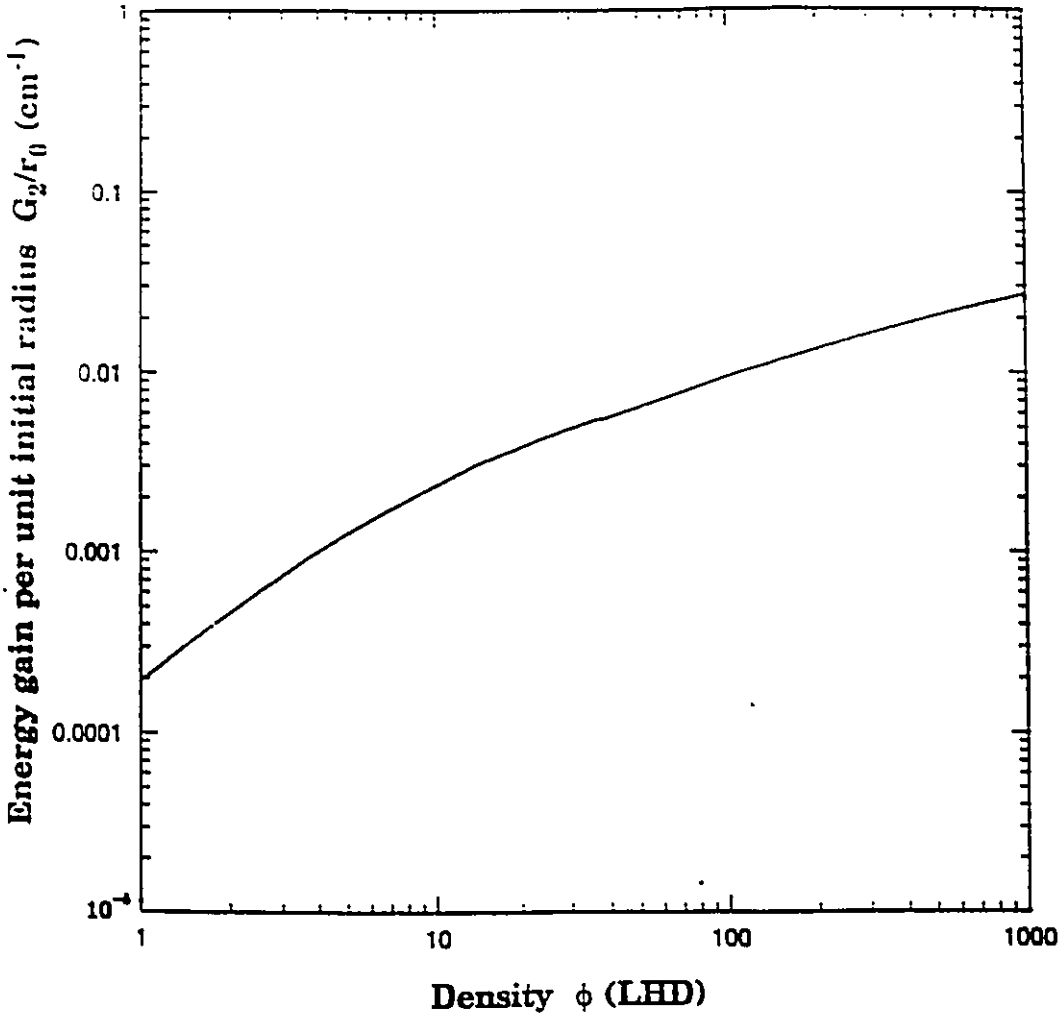

Figure 6.3 : Plot of the energy gain G_2 (not including efficiencies) of a compressed deuterium-tritium sphere injected with muon per unit initial pellet radius r_0 at an operating temperature of 30 eV.

6.4 Summary

The concept of μCF triggered ignition appears feasible, but significant technological advances in the area of muon injection are required before practical application will be possible. By contrast, the high density approach appears to be of marginal effectiveness because high cycling rates are restricted to low temperature regimes.

CHAPTER 7

CONCLUSIONS

7.1 Conclusions

An analysis of the complementary scientific and technical attributes of μCF and ICF approaches to an energy system was carried out. Two strategies for μCF-ICF synergetic interaction were examined in detail: μCF triggered ignition and high density μCF. The viability indicator, that is the energy gain of a single deuterium-tritium pellet, for the μCF triggered spark ignition concept suggests that energy production is possible if a sufficient quantity of muons can be effectively injected into a very small central volume. By contrast, the high density μCF approach was found to be non-viable, due to a low operating temperature and alpha particle poisoning. Based on analysis of the general technological implications of the μCF triggered ignition approach, we conclude that further development of muon production, moderation and compression drivers would be required for a μCF-ICF energy system to be practical.

In the course of the analysis of the μCF-ICF energy system concepts, the following two original analyses were undertaken:

1. the number of muons required to raise a spark region to the

ignition temperature and,

2. the energy production in a compressed deuterium-tritium sphere with muons.

In addition, the following original extensions to the understanding of relevant high temperature and density muon catalyzed fusion processes in deuterium-tritium were investigated:

1. the high temperature and high density muo-atom cascade,
2. the effect of excited state reverse muon transfer processes,
3. the effect of the energy structure on the break up of the μdt_{11} muo-molecule and,
4. the muon cycling rate and muon efficiency analyses encompassing all relevant high density μCF processes in deuterium-tritium.

7.2 Recommendations for Further Studies

The following worthwhile extensions of this analysis are suggested:

1. Investigation of methods to create, moderate and focus a large muon pulse into a small volume.
2. Inclusion of three body effects in the excitation of muons stuck to alpha particles. in the model of muon regeneration.
3. Inclusion of spatial simulation of the compression and μCF triggered ignition of a deuterium-tritium fuel pellet.
4. Exploration of three-body effects on the muo-atom cascade

and muon transfer.

5. Inclusion of high density μdd fusion processes.
6. Performance of experiments to determine μCF reaction rates in high density deuterium-tritium. This proposal is elaborated upon in Appendix E.

It is our expectation that the above investigations will provide further insight and understanding to support a μCF-ICF fusion energy system.

Appendix A

A.1 Ionization and Dissociation of Hydrogen

It is important to have suitable models of the physical state of the fuel, because this will determine the governing mechanisms in a muon catalysis chain. Whereas there are many possible states of hydrogen in the conditions of interest[123], the molecular, atomic, and ionized fuel fractions calculated from the following ionization and dissociation reaction mechanisms are likely to be dominant:

$$H_2 \rightarrow H + H - 4.50eV \tag{A.1}$$

$$H \rightarrow H^+ + e^- - 13.60eV \tag{A.2}$$

The dissociative and ionization properties for the heavy isotopic combinations of hydrogen (D_2, DT and T_2) are not significantly different from normal hydrogen, therefore simulation of hydrogen suffices.

The rate of molecular dissociation and atom ionization are much more rapid than μCF processes. Therefore, Saha type equilibrium relative fractions of deuterium and tritium molecules, atoms, and ions at a given temperature and density may be calculated.

The normal Saha equation[28,77], applied to the ionization reaction (Eq. A.2) must include the effect of pressure ionization at elevated densities[114]. As

density increases, the atomic spacing becomes smaller than the atomic orbits so ionization occurs at progressively lower energies and total ionization occurs at lower temperatures. For densities greater than about 37 times LHD, the atomic spacing distance (using the ion sphere model) is less then the ground state Bohr radius and the atoms are considered completely ionized for any temperature. For densities of 37 times LHD and less, we modify the normal Saha equation to include density dependent ionization potential yielding a modified Saha ionization equation for hydrogen:

$$\frac{\alpha_i^2}{1 - \alpha_i} = \frac{0.142\ (kT)^{3/2}}{\phi}\ e^{-\frac{I_i(\phi)}{kT}} \quad . \tag{A.3}$$

Here α_i is the ionization fraction, T is the fuel temperature and ϕ is the fuel density with respect to LHD. In Eq. A.3

$$I_i(\phi) = 13.6\left(1 - \frac{a_o}{r}\right)\ \ (eV)\ , \tag{A.4}$$

with $a_o = 5.29 \times 10^{-9}$ cm and r as the mean distance between hydrogen atoms and is calculated using the ion sphere model[115]

$$r = \left(\frac{3}{4\pi N\phi}\right)^{1/3} = 1.78 \times 10^{-8}\ \phi^{-1/3}\ \ (cm)\ , \tag{A.5}$$

where $N = 5 \times 10^{22}$ cm^{-3}. In this abrupt pressure ionization assumption, at fuel densities greater than 37 times LHD, all atoms are assumed to be ionized ($\alpha_i = 1$).

Using arguments similar to those employed to develop the modified Saha ionization equation, the modified Saha dissociation equation[28,77] is written as

$$\frac{\alpha_d^2}{1 - \alpha_d} = \frac{1.7\ (kT)^{1/2}\ e^{-\frac{I_d(\phi)}{kT}}}{Z_{vib}\ \phi}, \tag{A.6}$$

where α_d is the dissociation fraction, I_d is the dissociation potential of H_2, T is the temperature, ϕ is the fuel density with respect to LHD and Z_{vib} is the vibration partition function which is calculated by,

$$Z_{vib} = \sum_{v=0}^{v_{max}} e^{\frac{-\hbar\omega_o v}{kT}} . \tag{A.7}$$

Here $\hbar\omega_0/2$=0.27 eV is the H_2 ground state vibrational energy, v is the vibrational quantum number and v_{max} is the maximum allowed excitation before dissociation.

Pressure enhanced dissociation is included in the dissociation Saha equation by calculating the dissociation potential with the Morse potential[123] defined by the following:

$$I_d(\phi) = 4.75\ (e^{-2\alpha\cdot(r-d_o)} - 2\,e^{-\alpha\cdot(r-d_o)}) + 0.27\ \ (eV)\,, \tag{A.8}$$

where $d_o = 7.42 \times 10^{-9}$ cm, $\alpha = 1.94 \times 10^8$ cm^{-1} and r is defined from the ion sphere model. At low densities (ϕ << LHD) the dissociation potential reaches approximately 4.48 eV. As the atomic density increases, the dissociation potential decreases because the molecular size for successively lower vibrational modes equal or exceed the distance between atoms. Here the simple condition that molecules move freely prior to dissociation is assumed. As the fuel density increases, the value of v_{max} decreases, and the vibrational partition function tends to 1. At densities greater than ϕ ~ 7 times LHD the dissociation potential is approximately equivalent to the energy of the first vibrational state and suggests that any excitation will lead to molecular

dissociation. Using the modified dissociation Saha equation at densities higher than $\phi > 7$ times LHD produces inconsistent results. In order to simplify the molecular dissociation model it is assumed that there is abrupt and complete molecular dissociation for fuel densities greater than 7 times LHD.

Computing the values of α_i and α_d from the models above, the fraction of hydrogen molecules, $f_m = (1-\alpha_d-\alpha_i+\alpha_d\cdot\alpha_i)$, the fraction of hydrogen atoms, $f_a = \alpha_d(1-\alpha_i)$, and the fraction of hydrogen ions, $f_i = \alpha_i$ are plotted in Figs. A.1, A.2 and A.3 respectively for the temperature and density range of interest.

Since very high temperatures are being considered, density and temperature dependent muo-hydrogen ionization must be considered. The dynamics of the catalyzing processes are more complex with excited muo-atoms but it suffices to say that if the temperature of the medium exceeds the first excited state of muo-hydrogen, i.e., approximately 2 keV, then all muon reaction processes cease. A simple method may be used to simulate the effect of muo-atom excitation by multiplying f_μ, the muon ionization fraction defined by

$$f_\mu = 1-e^{-2keV/T} \tag{A.9}$$

with T as the fuel temperature in eV. The muo-ionization fraction will then be multiplied by any formation rate which includes muons.

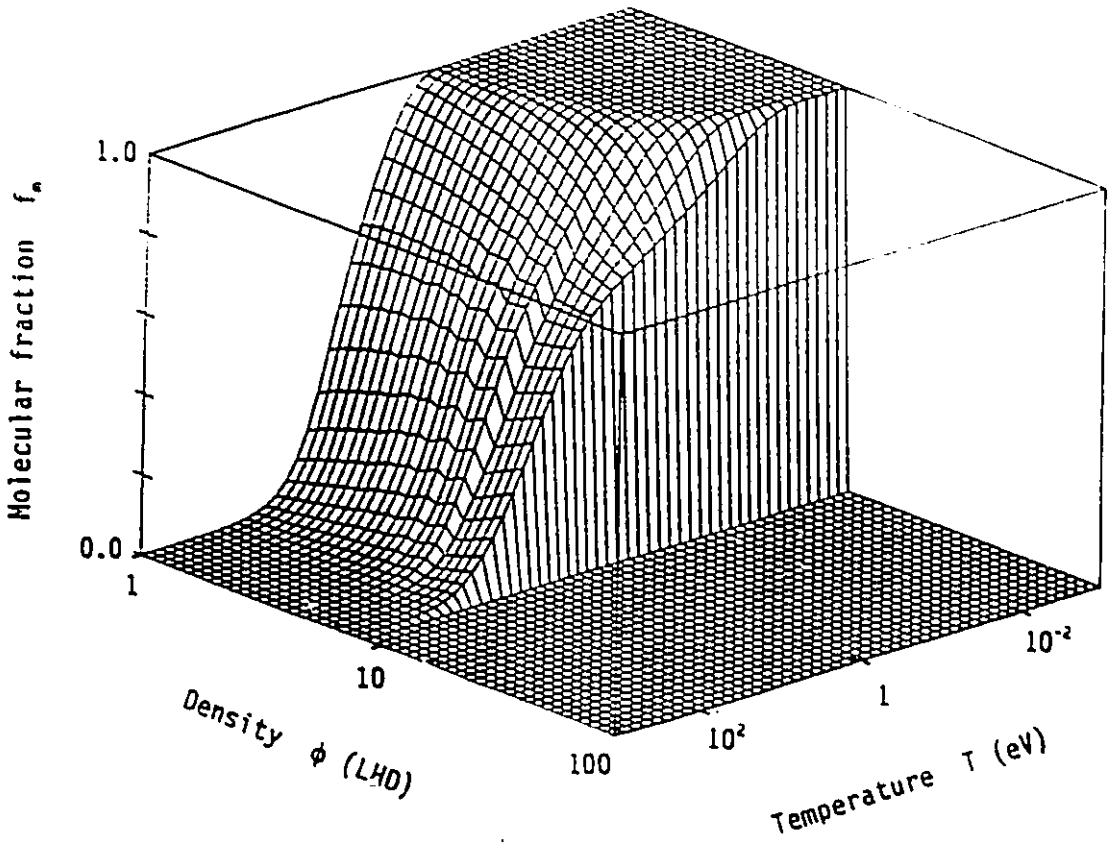

Figure A.1 : The density and temperature dependent molecular fraction of hydrogen.

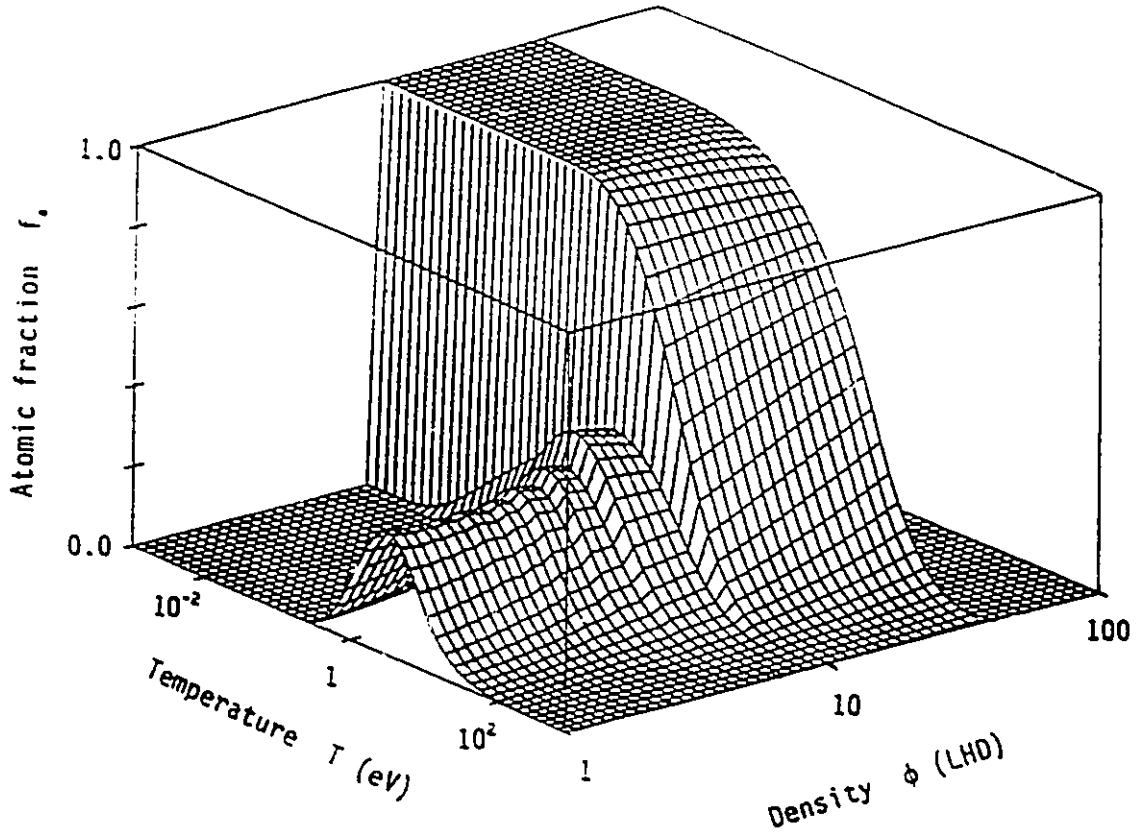

Figure A.2 : The density and temperature dependent atomic fraction of hydrogen.

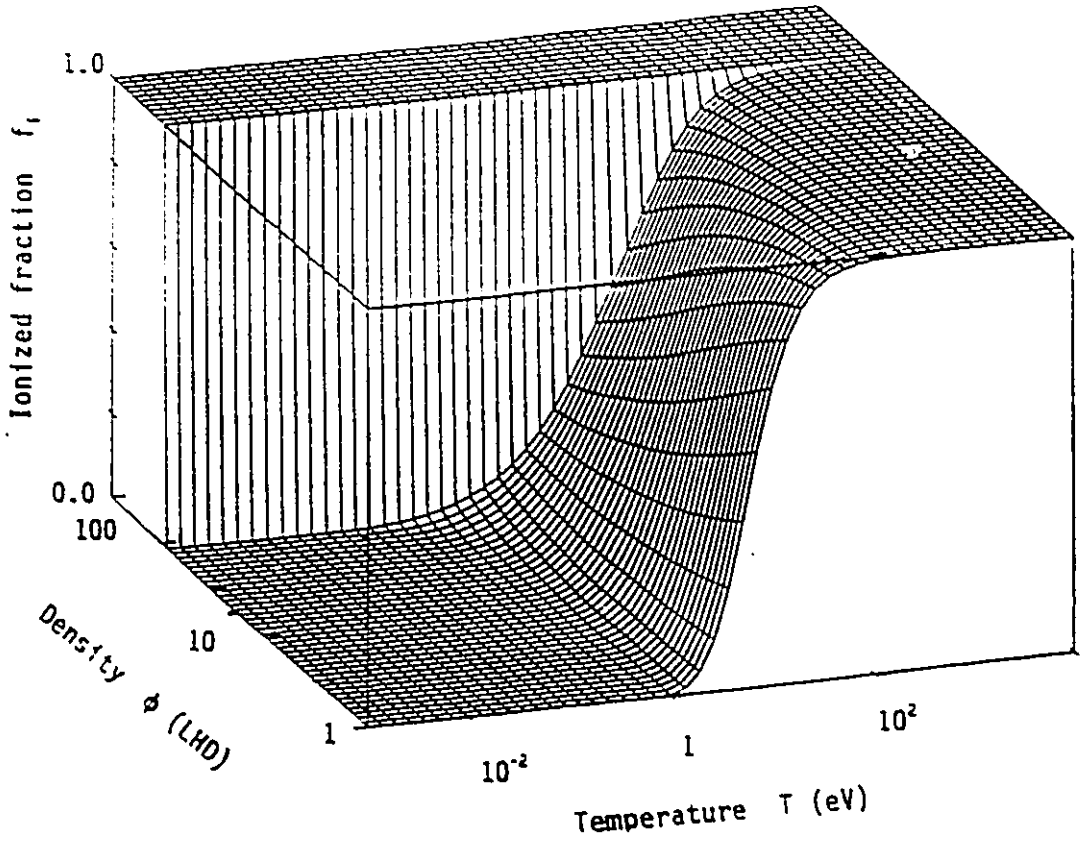

Figure A.3 : The density and temperature dependent ionized fraction of hydrogen.

Appendix B

B.1 Electron Degeneracy

A gas of free electrons will have a momentum distribution described by the Fermi-Dirac distribution. A key property of Fermi-Dirac particles is that only two of them may occupy the same point in momentum space. As a consequence, the fermi energy rises as the density of particles increases. The fermi level is defined as the energy above which the average occupation of the state is less than half. The Fermi-Dirac distribution is

$$f_{FD}(p) = \frac{1}{1 + \exp(\alpha + \frac{p^2}{2mkT})} \tag{B.1}$$

where

$$\alpha = \frac{-E_f}{kT}, \tag{B.2}$$

E_f is the fermi energy, p is the electron momentum, m is the electron mass, T is the temperature and k is Boltzmann's constant. The Fermi-Dirac distribution reduces to the following Maxwell-Boltzmann distribution at high temperatures or low densities:

$$f_{MB} = \exp(\frac{E_f}{kT} - \frac{p^2}{2mkT}). \tag{B.3}$$

The transition occurs when the so-called degeneracy temperature is exceeded. where the degeneracy temperature is defined by

$$kT_{deg} \sim E_f \ (eV) . \tag{B.4}$$

When the temperature is less than T_{deg}, the electrons are said to be degenerate and the degenerate electron pressure is defined as

$$P_f = \frac{2}{5} N E_f , \tag{B.5}$$

where

$$E_f = \frac{1}{8} (\frac{3}{\pi})^{2/3} \frac{h^2}{m_e} N_e^{2/3} \approx 5.1 \phi^{2/3} \ (eV) . \tag{B.6}$$

B.2 Effect of Electron Degeneracy on Reactions

Consider the following two and three body reactions that involve the excitation of an electron:

$$A + e \rightarrow A^* + e^* \tag{B.7}$$

$$A + B + e \rightarrow (AB)^* + e^* \tag{B.8}$$

The reaction rate of the above reactions will depend in part upon the probability that an electron will gain energy in the reaction. For both reactions, this probability can be represented by the following expression:

$$P = \int d^3p_e f(p_e) \int d^3p_e' (1 - f(p_e')) \times |M_{p_e - p_e'}|^2 \delta^3 (\frac{p_e'}{2m_e} - \frac{p_e}{2m_e} + \Delta E) . \tag{B.9}$$

Here p_e' is the final electron momentum, p_e is the initial electron momentum, ΔE is the transition energy released by reactants, M represents the probability of the transition and f(p) is the equilibrium distribution of the electrons. In the reactions depicted by Eqs. B.7 and B.8, the other reactants are assumed to follow a Maxwell-Boltzmann distribution for all conceivable temperatures and densities. By contrast, the electrons may follow Fermi-Dirac or Maxwell-Boltzmann statistics depending on the local temperature and density.

The difference in the reaction rates of the reactions depicted in Eqs. B.7 and B.8 for a Maxwell-Boltzmann distribution of electrons, compared with a Fermi-Dirac distribution, is an important consideration. It is assumed that the ratio of the reaction rates for the two distributions will be the ratio of the electron transition probabilities in Eq. B.9. Equation B.9 can be evaluated for each of the electron distributions using the following assumptions:

1. The transition probability is

$$|M_{p_e - p_e'}| \sim \frac{M}{p_e p_e'} \tag{B.10}$$

   where M is a constant,
2. The initial and final electron momentums are very close and therefore $p_e' \approx p_e$,
3. The transition energy is much smaller than the initial or final electron momenta and therefore $\Delta E \approx 0$,
4. The Maxwell-Boltzmann and Fermi-Dirac distributions are normalized by the following integral:

$$\int_0^\infty k^2 f(k)\, dk = 1 \tag{B.11}$$

yielding the following normalized Maxwell-Boltzmann distribution:

$$f_{MB}(p) = \frac{2}{\sqrt{\pi}\,(m\,kT)^{3/2}} \exp(-\frac{p^2}{2\,m\,kT}) \qquad \text{(B.12)}$$

and the following normalized Fermi-Dirac distribution:

$$f_{FD}(p) = \frac{1}{\sqrt{2}\,(m\,kT)^{3/2}\,F_{1/2}(\alpha)} \frac{1}{1 + \exp(\alpha + \frac{p^2}{2\,m\,kT})} \qquad \text{(B.13)}$$

where

$$F_{1/2}(\alpha) = \int_0^\infty \frac{\sqrt{u}\,du}{1 + \exp(\alpha + u)} \qquad \text{(B.14)}$$

which has an approximate solution of

$$F_{1/2}(\alpha) \sim \frac{2}{3}\,\alpha^{3/2} \qquad \text{(B.15)}$$

for strong electron degeneracy[19].

For the reactions described by Eqs. B.7 and B.8, using the above assumptions and solving Eq. B.9 with the normalized electron distributions defined in Eqs. B.12 and B.13, the ratio of the reaction rate assuming electron degeneracy λ_{FD}, over the reaction rate assuming a Maxwell-Boltzmann electron distribution λ_{MB}, is

$$\frac{\lambda_{FD}}{\lambda_{MB}} \sim (\frac{kT}{E_f})^{3/2}. \qquad \text{(B.16)}$$

Appendix C

C.1 Charged Particle Range

The range of energetic charged particles (alphas, muons, etc.) is

$$R(E) = \int_{E}^{0} \frac{dE}{S(E)} \tag{C.1}$$

where E is the initial energy of the muon and S(E) is the energy dependent stopping power of the medium.

C.2 Bethe Stopping Model

Charged particle energy loss in solid materials is caused predominantly by excitation of bound electrons and can be calculated using the Bethe Stopping model[18] with:

$$S(E) = \left(\frac{e^2}{4\pi\epsilon_0}\right)^2 \frac{4\pi N_a Z_1^2 Z_2 \rho e^4}{m_e c^2 \beta^2 A_2}$$

$$\times \left(\ln \frac{T(T + m_e c^2)^2 \beta^2}{2 \langle I \rangle^2 m_e c^2}\right) + (1 - \beta^2) + (2\sqrt{1 - \beta^2} - 1 - \beta^2) \ln 2 \tag{C.2}$$

$$- \frac{1}{8}(1 - \sqrt{1 - \beta^2}) - \beta^2 - \sum_i \frac{c_i}{Z_2} - \frac{\delta}{2}) .$$

where: T is the projectile kinetic energy,

Z_1 is the charge of the projectile.

Z_2 is the atomic number of the stopping medium.

A_2 is the atomic mass number of the stopping medium.

N_A = Avagadro's number = 6.023×10^{23}.

ρ is the density of the stopping medium.

$\beta = v/c$.

v is the projectile velocity,

c is the speed of light in a vacuum.

δ is the polarization effect correction term.

$\sum c_i/Z_2$ is the sum of shell corrections.

m_e is the mass of the electron.

e is the electronic charge,

<I> is the Bethe averaged electron ionization potential.

The Bethe averaged electron ionization potential is formally defined as

$$\ln\langle I\rangle = \frac{\sum_n f_n \ln E_n}{Z_2} \qquad \text{(C.3)}$$

where E_n and f_n are the energies of electronic transitions and corresponding dipole oscillator strengths of the stopping medium and a value of

$$\langle I\rangle \sim 18.8 \quad (eV) \qquad \text{(C.4)}$$

is assumed for deuterium-tritium[124].

C.3 Plasma Stopping Power

Jändel's muon reactivation model uses an analytic approximation to Maynard and Deutsch's Random Phase Approximation (RPA) for modelling of the plasma stopping power[12,120]. This stopping power model is a characteristic

example of the plasma stopping models that include degenerate electron effects and charged particle - plasma interactions by assuming the plasma is a polarizing medium which induces a braking electric field on a moving charge. An analytic expression of the plasma stopping power, which is approximately equivalent to the Maynard and Deutsch model but simpler to express and compute, is the following model by Skupsky[125] where a charged particle energy loss in a hydrogen plasma is expressed by,

$$\frac{dE}{dx} = -\sqrt{E}\, n_e \frac{Z^2\, e^4}{T^{3/2}} \left(\frac{m_e}{M}\right)^{1/2} \sqrt{\pi} \times \frac{8}{3} \left(\frac{\sqrt{\pi}}{2\, F_{1/2}(\eta)\, (e^{-\eta} + 1)}\right) \ln \Lambda_{RPA} \qquad \text{(C.5)}$$

where:

E is the projectile kinetic energy,

Z is the charge of the projectile,

n_e is electron density of the plasma,

M is the atomic mass of the plasma ions,

m_e is the mass of the electron,

e is the electronic charge,

T is the plasma temperature,

$F_{1/2}$ is the fermi function,

η is the ratio of the fermi and the kinetic energy of the electrons,

and $\ln\Lambda_{RPA}$ is the RPA coulomb logarithm.

Appendix D

D.1 3X3 System of Equations Solution

The set of three point kinetic equations of Eqs. 5.56 - 5.58 define a 3X3 System of Equations which determines the temporal evolution of the muon, muo-deuterium and muo-tritium populations. The solution of the 3X3 system in turn determines the important μCF parameters, the muon cycling rate λ_c and the muon efficiency X_μ.

The solution set of a general 3X3 system of equations is:

$$N_i(t) = \sum_{k=1}^{3} \left[\frac{J_i \lambda_k^2 + K_i \lambda_k + L_i}{\prod_{i \neq k} (\lambda_k - \lambda_i)} \right] e^{\lambda_k t} \qquad \text{(D.1)}$$

where λ_k are the eigenvalues of the 3X3 system calculated by following equation:

$$\det | \alpha - \lambda I | = 0 , \qquad \text{(D.2)}$$

where α is the system matrix.

The solution set of the 3X3 equation network of Eqs. 5.56 - 5.58 is obtained by using i={μ,μd,μt} and

$$\alpha = \begin{bmatrix} -(\lambda_a + \lambda_\mu) & 0 & \lambda_{\mu dt} C_d (1 - w_{dt}) \\ \lambda_a q_{1s} & -(\lambda_{dt}(1s) C_t - \lambda_\mu) & \lambda_{td}(1s) \\ \lambda_a (1 - q_{1s}) & \lambda_{dt}(1s) C_t & -(\lambda_{td}(1s) C_d + \lambda_{\mu dt} C_d + \lambda_\mu) \end{bmatrix}$$

in Eqs D.1 and D.2. The other parameters in Eq. D.1 are defined by the following:

$$J_i = N_i(0) \tag{D.4}$$

where $N_i(0)$ is the initial concentrations of the constituents,

$$K_i = trace(M_\alpha) - [\alpha]_{ii} \tag{D.5}$$

where M_α is the minor of the reaction matrix α and $[\alpha]_{ii}$ is the ii^{th} element of α and

$$L_i = \det(\alpha_i) , \tag{D.6}$$

where α_i is the matrix α, except that the i^{th} column is replaced by the initial concentration vector

$$N_0 = [N_\mu(0), N_{\mu d}(0), N_{\mu t}(0)] . \tag{D.7}$$

The eigenvalue equation of Eq. D.2 can be expressed as

$$\lambda^3 + a\lambda^2 + b\lambda + c = 0 \tag{D.8}$$

where

$$a = 3\lambda_\mu + A \tag{D.9}$$

$$b = 3\lambda_\mu^2 + 2A\lambda_\mu + B \tag{D.10}$$

$$c = \lambda_\mu^3 + A\lambda_\mu^2 + B\lambda_\mu + C \tag{D.11}$$

with

$$A = \lambda_a + \lambda_{dt}(1s)\,C_t + \lambda_{td}(1s)\,C_d + \lambda_{\mu td}\,C_d \tag{D.12}$$

$$\begin{aligned} B = {} & \lambda_a(\lambda_{dt}(1s)\,C_t - \lambda_{td}(1s)\,C_d) \\ & + \lambda_{\mu dt}\,C_d(q_{1s}\,\lambda_a + \lambda_{dt}(1s)\,C_t) \end{aligned} \tag{D.13}$$

$$C = \lambda_a\,\lambda_{dt}(1s)\,C_t\,\lambda_{\mu td}\,C_d\,w_{dt} \tag{D.14}$$

Using Cardan's formula to solve for the roots of a cubic equation in Eq. D.8 yields

$$\lambda_i = y_i - \frac{a}{3} = y_i - \lambda_\mu - \frac{A}{3}, \tag{D.15}$$

where y_i are the roots of the following cubic equation

$$y^3 + py + q = 0, \tag{D.16}$$

with

$$p = b - \frac{a^2}{3} = B - \frac{A^2}{3}, \tag{D.17}$$

and

$$q = c - \frac{ba}{3} + \frac{2a^3}{27} = C - \frac{BA}{3} + \frac{2A^3}{27}. \tag{D.18}$$

The type of roots of the eigenvalue equation in Eq. D.16 can be determined by the following determinant:

$$\Delta = \frac{q^2}{4} + \frac{p^3}{27}$$
$$= 4B^2(B - \frac{A^2}{4}) + 4CA(A^2 - \frac{9}{2}B) + 27C^2, \quad \text{(D.19)}$$

where if,	there is
$\Delta > 0$	One real root and two complex roots.
$\Delta = 0$	Three real roots and at least two are equal.
$\Delta < 0$	Three real roots.

For the density and temperature regime of interest, i.e. $\phi = 1 \rightarrow 1000$ LHD and $T = 10^{-3} \rightarrow 10^{4}$ eV, the value of Δ is found to always negative and thus three real roots are found. In addition, because the 3X3 system described by Eqs. 5.56 - 5.58 represents a dissipative system, the three roots of the eigenvalue equation are also all negative.

The case where Δ is negative is also the so-called "Casus Irreducibilis" where only trigonometric solutions of Eq. D.16 can be found. These solutions are:

$$y_1 = 2\sqrt{\frac{-p}{3}}\cos(\frac{\theta}{3}), \quad \text{(D.20)}$$

$$y_2 = 2\sqrt{\frac{-p}{3}}\cos\left(\frac{\theta}{3} + \frac{2\pi}{3}\right), \tag{D.21}$$

$$y_3 = 2\sqrt{\frac{-p}{3}}\cos\left(\frac{\theta}{3} + \frac{4\pi}{3}\right), \tag{D.22}$$

where

$$\tan(\theta) = \frac{-\sqrt{-\Delta}}{q\sqrt{27}}. \tag{D.23}$$

Assuming that the initial concentration vector is $N_0 = [1.0.0]$, the muon efficiency is calculated by

$$X_\mu(t) = \int_0^t \lambda_{\mu dt} C_d N_{\mu t}(t)\, dt \tag{D.24}$$

and using the solution of $N_{\mu t}(t)$ of Eq.D.1 yields

$$X_\mu = \int_0^\infty \lambda_{\mu dt} C_d \sum_{k=1}^{3} \left[\frac{B_{\mu t}\lambda_k + C_{\mu t}}{\prod_{l \neq k}(\lambda_k - \lambda_l)}\right] e^{\lambda_k t} \tag{D.25}$$

and reduces to the following expression

$$X_\mu = \frac{\lambda_{\mu dt} C_d}{\lambda_\mu^3 + A\lambda_\mu^2 B\lambda_\mu + C}. \tag{D.26}$$

In the density and temperature regime of interest, because the muo-atomic formation rate λ_a and the μd transfer rate $\lambda_{dt}(1s)$ are always larger than other reaction rates, the following expression is true:

$$N_\mu(t) \sim N_\mu(0)\exp(-\lambda_\mu + \lambda_c w_{dt}). \tag{D.27}$$

Appendix E

E.1 High Density Muon Catalyzed Fusion Experiment Proposal

Determination of the viability of the μCF-ICF energy system approach relies heavily upon the models of muon catalyzed fusion discussed in Chapter 5. An experiment to investigate some of the important reaction parameters at high density and temperature is suggested in order to validate these models.

Jones has suggested examining μCF fusion in deuterium and deuterium-tritium compressed in a diamond cell[91]. Static densities of hydrogen and deuterium up to 3 x LHD have been obtained for temperatures from less than 20 K up to 300 K (Ref.90). Introducing a diamond cell into current muon catalyzed fusion experiment designs seems to be a natural first step towards understanding the effect of fuel density upon the μdt_{11} resonance formation process as well as the muon regeneration process.

The next stage in high density muon catalyzed fusion research should involve dynamic compression processes with muons. A valuable experience base exists, in equation of state studies compressing hydrogen and deuterium to densities up to 10 x LHD with explosives[92,93]. Muons introduced into deuterium or deuterium-tritium fuel prior to shock compression and analysis

of the neutron flux emitted from during compression would yield data which could be used to determine the high density μCF reaction processes occurring. Performing experiments with varying pressure pulses and tritium : deuterium concentration ratios would allow specific process rates to be isolated (i.e. μdt_{11} formation rate).

REFERENCES

1. L.M. LIDSKY, "The Trouble with Fusion", *Technology Review*, p.32 (Oct.1983)

2. J.D. LINDL, R.L. McCRORY AND E.M. CAMPBELL, "Progress Towards Ignition and Burn Propagation in Inertial Confinement Fusion", *Physics Today*, p.32 (Sept. 1992).

3. W.J. HOGAN, R. BANGERTER AND G.L. KULCINSKI, "Energy from Inertial Fusion", *Physics Today*, p.42 (Sept. 1992).

4. D.H. CRANDALL, "Conclusions and Directions from the OFE Inertial Fusion Reactor Studies", *Fusion Technology*, **21**, p.1451 (May 1992).

5. A.A. HARMS, "The Synergetics of Fusion Energy", *J. of Fusion Energy*, in press, (1992).

6. A. HASEGAWA ET. AL., "Magetically Insulated and Inertially Confined Fusion - MICF", *Nuclear Fusion*, **28**, 3, p.369 (1988).

7. T. KAMMASH AND D.L. GALBRAITH, "A High Gain Reactor Based on the Magnetically Insulated Inertial Confinement Fusion (MICF) Concept", *Nuclear Fusion*, **29**, 7 p.1079 (1989).

8. YU. PETROV, "A Muon Catalyzed Reactor Concept", *Muon Catalyzed Fusion*, **1**, p.351 (1987).

9. T. TAJIMA, S. ELIEZER AND R.M. KULSRUD, "A New Concept for Muon Catalyzed Fusion Reactor", *AIP Conf. 181, Muon Catalyzed Fusion*, eds. S.E. Jones, J. Rafelski and H.J. Monkhorst, Sanibel Island, F, p.423 (1988).

10. S.E. JONES, "Can 250^{+} Fusions per Muon be Achieved?", in *Muon Catalyzed Fusion and Fusion with Polarized Nuclei*, eds. B. Brunelli and G.G. Leotta, Plenum Press, New York, p.73 (1987).

11. L.I. MEN'SHIKOV AND L.I. PONOMAREV, "Formation of dtμ muonic molecules in three-body collisions at high temperatures", *JETP Lett.*, **46**, 6, p.312 (1987).

12. M. JÄNDEL ET.AL., "Reactivation of αμ in Muon-Catalyzed Fusion under Plasma Conditions", *Phys. Rev. A*, **40**, 5, p.2799 (1989).

13. L.I. MEN'SHIKOV AND L.N. SOMOV, "Status of Muon Catalysis of Nuclear Fusion Reactions", *Sov. Phys. Usp.*, **33**, 8, p.616 (1990), L.I. MEN'SHIKOV, Report IAE-4589/2, Institute of Atomic Energy, Moscow (1988).

14. A.A HARMS, G. CRIPPS AND B. GOEL, "Energy Gain of ICF-μCF Symbiosis", *Proc. of the Fifth International Conference on Emerging Nuclear Energy Systems (ICENES 1989)*, Karlsruhe, FRG, eds. U. von Möllendorff and B. Goel, World Scientific Publishing, p.267 (1989).

15. G. CRIPPS, A.A. HARMS AND B. GOEL, "Muon Catalyzed Fusion under Compressive Conditions", KfK Report No. 4763, Kernforschungszentrum Karlsruhe, Karlsruhe, Germany (1991).

16. G. CRIPPS, A.A. HARMS AND B. GOEL, "Muon Catalyzed Fusion Chain-Length Extension under Compressive Conditions", *Fusion Technology*, **20**, 4, p.904 (1991).

17. G. CRIPPS, A.A. HARMS AND B. GOEL, "Muon Catalyzed Fusion of Deuterium-Tritium at Elevated Densities", *Hyperfine Interactions*, **77**, pp.181-199 (1993).

18. K.S. KRANE, *Introductory Nuclear Physics*, John Wiley and Sons, New York (1988).

19. D.D. CLAYTON, *Principles of Stellar Evolution and Nucleosynthesis*, McGraw Hill Book Company, New York (1968).

20. A. PERES, "Fusion Cross Sections and Thermonuclear Reaction Rates", *J. Appl. Physics*, **50**, 9, p.5568 (1979).

21. F.C. FRANK, "Hypothetical Alternative Energy Sources for the Second Meson Events", *Nature*, **160**, 4048, p.525 (1947).

22. A.D. SAKHAROV, Report to the Academy of Sciences USSR (1948).

23. G. ZWEIG, "Quark Catalysis of Exothermal Nuclear Reactions", *Science*, **201**, 4360, p.973 (1978).

24. D. HARLEY, "Nuclear and Molecular Processes in Muon Catalyzed Fusion", PhD. Thesis, University of Arizona (1991).

25. L.I. PONOMAREV, "Muon Catalysed Fusion", *Contemporary Physics*, **31**, 4, p.219 (1990).

26. S.S. GERSHTEIN, YU.V. PETROV AND L.I. PONOMAREV, "Muon Catalysis and Nuclear Breeding", *Sov.Phys.Usp.*, **33**, 8, p.591 (1990).

27. L. BRACCI AND G. FIORENTINI, "Mesic Molecules and Muon Catalyzed Fusion", *Physics Reports*, **86**, 4, p.169 (1982).

28. YA. B. ZEL'DOVICH AND YU. P. RAIZER, *Physics of Shock Waves and High Temperature Hydrodynamic Phenomena*, Academic Press, New York (1966).

29. K. A. BRUECKNER AND S. JORNA, "Laser Driven Fusion", *Rev. Mod. Phys.*, **46**, 2, p.325 (1974).

30. B. GOEL AND W. HÖBEL, " The Role of Neutrons in the Performance of ICF-Traget", in *Proceedings of the 10th International Conference on Plasma Physics and Controlled Nuclear Fusion*, London, Sept. 12-19, 1984, Nucl. Fus. Supplement, 3, p.345 (1985).

31. J.D. LAWSON, "Some Criteria for a Power Producing Thermonuclear Reactor", *Proc. Phys. Soc. London*, **B70**, 6, p.6 (1957).

32. J. RAEDER ET.AL., *Controlled Nuclear Fusion : Fundamentals of its Utilization for Energy Supply*, John Wiley and Sons (1986).

33. S.K. SOOD, J. QUELCH AND R.B. DAVIDSON, "Fusion Technology Experience at Ontario Hydro's Darlington Tritium Removal System and Heavy Water Upgrader", *Fusion Eng. and Design*, **12**, 3, p.365 (1990).

34. HOLDREN, J.P., "Adequacy of Lithium Supplies as a Fusion Energy Source", LLNL, Livermore, CA, UCID-15953 (1971).

35. R.W. MOIR, "HYLIFE-II Inertial Confinement Fusion Power Plant Design", *Fusion Technology*, **19**, p.617 (1991).

36. R.W. MOIR, "Hylife-II Inertial Fusion Energy Power Plant Design", *Fusion Technology*, **21**, p.1475 (1992).

37. J. NUCKOLLS, L. WOOD, A. THIESSEN AND G. ZIMMERMAN, "Laser Compression of Matter to Super-High Densities: Thermonuclear (CTR) Applications", *Nature*, 239, p.139, 15 Sept. 1972.

38. YU. V. ASFANAS'EV ET.AL., "Laser Initiation of Thermonuclear Reaction in Inhomogenous Spherical Targets", *Soviet Physics JETP Letters*, 21, 2, p.68 (1975).

39. S. ELIEZER, A. GHATAK AND H. HORA, *An Introduction to the Equation of State : Theory and Applications*, Cambridge University Press, Cambridge, UK (1986).

40. G. TAYLOR, " The Instability of Liquid Surfaces when Accelerated in a Direction Perpendicular to their Planes", *Proc. Roy. Soc.*, **A201**, p.192 (1950).

41. K.A. BRUECKNER, S. JORNA AND R. JANDA, "Hydrodynamic Stability of a Laser-Driven Plasma", *Phys. Fluids*, **17**, p.1554 (1974).

42. W. SEIFRITZ and B. GOEL, "Muonic and polarized fusion for inertial confinement fusion", *Atomenergie-Kerntechnik*, **43**, *3* (1983).

43. G.L. KULCINSKI, "First Wall Protection Schemes for Inertial Confinement Fusion Reactors", *J. of Nucl. Mat.*, **85 & 86**, p.87 (1979).

44. W.J. HOGAN AND G.L. KULCINSKI, "Advances in ICF Power Reactor Design", UCRL-91647 Preprint (1985).

45. J. POWELL ET.AL., "A Liquid Wall Boiler and Moderator (BAM) for Heavy Ion Pellet Fusion Reactors", BNL-50744 (1977).

46. J.J. DUDERSTADT AND G.A. MOSES, *Inertial Confinement Fusion*, John Wiley and Sons, New York (1982).

47. P.K. IYENGAR AND M. SRINIVASAN, "Overview of Inertial Confinement Fusion (ICF)", Preprints of papers presented at the Indian Physics Association Seminar on Physics of Fusion Plasmas, Matheran, India, Dec. 14-18, 1982.

48. R.L. McCRORY ET.AL., "Laser Driven Implosion of Thermonuclear Fuel to 20 to 40 g/cm^{-3}, *Nature*, **335**, p.225, 25 Sept. 1988, T.R. BOEHLY ET.AL., "The Upgrade to the Omega Laser System", *Proc. SPIE OE/LASE* (1992).

49. Second Review of the Department of Energy's Inertial Confinement Fusion Program, National Acadamy Press, Washington (1990).

50. C. YAMANAKA, "Recent Inertial Fusion Research at Osaka", *Fusion Technology*, **20**, p.769 (1991).

51. T.P. TURNER ET.AL., "Configuration and Performance of the Los Alamos Aurora KrF/ICF Laser System", *Proc. SPIE - Int. Soc. Opt. Eng.*, **1225**, p.23 (1990).

52. D.L. COOK, "Progress in Light Ion Fusion", *Proceedings of the 1991 IEEE Particle Accelerator Conference*", San Francisco, CA, 91CH-3038-7, p.537 (1991).

53. C.G. FONG ET.AL., "Engineering Study of a 10 MeV Heavy Ion Linear Accelerator", *Proceedings of the 1989 Particle Accelerator Conference*, IEEE Cat. #89CH2669-0, p.962 (1989), R. BOCK, "German Heavy-Ion ICF activities: Status and Prospects", *Laser and Particle Beams*, **8**, 4, p.563 (1990), GESELLSCHAFT FÜR SCHWERIONENFORSCHUNG, Annual Report, "High Energy Density and Matter Produced by Heavy Ion Beams", GSI-91-27 (1991).

54. R.F. BOURQUE, W.R. MEIER AND M.J. MONLER, "Overview of the Osiris IFE Reactor Conceptual Design", *Fusion Technology*, **21**, p.1465 (May 1992), W.R. MEIER AND R.L. BIERI, "Economic Modelling and Parametric Studies for Osiris - A HIB-Driven IFE Power Plant", *Fusion Technology*, **21**, p. 1547, May 1992.

55. I.N. SVIATOSLASKY ET.AL., "A KrF LAser Driven Inertial Fusion Reactor SOMBRERO", *Fusion Technology*, **21**, p.1470 (May 1992), W R MEIER AND C.W. VON ROSENBERG JR.,"Economic and Parametric Studies for SOMBRERO - A Laser Driven IFE Power Plant", *Fusion Technology*, **21**, p.1552 (May 1992).

56. G.A. MOSES ET. A, "LIBRA- A Light Ion Beam Inertial Confinement Fusion Reactor Conceptual Design", *Laser and Particle Beams*, **7**, 4, p.721 (1989).

57. Review of the Department of Energy's Inertial Confinement Fusion Program, National Acadamy Press, Washington, p.7 (1986).

58. L.W. ALVAREZ ET.AL., "Catalysis of nuclear reactions by μ mesons", *Phys. Rev.*, **105**, p.1157 (1957).

59. E.A. VESMAN, "Concerning One Possible Mechanism of Production of the Mesic Molecular Ion ddμ", *Soviet Physics JETP Letters*, **5**, 1, p.91 (1967).

60. S.E. JONES, "Status and Prospects of Muon Catalyzed Fusion Research", Internal Report of EG&G Idaho, Inc., EGG-SE-6290 (1983).

61. S.E. JONES ET.AL.,"Experimental Investigation of Muon Catalyzed d-t Fusion", *Phys. Rev. Lett.*, **51**, p.1757 (1983).

62. A.J. CAFFREY ET.AL., "Muon Catalyzed Fusion Experiments at LAMPF", *Muon Catalyzed Fusion*, **1**, p.53 (1987).

63. S.E. JONES ET.AL., "Observation of Unexpected Density Effects in Muon Catalyzed d-t Fusion", *Phys. Rev. Lett.*, **56**, 588 (1986).

64. S.E. JONES, "Survey of Experimental Results in Muon-Catalyzed Fusion", *AIP Conf. 181, Muon Catalyzed Fusion*, eds. S.E. Jones, J. Rafelski and H.J. Monkhorst, Sanibel Island, FL, p.2 (1988).

65. M. LEON, "Resonant Formation of Muonic Molecules", *Muon Catalyzed Fusion*, **5/6**, p.127 (1990/91).

66. C. PETITJEAN, " Sticking in Muon Catalyzed D-T Fusion", *Muon Catalyzed Fusion*, **1**, p.89 (1987).

67. C. PETITJEAN ET. AL., "New Results in Muon Catalyzed DT Fusion at Low Temperatures", *Hel. Phys. Acta*, **60**, 5-6, p.736 (1987).

68. C. PETITJEAN, "Muon Catalyzed Fusion", *Fusion Engineering and Design*, **11**, p.255 (1989).

69. P.C. SOUERS, *Hydrogen Properties for Fusion Energy*, University of Califonia Press (1986)

70. H. TAKAHASHI ET.AL., *Atomenergie*, **36**, 3, p.593 (1961).

71. A.S.WIGHTMAN, "Moderation of Neagative Mesons in Hydrigen I : Moderation from High Energies to Capture by an H_2 Molecule", *Phys. Rev.*, **77**, 4 (1950).

72. S. ELIEZER, "Muon Catalyzed Nuclear Fusion for Energy Production", in *Muon Catalyzed Fusion and Fusion with Polarized Nuclei*, eds. B. Brunelli and G.G. Leotta, Plenum Press, New York, p.19 (1987).

73. L.I. MEN'SHIKOV AND L.I. PONOMAREV, "Effect of the reaction $d\mu(n)+t\rightarrow d+t\mu(n)$ on the kinetics of muon-catalysis processes in a D_2+T_2 mixture", *Sov. Phys. JETP Lett.*, **39**, 12 p.663 (1984).

74. B. MÜLLER, J. RAFELSKI, M. JÄNDEL AND S.E. JONES, "Possible influence of Vacuum Polarization on Q_{1s} in Muon Catalyzed D-T Fusion", *AIP Conf. 181, Muon Catalyzed Fusion*, eds. S.E. Jones, J. Rafelski and H.J. Monkhorst, Sanibel Island, FL, p.105 (1988).

75. H.E. RAFELSKI, D. HARLEY, G.R.SHIN AND J. RAFELSKI, "Cold Fusion: Muon Catalyzed Fusion", *J. Phys. B: At. Mol. Opt. Phys.*, **24**, p.1469 (1990)

76. M.P. FAIFMAN, "The Resonant Formation of ddμ and dtμ Mesic Molecules", *Muon Catalyzed Fusion*, 2, p.247 (1988).

77. A. KUMAR AND S. SAHIN, 'Potential of Muon Catalyzed Fusion-Fission (Hybrid) Reactors', *Alternative Energy Sources V, Part E - Nuclear / Conservation / Environment*, ed. T.N. Veziroglu, Elsevier Science Publishers B.V., Amsterdam (1983).

78. A.M. LANE, "Back-Decay of Molecular Resonances in Muon Catalyzed Fusion", *Physics Letters*, **98A**, 7, p.337 (1983).

79. S.S. GERSHTEIN ET.AL., "Kinetics of Muon Catalysis Processes in a Mixture of Deuterium and Tritium", *Sov. Phys. JETP*, **51**, 6, p.1053 (1981).

80. A.A. HARMS AND G. SHANI, "Analysis of a Cosmic Ray Source Muon Energy System", *Proceedings of the 4th International Conference on Emerging Nuclear Energy Systems (ICENES 86)*, Madrid, Spain, eds. G. Verlade and E. Minguez, World Scientific, p. 178 (1987).

81. W. FUNDAMENSKI AND A.A. HARMS, "On the Feasibility of Cosmic Ray Muon Focussing", submitted to *Nucl. Inst. and Meth.* (1992).

82. V.V. ARTISYUK, YU. V. KOROVIN AND V.N. SOSNIN, "Computation of Electronuclear Channel Impact on the Energy Balance of the Muon Catalyzed Hybrid Reactor", *Muon Catalyzed Fusion*, 4, p.223 (1989).

83. A.V. DANIEL ET.AL., "Contribution of Fast Nucleons to the Energy Balance of a Hybrid Mesocatalytic Reactor", *Muon Catalyzed Fusion*, 4, p.133 (1989).

84. A.A. HARMS AND M. HEINDLER, *Nuclear Energy Synergetics*, Plenum Press, New York (1982).

85. W.P.S. TAN, "Muon Catalysed Fusion for Pellet Ignition", *Nature*, **263**, p.656 (1976).

86. E.P.HINCKS ET.AL., "Muon Catalysis of Hot Fusion", *Nature*, **269**, p.584 (1977).

87. D. HARLEY AND J. RAFELSKI, "Muon Catalyzed Fusion at High Density", U. of Arizona Preprint (1990).

88. H. TAKAHASHI, "Muon Catalyzed Fusion in the Degenerated Electron DT Plasma Mixture", *Muon Catalyzed Fusion*, **5/6**, p.363 (1990/1991).

89. A.L. RUOFF, "Prospects for Metallic Hydrogen", in *High Pressure and Low Temperature Physics*, ed. C.W. Chu and J.A. Woollam, Plenum Press (1978).

90. A.K. McMAHAN, "Metallic Hydrogen: Recent Theoretical Progress", in *High Pressure and Low Temperature Physics*, ed. C.W. Chu and J.A. Woollam, Plenum Press (1978).

91. S.E. JONES, poster presented at the Sixth International Conference on Emerging Nuclear Energy Systems (ICENES'91), June 16-22, Monterey, California.

92. W.J. NELLIS ET.AL., "Equation of State Data for Molecular Hydorgen And Deuterium at Shock Pressures in the Range 2-76 GPa", *J. Chem. Phys.*, **79**, 3, p.1480 (1983).

93. M. ROSS, F.H. REE AND D.A. YOUNG, "The Equation of State of Molecular Hydrogen at Very High Density", *J. Chem. Phys.*, **79**, p.1487 (1983).

94. R.E. KIDDER, "Theory of Homogenous Isentropic Compression and it's Application to Laser Fusion", *Nuclear Fusion*, **14**, p.53 (1974).

95. R.E. KIDDER, "Laser-Driven Compression of Hollow Shells: Power Requirements and Stability Limitations", Nuclear Fusion, **16**, 1 p.3 (1976).

96. T.K. LARSON, J.F. WHITBECK AND R.L. BENEDETTI, "Analysis of System Requirements for a Commercially Feasible Muon-Catalyzed Fusion Power Plant", internal document EG&G Idaho, Inc.

97. T. NIKSHIKAWA, "High Energy Accelerators, Perspectives" *Part. Accel.*, **26**, 1-4, p.7 (1990).

98. YU. V. PETROV AND YU.M. SHABELSKI, "Estimate of the Expenditure of Energy in Production of π Mesons by Nucleons in Light Nuclei", *Sov. J. Nucl. Phys.*, **30**, 1, p.66 (1980).

99. H. TAKAHASHI, "π Meson Production using Fixed Target and α-Sticking and Reactivation Factor", Contributions to the Muon Catalyzed Fusion Workshop, Jackson Hole, Wyoming (1984).

100. E.H. OTTEWITTE, " Efficient Pion/Muon Production and use for Muon Catalyzed Fusion", Contributions to the Muon Catalyzed Fusion Workshop, Jackson Hole, Wyoming (1984).

101. G. CHAPLINE AND R. MOIR, "Some Thoughts on the Production of Muons for Fusion Catalysis", *J. of Fusion Energy*, **5**, 3, p.191 (1986).

102. G.R. SHIN AND J. RAFELSKI, "Pion Production for μCF", *Nuclear Instr. and Meth.*, **A287**, p.565 (1990).

103. M. JÄNDEL, "Design Principles for Efficient Muon Production in Muon Catalyzed Fusion Reactors", *J. of Fusion Energy*, **8**, 1/2, p.81 (1989).

104. R.A. LEWIS ET.AL., "Pion and Muon Production by Anti-protons on Light and Heavy Nuclei ", *AIP Conf. 181, Muon Catalyzed Fusion*, eds. S.E. Jones, J. Rafelski and H.J. Monkhorst, Sanibel Island, FL, p.415 (1988).

105. H. DANIEL, "Cheap Muon Production and Artificial Muon Reactivation", *Muon Catalyzed Fusion*, **5/6**, p.335 (190/1991).

106. A.P. CHEPLAKOV ET.AL., "π^- Meson Production in Interactions of Deuterons with Extended Carbon And Beryllium Targets at 1 GeV/Nucleon", *Muon Catalyzed Fusion*, **7**, p.231 (1992).

107. YU.V. PETROV AND E.G. SAKHNOVSKY, "Efficiency Estimates of Two Ways of Muon Production in HMC-Reactor", *Muon Catalyzed Fusion*, **3**, p.571 (1988).

108. M.D. GABOVICH, N.V. PESHIVTSEV AND N.N SEMASHKO, *Ion and Atomic Beams for Controlled Fusion and Technology*, Consultants Bureau, New York (1989).

109. A. BERTIN ET.AL., " Muon Losses in Deuterium-Tritium Muon-Catalyzed-Fusion Due to Fast Transfer Reactions to Helium Nuclei", *AIP Conf. 181, Muon Catalyzed Fusion*, eds. S.E. Jones, J. Rafelski and H.J. Monkhorst, Sanibel Island, FL, pp.161-168 (1988).

110. H.E. RAFELSKI ET.AL., "Muon Reactivation in Muon-Catalyzed D-T Fusion", *Progress in Particle and Nuclear Physics*, **22**, p.279 (1989).

111. J.S. COHEN,"Kinetics of Muonic Helium in Muon-Catalyzed d-d and d-t Fusion", *Phys. Rev. Lett.*, **58**, 14, p. 1407 (1987).

112. J.S. COHEN, "Stripping and X-ray Production in Muon-Catalyzed d-d and d-t Fusion", *Muon Catalyzed Fusion*, **3**, p.421 (1988).

113. J.S. COHEN, "Cross-Sections for Kinetics of Muonic Helium Created in Muon Catalyzed d-d and d-t Fusion", *Muon Catalyzed Fusion*, **3**, p.499 (1988).

114. R.M. MORE, 'Atomic Physics in Inertial Confinement Fusion', *Lawrence Livermore Laboratory Preprint*, UCRL-84991 Part I and II (1981).

115. H.E. RAFELSKI AND B. MÜLLER "Density Dependent Stopping Power and Muon Sticking in Muon Catalyzed D-T Fusion", *AIP Conf. 181, Muon Catalyzed Fusion*, eds. S.E. Jones, J. Rafelski and H.J. Monkhorst, Sanibel Island, FL, p.355 (1988).

116. T.J. DOLAN, *Fusion Research*, Pergamon Press, New York (1982).

117. E. FERMI AND E. TELLER, "The Capture of Negative Mesotrons in Matter", *Phys. Rev.*, 72, 5, p.399 (1947).

118. H. TAKAHASHI, "Muon Catalyzed Fusion in Plasma State DT Mixture", *Proceedings of An International Symposium on Muon Catalyzed Fusion μCF - 89*, Ed. J.A. Davies, RAL-90-022, p.93 (1990).

119. A. DAR, J.GRUNZWEIG-GENOSSAR, A. PERES AND A. RON, "Slowing Down of Ions by Ultra-high Density Electron Plasma", *Phys. Rev. Letts.*, **32**, 23,p.1299 (1974).

120. G. MAYNARD AND C. DEUTSCH, "Born Random Phase Approximation for Ion Stopping in an Arbitrarily Degenerate Electron Fluid", *Journal de Physique*, **46**, p.1113 (1985).

121. L.BRACCI AND FIORENTINI, "Enhancement of the Number of Muon Catalyzed Fusions", *Nature*, **297**, p.134 (May 1982).

122. C. TENG, "Accelerator Projects Worldwide", *AIP Conf Proceedings 184, Physics of Particle Accelerators*, Eds. M. Month and M. Dienes, p.2117 (1989).

123. G. HERZBERG, *Molecular Spectra and Molecular Structure I : Spectra of Diatomic Molecules*, 2nd Edition, Van Nostrand Reinhold and Company (1950).

124. N.K. GUPTA AND B. GOEL, "Bethe's <I> for the Calculation of Proton Stopping Power in ICF Plasma", *Proc. of the Fifth International Conference on Emerging Nuclear Energy Systems (ICENES 1989)*, Karlsruhe, FRG, eds. U. von Möllendorff and B. Goel, World Scientific Publishing, p.153 (1989).

125. S. SKUPSKY, "Energy loss of ions moving through high-density matter", *Phys. Rev. A*, **16**, 2, p.727 (1977).

126. J.V. USPENSKY, *Theory of Equations*, McGraw Hill Book Co., New York (1948).